ON THE PROPAGATING BUCKLE AND ITS ARREST

Thesis by

Stelios Kyriakides

In Partial Fulfillment of the Requirements

For the Degree of

Doctor of Philosophy

California Institute of Technology

Pasadena, California

1980

(Submitted April 14, 1980)

DEDICATION

This work is dedicated to my parents whose encouragement, guidance and sacrifices I could not have done without.

ACKNOWLEDGEMENTS

I would first like to express my sincere thanks and appreciation to Professor Chuck Babcock for his guidance, encouragement and friendship during the course of this investigation. The advice and suggestions of other members of the Engineering Staff is also appreciated.

Special thanks to the graduate students of the Solid Mechanics group of GALCIT for providing a warm atmosphere to work in. I would also like to thank my friends Rohan Abeyiaratne and John Psycharis for their help in numerous ways.

I am also grateful to the technicians of GALCIT and to Doug Brisky, Charles Narty and Sam Chang who patiently assisted in the experimental work. Mrs. Betty Wood, Mr. Harry Hamaguchi, Mrs. Marlys Ricards, Mrs. Maureen Matteson and Mrs. Karen Valente are all thanked for all they've done in preparing this manuscript.

Finally, the financial assistance of the California Institute of Technology, the American Petroleum Institute and the Department of Energy is gratefully acknowledged.

ABSTRACT

If an offshore pipeline locally buckles in the presence of sufficiently large external pressure, a propagating buckle is initiated. The buckle propagates along the pipeline until it encounters a region of adverse conditions -- low pressure or an arresting device. The lowest pressure at which a buckle propagates is defined as the Propagation Pressure. An experimental study of this quantity is presented and a semi-empirical expression derived by examining various models of the phenomenon. The dynamics of the Propagating Buckle are also examined and a parametric study of the steady state velocity of Propagation is carried out. A systematic way of empirically deriving the parametric dependence of arresting devices is presented and experimental results of two such arrestors are discussed. During this study a unique "flip-flop" mode of propagation was discovered and studied. An explanation of the phenomenon is also attempted.

TABLE OF CONTENTS

NOMENCLATURE

a	Buckle Profile Length
D	Pipe Diameter, O.D.
E	Young's Modulus
E'	Post-Yield Slope of Bilinear σ-ε Curve
E_s	Secant Modulus
E_t	Tangent Modulus
G	Gap Size
G	Normalized Curvature
h	Arrestor Thickness
H	Horizontal Force at any point in Ring
$\bar{H}$	Normalized Horizontal Force
ℓ	Arrestor Spacing
L	Arrestor Length
M	Moment
$\bar{M}$	Normalized Moment
M_o	Yield Moment
P	Pressure
P_c	Buckling Pressure of Pipe under External Pressure
P_{col}	Collapse Pressure
P_{cp}	Inelastic Buckling Pressure
P_i	Initiation Pressure
P_{ff}	Lowest Pressure at which Flip-Flop Occurs
P_o	Arrestor Crossover Pressure
P_{oD}	Arrestor Dynamic Crossover Pressure
P_p	Propagation Pressure

Q	Normalized Pressure
R	Pipe Radius
s	Normalized Ring Mid-Plane Coordinate
t	Pipe Thickness
T	Time
$\underline{u}$	Vector $(\bar{H}, \bar{V}, \bar{M}, \theta)$
U	Buckle Velocity
U_o	$\sqrt{\sigma_0/\rho}$
V	Vertical Force at any Point on Ring
$\bar{V}$	Normalized Vertical Force
w_0	Amplitude of Initial Imperfection
W	External Work done on Ring
W_{PL}	Plastic Strain Energy in Pipe
W_{KP}	Kinetic Energy of Pipe
W_{KF}	Kinetic Energy of Fluid
W_{PR}	Work Done by External Pressure
x,y	Cartesian Coordinates
$\bar{x},\bar{y}$	Normalized Cartesian Coordinates
α	E/E'
Δ	Displacement of Ring at $\bar{y}(1)$
η	Arrestor Efficiency
η_y	Inelastic Correction Factor for Buckling Pressure
η_{Dy}	Arrestor Dynamic Efficiency
η_{St}	Arrestor Static Efficiency
θ	Angle between Normal and x-axis

κ Curvature

κ_o Curvature at First Yield

ν Poisson Ratios

ρ Pipe Material Density

ρ_f Fluid Density

σ_0 Yield Stress, Pipe (stress at $\varepsilon = 0.005$)

σ_0' Yield Stress, Arrestor

1. INTRODUCTION

In recent years the seas, off the continents, and the oceans beyond are being looked upon with ever increasing interest as main sources of fossil energy for the future (30% of total U.S. oil production by 1983). As exploration of the continental shelf continues the deeper waters beyond are being leased by the government and exploration of oil and gas in depths of up to 5000 ft. (1.5 km) is already under way.

This endeavor has demanded a whole new technology to be established rather quickly and in many cases industry is hard pressed to meet the demand. Existing technology was modified to suit the new field conditions. In many cases restricted methods are used in order to obtain quick answers to new problems.

Offshore pipeline design, construction and operation is one of the new industries which had to be developed. Based on the experience obtained from pipelines laid in shallow waters as early as the 1940's, a number of pipelaying methods have been developed. Ref. 1.1 gives an up to date summary of these. Pipelaying off a barge, an early favorite, still remains the most commonly used method. References 1.2-1.6 give extensive studies of the equilibrium of a pipe during such laying operations (fig. 1.1). Although a few problems still exist, such as the stinger contact problem and elastic-plastic

pipe material behavior, this problem area is fairly well understood. In recent years the development and deployment of barges equipped with reels [1.1, 1.7] have made this type of process much faster.

During such a pipelaying operation (fig. 1.1) the pipe is under the combined effect of bending, pressure, tensional and buoyancy loads. The tension applied at the barge usually controls the bending stresses in the pipeline. If tension is lost either due to sudden ship movement or malfunctioning of the tensioner the bending stresses in the sag bend area (area of maximum moment) can exceed the buckling limit and cause a bending buckle. Bending buckles are local in nature affecting a region less than ten diameters long (fig. 1.2a,b). If the external pressure at this point is high enough the local buckle transforms itself into one that propagates, driven by the pressure (fig. 1.2c). Once initiated this buckle continues propagating, completely flattening the pipe behind it. This continues until an area of low pressure is reached, where propagation cannot be sustained or until some mechanical obstacle is encountered which hinders further flattening of the pipe. In any case, it is clear that practically the whole pipeline is potentially in danger.

It is important to make clear that the role of the bending moment is important only until the initial local buckle is formed which initiates the Propagating Buckle. In fact, a buckle can be initiated from any type of local dent or damage. For example, once the pipe becomes

operational, many external factors can cause damage to the pipeline even though the pipeline is not under the effect of any substantial bending moments. Earthquakes, sea bottom instabilities and sea floor currents can all cause local buckles or damage to the pipeline. Another common cause of damage is heavy equipment or debris falling onto the pipe. Ship anchors falling onto the pipe or becoming hinged to it is another serious danger.

Other ocean energy extraction schemes such as Ocean Thermal Energy Conversion (OTEC) and Kelp Farming involve suspended pipes up to 15,000 ft. (4.57 km) in length [1.8] (fig. 1.3). Through these pipes, large quantities of water are pumped from deep down in the sea to the surface, providing the temperature difference for a heat engine or for nutrients for growing kelp. The pipes are subjected to loads due to currents, to pumping pressure differences and motion induced by the floating structure to which they are attached. Buckling of these structures can occur from the combined effect of bending and external pressure. This can create the conditions necessary for a Propagating Buckle to be initiated.

Although this problem has been observed primarily in offshore pipeline applications it is by no means restricted to these. In fact, any long cylindrical structure under external pressure can be Propagating Buckle critical provided the potential danger of local dents, buckles or other damage occurring, exists. One rather interesting example is described in ref. 1.9. In that case a small diameter gas

pipeline is placed inside an existing large diameter one. (See fig. 1.4.) In some circumstances water fills the space between the two pipes. During the winter this water freezes and for a range of pipe diameter ratios the expansion of ice can cause buckling and complete flattening of the pipe. In a case like this buckling always occurs at the weakest point along the pipeline. The result is a long pipe with a section that is damaged. This acts as an initiating point for a Propagating Buckle. It is driven by the pressure provided by the expanding ice. The rate of propagation depends on the rate of ice expansion.

The problem of the Propagating Buckle and its potentially catastrophic results were first noticed by a number of different researchers in the early seventies. The first published report on the problem came from researchers at Battelle in July 1973 [1.10]. Industry responded by sponsoring a multiyear research program for tackling this and other related buckling problems of offshore pipelines [1.11]. Quite independently Palmer, in a short article [1.12], made a first attempt at quantifying the so called Propagation Pressure. His experimental and theoretical work were not taken far enough to produce a useful formula for this critical quantity. In 1976 (ref. 1.13) the Battelle group expanded on their earlier report. Although practically all aspects of the problem were touched, the restrictive nature of these projects caused the fundamental underlying mechanics problems to be slighted. In all fairness

many of the problems involved are rather difficult in nature involving large deformation plasticity, post buckling effects as well as hydrodynamic effects. However, the above reports served the very useful purpose of making industry conscious of the problem.

This report is a record of a systematic effort, which started in the summer of 1976, to better understand the mechanics of the problem in all its stages. Experiments on model pipes carried out in controlled environments were conducted in order to decide the importance of the various parameters on the exhibited phenomena. With these results established, modelling of some of the problems involved was attempted with the general objective of obtaining approximate but useful expressions for the various critical quantities.

In order to help understand the various aspects of the problem and the mechanical processes involved in initiating, propagating and arresting a buckle, the problem has been subdivided into 6 sub problems. Each of these is briefly described below.

(a) Causes of Local Buckles

As already mentioned a Propagating Buckle is always initiated from some local damage or dent on the pipe. Clearly the best way of avoiding the problem is to make sure that the conditions that cause these local imperfections are restricted. As far as the pipelaying operations are concerned this goal has been achieved to a great

extent due to the addition of a number of new pipelaying methods for special applications [1.1] and the perfection of existing techniques. The advent of dynamically positioned laying vessels (barges, reel ships and semi-submersibles) has also helped reduce accidents due to sea roughness. It is safe to say that today most buckling problems during offshore pipelaying are caused by human error. In addition, better trenching and dredging techniques [1.14-1.16] coating the pipe with protective coating, securing the pipe to the ocean floor, [1.17], better sea bottom survey methods, etc., have all contributed to increasing the safety of the pipeline during its operation.

(b) Buckling of a Circular Pipe Under External Pressure

Since offshore pipelines are under the influence of a variety of compressive loads there exist conditions under which the pipe becomes buckling critical. For the purposes of this report the simplifying assumption that the pipe is under external pressure loading only, will be made. In such a case the buckling pressure of an infinitely long pipe is given by the classical result:

$$P_c = \frac{2E}{1-\nu^2}\left(\frac{t}{D}\right)^3 \qquad (1.1)$$

This equation assumes purely elastic buckling. For typical steel alloys ($\sigma_o \sim 50 \times 10^3$ psi) this formula is good for $D/t \geq 25$. For pipes having diameter: thickness ratios smaller than the above an elastoplastic buckling correction

factor for 1.1 as calculated by ref. 1.18 can be used.

$$P_{cp} = \eta_y P_c \qquad (1.2)$$

$$\eta_y = \frac{E_s}{E}\left[\frac{1}{4} + \frac{3}{4}\frac{E_t}{E_s}\right]$$

(c) Initiation of a Propagating Buckle

As already mentioned a Propagating Buckle will only occur if a local damage exists from which it can be initiated. The pressure at which such a local imperfection transforms itself into a propagating one is called the Initiation Pressure (P_i). If a pipe under purely lateral pressure is considered, it has been shown experimentally that a Propagating Buckle prefers a "dogbone" type of collapse. This is independent of the way the buckle was initiated. The Initiation Pressure then can be looked at as the pressure at which an imperfection, having a general shape, transforms itself into the correct profile which collapses the pipe into the dogbone shape. It is clear that the value of pressure at which this happens depends on the characteristics of the specific imperfection considered. These include the type of imperfection (e.g., local dent of the type introduced by bending buckles or some kind of random imperfection) and its magnitude (i.e., length and amplitude). The relation of the geometry of the imperfection to the required profile of a Propagating Buckle is another factor. For example, a longitudinally extending and symmetrically placed dent of small

amplitude, can have a lower initiation pressure than an irregular and awkwardly oriented dent of much bigger amplitude. If one considers the more complicated case of pressure, moment and tension interacting, then the additional problem of the local stress state has to be considered.

It became clear that since an infinite number of initial dents can be defined, the problem of quantifying the Initiation Pressure in a systematic way (analytical or experimental) is enormous. On the other hand,one is faced with the real demand for this knowledge in the field. Some kind of rule that will enable an evaluation of the seriousness of a given situation where a dent exists on a pipeline is necessary in order to make a decision about the course of action to be taken. Stopping a laying operation or the pumping process are extremely costly decisions. Any advice that might help in evaluating the seriousness of the damage is very useful.

If engineering judgment and experience derived from recorded mishaps are used, the imperfections to be considered can be restricted to a manageable small number and in such a case the parametric dependence of the Initiation Pressure can be studied in a systematic way with the hope that the results derived will apply to a high percentage of the cases encountered.

Such a study has not been one of the objectives of the reported work but represents a long term objective of the investigator.

(d) Buckle Propagation

Once a buckle is initiated it propagates down the pipe flattening it. Typical pictures of Propagating Buckles on three different size pipes are shown in fig. 1.5. It is clear that the damage is extensive and terminal.

Due to the large deformation, cracking at the sharp corners sometimes occurs. This can be very hazardous because any oil in the pipe at the time of the accident spills into the ocean with adverse effects to the environment. In addition if this occurs during the laying operation flooding of the pipe occurs which can cause loss of the pipeline. Any analysis of the above problems has to involve the nonlinear material behavior as well as nonlinear large deformation kinematics.

As mentioned by ref. 1.10 there exists a critical pressure below which a Propagating Buckle cannot be sustained. This is given the name Propagation Pressure (P_p) and an empirical value for this pressure is given by ref. 1.10 as

$$P_p \simeq 34\sigma_0 \left(\frac{t}{D}\right)^{2.5} \quad . \tag{1.3}$$

The validity of this expression is tested experimentally in chapter 2 and an effort to derive a more general expression is also made. It is important to note that for each pipe

$$P_p \leq P_i \leq P_c^* \quad . \tag{1.4}$$

For buckles initiated at pressures higher than P_p the buckles were recorded to propagate at substantial velocities.

*At least for $D/t < 100$ and metallic pipes.

The dynamics of this propagation and the dependence of the velocity on the various parameters of the problem is studied in chapter 3. Chapter 4 deals with a new mode of propagation termed the "flip-flop" discovered during the process of this investigation.

(e) Propagating Buckle Arrest

Accepting the potentially catastrophic results of the Propagating Buckle one would like to restrict its effects to as small a section of pipe as possible. This is done by using strengthening devices called Buckle Arrestors so that if an accidental buckle occurs the damage is restricted to a sacrificial length of the pipeline. The final chapter deals with the design of such devices.

2. ON THE PROPAGATION PRESSURE

2.1 Introduction

When a circular cylindrical pipe is subjected to external pressure there exists a pressure above which a Propagating Buckle can occur. Above this pressure plastic deformations of a local nature that might arise from a variety of sources, such as local buckles or local dents, can cause a Propagating Buckle. The magnitude and configuration of these local imperfections required to cause such a buckle depends primarily on the operating pressure. *The lowest pressure at which a Propagating Buckle can be sustained is defined as the pipe's Propagation Pressure,* (P_p). As shown in fig. 2 the Propagation Pressure is well below the critical buckling pressure of the same pipe under external pressure, at least for pipes with D/t of interest for pipeline applications ($25 \leq D/t \leq 100$). Thus buckle propagation can occur for pressures anywhere between $P_p \leq P \leq P_c$. For pressures closer to the buckling pressure, any kind of local imperfection that will cause local buckling will automatically cause a Propagating Buckle. For pressures closer to the Propagation Pressure a Propagating Buckle is more difficult to initiate. Propagating Buckles prefer a dogbone type of collapse. This is independent of the way the buckle is initiated. As a result, an $n = 2$ imperfection is much more likely to cause a Propagating Buckle, at pressures closer to P_p, than other modes of imperfection are. Investigation of the problem of buckle initiation has not been one of the

objectives of this study. In this section a concentrated effort is made to understand the governing parameters that determine the value of the Propagation Pressure once it is initiated. The problem is simplified even further by avoiding the perplexing issue of propagation under combined loading such as bending, pressure and tension. Instead, propagation under purely external pressure conditions is considered.

The problem is first examined experimentally and then some simplifying models are considered in order to help explain some of the experimental results.

2.2 Experimental Determination of the Propagation Pressure

2.2.1 Experimental Set-up

The experiments were conducted in a specially built pressure tank shown in fig. 2.1. This tank has a diameter of 8 in. (.2m) and a length of 12 ft. (3.61m). It is made from three different segments each one of which can be used independently. The first is a 2 ft. (.6m) long initiator section shown in fig. 2.2. A pneumatically operated knife edge is part of this assembly and was used for initiating a buckle at one end of the pipe under test. The pneumatic cylinder was operated through a solenoid valve remotely and used up to 125 psi (8.62 bar) air pressure. This device was essential for the dynamic tests, described in chapters 3 and 4 where it was necessary that a buckle be initiated at a specific pressure.

Two more sections can be added to the initiator section making the tank 6 or 12 ft. (1.8 or 3.6m) in total length.

The tank was pressure tested to 1000 psi (69.0 bar) but has an operating pressure of 800 psi (55.2 bar). Fig. 2.3 shows a 4 ft. (1.2m) long transparent section which was designed, fabricated and used for observation of the Propagating Buckle. It is made of a floating (no axial stresses present) inner cylindrical acrylic transparent tube turned to the design diameter and repolished. This was slid into a steel casing which was honed allowing only 0.01 in. (.25mm) between the two cylindrical surfaces. Two "O"-rings provided the necessary sealing. Through this design the hoop stresses were taken primarily by the acrylic tube and the axial stresses wholly by the steel casing. The discontinuity at the window was designed as shown in the figure to reduce stress concentrations.

This section was pressure tested to a pressure of 240 psi (16.6 bar) but had a working pressure of 200 psi (13.8 bar). It was used primarily for experimental visualization as it restricted the range of D/t that could be tested. The tank was periodically pressure tested for possible failure of the acrylic due to the cyclic loads that the tank was subjected to. A release safety valve was added to the system when this section of the pressure tank was in operation.

The complete tank assembly is shown in fig. 2.1. The tank can be pressurized with a totally liquid medium, a totally gaseous medium or it can be partly filled with a liquid and pressurized by a gas. In our case all three

situations were encountered; the liquid was water and the gas, air or just nitrogen.

For quasistatic experiments, the tank had to be completely filled with water in order to allow control over the speed of propagation. To achieve this the tank was positioned at an inclination of 2^{o} to the horizontal. The test procedure was as follows. The tube to be tested was prepared and placed into the tank. One end of the tube was directly connected to the atmosphere in order to ensure the pressure inside the tube was atmospheric as the buckle propagated (decreasing its volume). The end flanges were secured to place. "O"-rings between the end flanges and the slip-on flanges of the tank provided the necessary seals. Referring to fig. 2.1 with valves D, E, and F closed and A, B, and C open, water was pumped into the tank. As water filled the tank the air escaped through B-C. Valve B is positioned at the highest possible point ensuring that all the air escaped out of the tank through B-C. Water was pumped until it started escaping through exhaust C. Valve C was first closed and then valve A.

A Teledyne S-216-C single piston air driven pump with a pressure ratio of 10 was used for pressurizing the tank (fig. 2.1). This pressurizing procedure was as follows. With valves A, C, and D closed, valve E was opened. Valve F was used to control the rate of pumping and to monitor the pressure. The pressure in the tank could be read from a calibrated pressure gage. In addition a pressure transducer

signal was recorded on a chart recorder giving a continuous time-pressure reading.

For experiments in air the tank was pressurized with compressed air or nitrogen from high pressure cylinders through valve D with A, E and F closed.

For dynamic experiments in water the tank was partially filled with water leaving an air gap at the top. The system was then pressurized with compressed air. The air gap was big enough to allow near constant pressure experiments. (Pressure difference from the beginning to the end of the experiment was 2-3%; for the case of the tank being completely filled with air the pressure difference was less than 1% - these apply to the biggest diameter pipes used in dynamic experiments 1.5 in. (.38m) OD).

2.2.2 Experimental Procedure

As defined earlier the Propagation Pressure is the lowest pressure at which a buckle will propagate. A series of experiments were carried out on a number of aluminum alloy as well as on stainless steel pipes to find an experimental value for the Propagation Pressure of each. The geometric characteristics of the pipes tested can be found in Table 2.1. Longitudinal tensile test specimens were cut from each of the pipes tested and the stress-strain behavior of the pipe material was obtained up to a maximum strain of about 1%. Typical results from these tests are shown in fig. 2.4.

The experimental procedure was as follows. A pipe was sealed and placed in the tank as shown in fig. 2.1. A large

local initial imperfection was inflicted to the pipe either externally or by the knife edges available in the initiator section. The tank was completely filled with water and slowly pressurized by the water pump. A typical pressure time history of how the experiment progressed is shown in fig. 2.5. For $T_0 \leq T \leq T_1$ the pressure rises to a maximum value P_i called the Initiation Pressure of the specific imperfection. For $T_1 \leq T \leq T_2$ the initial imperfection deforms plastically and rapidly until at T_2 it has taken the geometry of the profile of a Propagating Buckle. A typical profile of a quasistatically Propagating Buckle is shown in fig. 2.5. For $T_2 < T \leq T_4$ the buckle slowly propagates in a dogbone type of collapse. (Typical crossections of collapsed pipes are shown in fig. 2.6.) The rate of propagation depends wholly on the rate water is pumped into the tank; this was usually left constant for $T_2 < T \leq T_4$. The buckle continues to propagate at relatively constant pressure until it starts "feeling" the effect of the end plug, at about 15 pipe diameters away from the end. At this point the constraining effect of the plug makes the pressure rise and this usually signalled the end of the experiment.

Due to the fact that the pump used is a single piston pump, small variation in pressure occurred in the experiment. These variations were of periodic nature and the mean pressure was very easily obtained. This was taken to be the Propagation Pressure.

As shown later the Propagation Pressure is very sensitive

to pipe thickness variations as well as to yield stress variations. Wall thickness irregularities of about max $|\Delta t| = 7\%$ exist in all drawn tubes. As a result sometimes the Propagation Pressure was position dependent. Careful measurement of wall thickness at different points along the pipe and at different points around the perimeter partly negated this error. Other sources of error were instrumentation inaccuracies and human error. The Propagation Pressure results are tabulated in Table 2.1.

2.2.3 Experimental Results-Discussion

Accepting the fact that this phenomenon is primarily governed by rather large plastic deformations, in a first attempt to plot the results in some logical fashion, the assumption that the whole stress-strain behavior of the material can be characterized by one parameter only, i.e., the yield stress, is accepted (see ref. 2.1). For comparison reasons the yield stress σ_0 is taken to be the same as ref. 2.1, i.e.,

$$\sigma_0 = \{\sigma | \ \varepsilon = 0.005\} \quad .$$

This definition has been standardized by API for steel pipes. From fig. 2.4 it can be seen that for steel, this definition gives 4-8% higher values for the yield stress compared to the .2% offset strain criterion. On the other hand in the case of aluminum alloys the first criterion gives 5-15% lower values than the latter one.

The Propagation Pressure normalized by the yield stress

is plotted on log-log scales, vs D/t in fig. 2.7. The results are fitted with a straight line (least squares fit). This straight line has a slope of -2.281. The small scatter of the results is due to experimental errors described above but probably the biggest contribution is due to discrepancies in the determination of the yield stress. As mentioned earlier the yield stress was obtained from tests carried out on specimens cut along the axis of the pipes. In the case of drawn tubes the properties in the transverse direction are different by as much as $\pm$ 5%. Due to the size of the pipes used, obtaining the properties in the transverse direction was very involved so the compromise solution of longitudinal specimens was accepted. Using the slope obtained from fig. 2.7 the results are plotted on natural scales in fig. 2.8.

On the same figures results from ref. 2.1 are also plotted. These were carried out using 2 in. (.051m) and 12 in. (.305m) OD steel pipes of different thicknesses. The slope of the fitted straight line is -2.254. Comparing the steel results with those from aluminum alloys, it is evident that the slope is practically the same (1% difference) but the two straight lines are shifted in the log-log plane. Two experiments carried out by the author on stainless steel pipes (SS-304) which has similar $\sigma - \varepsilon$ behavior as the steels used by ref. 2.1 are also shown in fig. 2.8. They are in good agreement with the other steel results reinforcing the suspicion that a fundamental difference exists between the two sets of results.

The equations of the fitted curves for the two sets of results are as follows:

$$\frac{P_p}{\sigma_0} = A \left(\frac{t}{D}\right)^{\beta} \qquad (2.2.1)$$

	A	β
Aluminum Alloys	11.3	2.281
Steel Alloys	14.5	2.254

Very clearly, replacing the complete stress-strain behavior by one parameter only is not a very good approximation. A more realistic assumption seems to be

$$\frac{P_p}{\sigma_0} = f\left(\frac{E}{\sigma_0}, \alpha\right)\left(\frac{t}{D}\right)^{\beta} \qquad (2.2.2)$$

where E is the Young's modulus of the material and α is a strain hardening parameter which could depend on the stress state. The effect of the elastic deformation and strain hardening will be examined in conjunction with some simplified models of the phenomenon, which follow.

2.3 Theoretical Modeling

Having obtained some knowledge about the phenomenon, effort was made to somehow model it in some simplified way that included the main mechanical parameters of the problem.

Remseth, Holthe, Bergan and Holland in ref. 2.2 looked at the problem of combined bending and external pressure acting on a pipe and the associated initiation and propagation of a buckle. Due to the combined loading considered

most of their effort went into initiating the buckle which as will be explained later depends very much on the load time history used or in deformation terms it depends on the initial imperfection. This is because in practical sense all the bending moment does is induce an initial local imperfection. Once the buckle was initiated their solution became unstable and no data, of usable value, for the propagation pressure are presented in their paper. Possible modifications to their loading and procedure are suggested at the end of this chapter.

Although solution of the problem numerically, through a large deformation shell numerical analysis with plasticity included, is feasible this route was avoided due to the complicated numerical work necessary. Instead it was decided to look at various simplified models of the problem with a varying degree of complexity. The purpose of these models was first to understand the governing physical processes that go on when the buckle quasistatically propagated a distance x; second, to look in more detail at the structure of f in equation (2.2) and third, to obtain, if possible, an approximate theoretical expression for P_p.

2.3.1 One-dimensional Model

As a first approximation to the problem, collapse of a circular ring (or infinitely long pipe) under external pressure is examined. At first this is done through the limit load placticity theory and at a more advanced stage the problem is examined numerically.

(a) Collapse load of a circular ring under external pressure.

Consider a ring of radius R, thickness t, under external pressure P. The limit theorems of plasticity will be used to establish bounds on the collapse load of this ring. (See refs. 2.3, 2.4, and 2.5.)

(i) Upper Bound Theorem

Let the ring material be idealized to a rigid (or elastic)-perfectly plastic one. Consider the kinematically admissible deformation field shown in fig. 2.9a. Four hinges are placed as shown and the ring quadrant between the hinges are made rigid. The system becomes a mechanism whose motion is restricted to the one shown in fig. 2.9b. The moment at the hinges is assumed to be the full plastic moment

$$M_o = \frac{\sigma_0 t^2}{4} \quad .$$

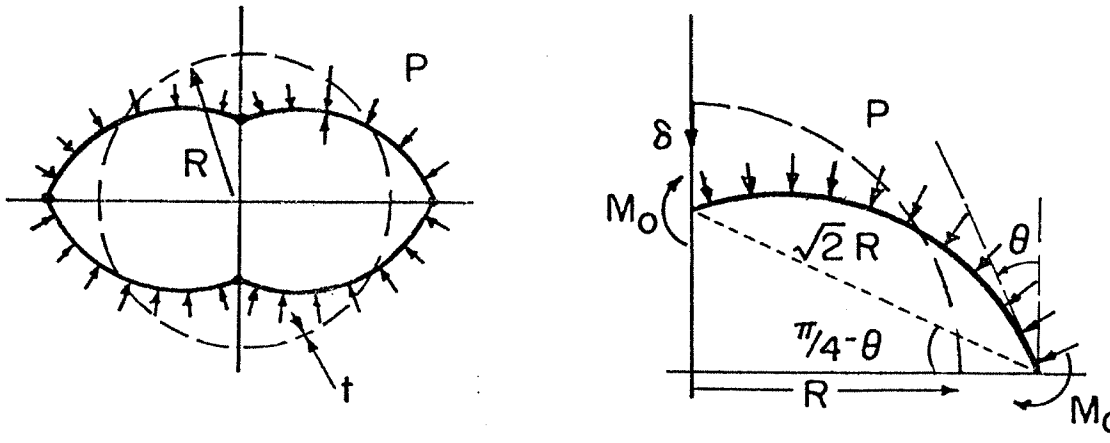

FIG. 2.9. A KINEMATICALLY ADMISSIBLE DEFORMATION FIELD FOR A COLLAPSING RING

If the hinges are rotated as shown in fig. 2.9b through an angle θ the internal energy dissipated is given by

$$U = 8M_0\theta = 2\sigma_0 t^2\theta \tag{2.3.1}$$

The volume change is given by

$$\Delta V = 2R^2\left\{1 - \sin\left(\frac{\pi}{2} - \theta\right)\right\}$$

or

$$\Delta V = 2R^2\left\{1 - \left(1 - \frac{\delta}{R}\right)\left[1 + 2\frac{\delta}{R} - \left(\frac{\delta}{R}\right)^2\right]\right\} \tag{2.3.2}$$

Since

$$\theta = \frac{\pi}{4} - \sin^{-1}\left(\frac{1 - \frac{\delta}{R}}{\sqrt{2}}\right) \tag{2.3.3}$$

Thus the external work done is

$$W = P\Delta V = 2PR^2\left\{1 - \left(1 - \frac{\delta}{R}\right)\left[1 + 2\frac{\delta}{R} - \left(\frac{\delta}{R}\right)^2\right]^{\frac{1}{2}}\right\} \tag{2.3.4}$$

The upper bound limit theorem says that "the structure must collapse if for any kinematically admissible deformation the rate at which the external forces do work is equal (or bigger) to the rate of internal dissipation." Thus for <u>no</u> collapse from (2.3.1), (2.3.3) and (2.3.4)

$$P \leq \sigma_0\left(\frac{t}{R}\right)^2\left[\frac{\frac{\pi}{4} - \sin^{-1}\left(\frac{1 - \delta/R}{\sqrt{2}}\right)}{1 - \left(1 - \frac{\delta}{R}\right)\left[1 + 2\frac{\delta}{R} - \left(\frac{\delta}{R}\right)^2\right]^{\frac{1}{2}}}\right] \tag{2.3.5}$$

Note: from (2.3.5)

$$\frac{\delta}{R} = 1 \quad \Rightarrow \quad P = \frac{\pi}{4}\sigma_0\left(\frac{t}{R}\right)^2$$

$$\frac{\delta}{R} \to 0 \quad \Rightarrow \quad P \to \infty$$

Thus

$$P_{collapse} < \frac{\pi}{4}\,\sigma_0\left(\frac{t}{R}\right)^2$$

(ii) Lower Bound Theorem

The same assumptions are made for the ring as in (i). Due to the double symmetry consider the equilibrium of only one quadrant as shown in fig. 2.10.

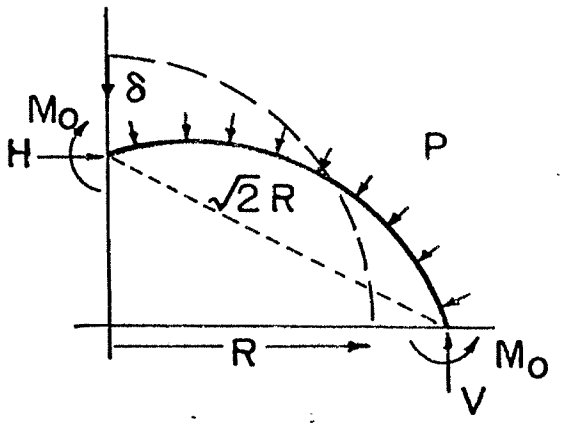

FIG. 2.10. STATICALLY ADMISSIBLE STRESS FIELD

H, V, and M_o define a statically admissible force field if the ring is in equilibrium.

$$V = PR\sqrt{2 - \left(1 - \frac{\delta}{R}\right)^2}$$

$$H = PR\left(1 - \frac{\delta}{R}\right) \qquad (2.3.6)$$

$$M_o = \frac{1}{2}\left[PR^2 - HR\left(1 - \frac{\delta}{R}\right)\right] = \frac{PR^2}{2}\left(2 - \frac{\delta}{R}\right)\left(\frac{\delta}{R}\right)$$

The lower bound theorem states that if the internal forces equilibriate the external forces and the material is at yield or below yield the structure will not collapse.

From (2.3.6) then, for collapse

$$P > \sigma_0 \left(\frac{t}{R}\right)^2 \frac{1}{2\frac{\delta}{R}\left(2 - \frac{\delta}{R}\right)}$$

Note $\frac{\delta}{R} \to 0 \Rightarrow P \to \infty$ (2.3.7)

$$\frac{\delta}{R} \to 1 \Rightarrow P \to \frac{1}{2}\sigma_0\left(\frac{t}{R}\right)^2$$

If we thus combine the results of (2.3.5) and (2.3.7) and define collapse when $\frac{\delta}{R} = 1$, then

$$\frac{1}{2}\sigma_0 \left(\frac{t}{R}\right)^2 < P_{\text{collapse}} < \frac{\pi}{4} \sigma_0 \left(\frac{t}{R}\right)^2 \qquad (2.3.8)$$

Expressions (2.3.5) and (2.3.7) are plotted as functions of $\Delta \left(\Delta = \frac{2}{\pi} \frac{\delta}{R}\right)$. in fig. 2.11. The problem of collapse of a circular ring under external pressure is solved numerically in the next section. The post buckling displacement of point A is also plotted on fig. 2.11. (Note $\alpha = 10^4$.) Excluding the behavior for $\Delta < .1$ the equilibrium path of the statically admissible path described above is very close to the exact one. For $\Delta > .1$ the error in pressure is $1.5 \leq \Delta\rho \leq 2.5\%$, but is always positive. According to the lower bound theorem the error should be negative. It is thought that since the error is so small this discrepancy is probably due to truncation and roundoff errors in the numerical scheme used to solve the problem exactly. The kinematically admissible mechanism gives a clear upper bound at all points.

If we associate the propagation pressure with the collapse pressure and remember that we have assumed a rigid

perfectly plastic material behavior from (2.3.8), we can say that

$$\frac{1}{(1-\nu'^2)}\frac{1}{2}\sigma_0\left(\frac{t}{R}\right)^2 \leq P_p \leq \frac{1}{(1-\nu'^2)}\frac{\pi}{4}\sigma_0\left(\frac{t}{R}\right)^2$$

where $\nu' = \frac{1}{2}$. Thus, (2.3.9)

$$\frac{P_p}{\sigma_0} = A\left(\frac{t}{R}\right)^2 \qquad \frac{2}{3} \leq A \leq 1.047$$

As expected this model does not give us a good representation of the propagation pressure. The material σ-ε behavior is represented by only one parameter σ_0 and the power of $\left(\frac{t}{R}\right)$ is only 2. Of course this is to be expected due to the fact that the third dimension of the problem has been neglected. If we take the maximum value for A then in fig. 2.12 we see the difference between the experimental and the predicted result.

As a next step we look at the exact solution of the problem of the collapse of a ring, numerically. Examining the collapsed cross sectional configuration of a buckled pipe in fig. 2.6 we see that the configuration of the actual cross section is not very different from what assumed, if the region close to the plastic hinge is neglected. In fact the four quadrants remain practically undeformed on collapse. This leads us to the next problem where the effects of including the complete σ-ε behavior (Elastic-Linear strain hardening) to the problem of ring collapse under external pressure are examined numerically.

(b) Large Deformation Collapse Analysis of an Inelastic Ring Under External Pressure

In the last section the collapse analysis of a ring was examined assuming a rigid perfectly plastic material and using theorems of limit load plasticity. It has already been mentioned that the effect of including the complete σ-ε behavior in the problem is probably critical. Since the complete problem will not be solved it was thought prudent to examine the effect this has on at least the ring model which, after all, includes the fundamental mode of deformation that the pipe undergoes (Strip Theory Approximation). For this reason the large deformation response of an inextentional ring under external pressure is examined. The nonlinear equilibrium equations are used and the material behavior is approximated by an elastic linear strain hardening σ-ε curve symmetric about the zero strain axis. The problem is solved numerically and the deformations are followed until complete collapse of the ring. A parametric study of the problem is carried out in order to examine the dependence of the collapse load on the various parameters of the problem.

(c) The Problem

Consider a circular ring of radius R and thickness t, as shown in fig. 2.13. The ring can have an initial imperfection. For convenience this will be taken to be of the form

$$w_i = w_o \cos 2\phi \qquad (2.3.10)$$

Equilibrium Equations

The nonlinear equilibrium equations can be obtained by considering an elemental segment of the ring as shown in fig. 2.14.

$$\frac{dH}{dS} = -P \cos \theta$$

$$\frac{dV}{dS} = -P \sin \theta \qquad (2.3.11)$$

$$\frac{dM}{dS} = H \cos \theta + V \sin \theta$$

H and V are the horizontal and vertical forces whereas M is the moment as defined by fig. 2.14. S is the coordinate along the midsurface of the ring and θ is the angle the normal at any point makes with the x-axis.

Geometry

Only inextensional deformations of the ring will be considered, as a result

$$\frac{dx}{dS} = - \sin \theta$$

$$\qquad (2.3.12)$$

$$\frac{dy}{dS} = \cos \theta$$

where (x, y) defines a point on the deformed ring relative to the Cartesian frame shown in fig. 2.14.

Constitutive Behavior

The main purpose of this exercise is not to fit any stress strain curve exactly, but to see how the response of the ring depends on some well defined material parameter.

For this reason a material with σ-ε curve as shown in fig. 2.15 was chosen. The symmetry of the σ-ε curve about the zero strain axis should be noted.

The inelastic moment curvature relationship for such a material is derived in Appendix A and is given by

$$M = \frac{\sigma_0 t^2}{6}\left[\frac{1}{\alpha}\left(\frac{\kappa}{\kappa_0}\right) - \frac{1}{2}\left(1 - \frac{1}{\alpha}\right)\left(\frac{\kappa_0}{\kappa}\right)^2 + \frac{3}{2}\left(1 - \frac{1}{\alpha}\right)\right]$$

where (2.3.13a)

$$\kappa = \frac{d\theta_c}{dS} - \frac{d\theta}{dS} \quad .$$

This is the nonlinear curvature displacement relationship for a curved beam. $\frac{d\theta_0}{dS}$ is the initial curvature.

$$\kappa_0 = \left\{\kappa \mid M = \frac{\sigma_0 t^2}{6}\right\} \tag{2.3.13b}$$

Let $G = \frac{\kappa}{\kappa_0}$.

With these definitions the moment curvature relationship becomes

$$G^3 + \left[\frac{3}{2}(\alpha - 1) - \alpha\bar{M}\right]G^2 - \frac{1}{2}(\alpha - 1) = 0 \quad ; \tag{2.3.14a}$$

$$\bar{M} = M \Big/ \frac{\sigma_0 t^2}{6} \quad .$$

Let the required root of this cubic be

$$G = G(\alpha, \bar{M}) \quad . \tag{2.3.14b}$$

Note that $G(1, \bar{M}) = \bar{M}$.

(2.3.12b), (2.3.14a), (2.3.14b) $\Rightarrow$.

$$\frac{d\theta}{ds} = \frac{d\theta_0}{ds} - \pi\left(\frac{R}{t}\right)\left(\frac{\sigma_0}{E}\right)G(\alpha, \bar{M}) \tag{2.3.15}$$

Because of symmetry about the x-axis and y-axis only one quadrant of the ring need be considered. The boundary conditions then are:

$$\begin{aligned} H(0) &= 0 & \theta\left(\frac{\pi}{2}R\right) &= \pi/2 \\ \theta(0) &= 0 & V\left(\frac{\pi}{2}R\right) &= 0 \end{aligned} \qquad (2.3.16)$$

Non-dimensionalizing equations (2.3.11), (2.3.15) and (2.3.16) appropriately, one obtains:

$$\frac{d\bar{H}}{ds} = -Q \cos\theta$$

$$0 \leq s \leq 1$$

$$\frac{d\bar{V}}{ds} = -Q \sin\theta$$

$$\frac{d\bar{M}}{ds} = \bar{H} \cos\theta + \bar{V} \sin\theta$$

$$\frac{d\theta}{ds} = \frac{d\theta_0}{ds} - \pi\left(\frac{R}{t}\right)\left(\frac{\sigma_0}{E}\right) G(\alpha, \bar{M}) \qquad (2.3.17)$$

$$G(1, \bar{M}) = \bar{M}$$

$$G(\alpha, \bar{M}) = \bar{M} \text{ for } \bar{M} \leq 1.$$

with B. C.

$$\bar{H}(0) = 0$$

$$\theta(0) = 0$$

$$\theta(1) = \pi/2$$

$$\bar{V}(1) = 0$$

In addition (2.3.12) becomes

$$\frac{d\bar{x}}{ds} = -\sin\theta \qquad 0 \leq s \leq 1 \qquad (2.3.18)$$

$$\frac{d\bar{y}}{ds} = \cos\theta$$

$$\bar{x}(1) = 0$$

$$\bar{y}(0) = 0$$

where

$$s = 2S/\pi R \ , \quad \bar{x} = 2x/\pi R \ , \quad \bar{y} = 2y/\pi R \ ,$$

$$\bar{M} = 6M/\sigma_0 t^2 \ , \quad \bar{H} = 3\pi HR/\sigma_0 t^2 , \bar{V} = 3\pi VR/\sigma_0 t^2 \ , \tag{2.3.19}$$

$$Q = \frac{3}{2}\pi^2 \left(\frac{R}{t}\right)^2 \left(\frac{P}{\sigma_0}\right) \ .$$

(2.3.17) can be expressed in vector form as:

$$\frac{d\underline{u}}{ds} = \underline{f}(s, \underline{u}) \ ,$$

$$\underline{u} = (\bar{H}, \bar{V}, \bar{M}, \theta) \ , \qquad 0 \leq s \leq 1 \tag{2.3.20}$$

$$u_1(0) = 0 \ , \qquad u_2(1) = 0 \ ,$$

$$u_4(0) = 0 \ , \qquad u_4(1) = \pi/2 \ .$$

(2.3.20) describes a set of four nonlinear ordinary differential equations in the form of a two point boundary value problem. Newton's iterative numerical method is used to solve for $\underline{u}$. The interval $s \in \left]0, 1\right[$ is discretized into N discrete points where $26 \leq N \leq 50$, depending on the situation.

The convergence criterion used was as follows:

$$\max_j \left| u_j^{(\nu+1)} - u_j^{(\nu)} \right| \leq 10^{-4}$$

The numerical method used is described in more detail in ref. 2.6.

The solution of the elastic small deformation linearized problem -- ref. 2.7 -- was used as initial guess $\underline{u}^{(0)}$ to start

the iteration. The calculation of the initial guess is shown in Appendix B:

The pressure parameter Q was increased by ΔQ and the solution at Q was used as initial guess for $Q+\Delta Q$, i.e.,

$$\underline{u}\,(Q)^{(\nu)} \rightarrow \underline{u}^{(0)}(Q + \Delta Q)$$

(i) Linearly Elastic Case ($\alpha = 1$)

Linearly elastic material behavior is obtained if $\alpha = 1$ in (2.3.17). The procedure described above is used to find the different configurations as a function of pressure (see fig. 2.16). The ring was assumed to have collapsed when $(y(1), 0) = (0, 0)$. Figure 2.16 shows how the displacement (non-dimensional) of the point $(y(1), 0)$ varies with pressure. The same study was done for five different values of the imperfection. For zero imperfection the following procedure was used for solution:

Define $\underline{u}^{(\nu)} = \underline{u}^{(\nu)}\left(Q, \frac{w_0}{R}\right)$ the νth iteration value of $\underline{u}$ pressure Q and imperfection $\frac{w_0}{R}$.

Suppose that on the νth iteration the solution converged. Using this definition

$$\underline{u}^{(\nu)}\ (1.5,\ .009) \rightarrow \underline{u}^{(0)}\ (1.5,\ 0)$$
$$\underline{u}^{(\nu)}\ (1.5,\ 0) \rightarrow \underline{u}^{(0)}\ (1.4,\ 0)$$
$$\underline{u}^{(\nu)}\ (1.4,\ 0) \rightarrow \underline{u}^{(0)}\ (1.3,\ 0) \quad , \text{ etc.}$$

Of course once the first point on the curve was obtained then the same procedure was followed as before.

The problem of collapse of an elastic ring with no imperfection has been studied in detail by ref. 2.8, where the

existence of solution is proved both above and below $P/P_c = 1$. In the same reference Newton's method was used to find the deformed shape as a function of pressure. For collapse as defined above, $P/P_c = 1.68$. This compares with a value of 1.75 found in our case. The error depends both on the mesh as well as on the convergence criterion.

More recently Budiansky and Sills [2.9] looked at the "initial post-buckling" of a ring with no imperfection, under external pressure. They showed that the buckling pressure is not imperfection sensitive. This was in disagreement with the results of ref. 2.10. The complete pressure-displacement curves clearly agree with the conclusion of Budiansky and Sills.

Pressure vs. the volume change curves have also been drawn and have the same nature as those of fig. 2.1.6 as a result they are not included.

(ii) Linear Strain Hardening Case ($\alpha \geq 1$)

If $\alpha > 1$ then $G = G(\alpha, \bar{M})$ is used in equations (2.3.17) where G is the solution of (2.3.14a). For most metals of interest $\alpha \varepsilon (50, 250)$. If this range of α is considered then the pressure-displacement response changes drastically in nature. A distinct limit load appears and the ring becomes unstable beyond this point. Using load increments (ΔQ) the solution had difficulty converging for points around the limit point. Arbocz in ref. 2.11, facing the same problem but using the double shooting technique, successfully modified his equations so that increments of deformation were prescribed

instead of load. This enabled him to extend the curve beyond the limit point. The same idea is used in this case but a different constraint is used.

From (2.3.18)

$$\frac{d\bar{y}}{ds} = \cos\theta \ , \quad \bar{y}(0) = 0$$

Suppose we add the constraint that

$\bar{y}(1) = \Delta$, where Δ is to be prescribed each time.

Since displacement cannot be prescribed simultaneously, and traction at a point, Q is treated as a new unknown to the problem. Since Q = const

$$\frac{dQ}{ds} = 0 \ .$$

Equations (2.3.17) then become

$$\frac{d\bar{H}}{ds} = -Q\cos\theta$$

$$\frac{d\bar{V}}{ds} = -Q\sin\theta \qquad 0 \leq s \leq 1 \qquad (2.3.21)$$

$$\frac{d\bar{M}}{ds} = \bar{H}\cos\theta + \bar{V}\sin\theta$$

$$\frac{d\theta}{ds} = \frac{d\theta_0}{ds} - \pi\left(\frac{R}{t}\right)\left(\frac{\sigma_0}{E}\right)G(\alpha, \bar{M}) \qquad G(1, \bar{M}) = \bar{M}$$

$$G(\alpha, \bar{M}) = \bar{M} \quad \bar{M} \leq 1$$

$$\frac{d\bar{y}}{ds} = \cos\theta$$

$$\frac{dQ}{ds} = 0$$

with B. C's.

$$\bar{H}(0) = 0$$

$$\theta(0) = 0$$

$$\theta(1) = \pi/2$$

$$\bar{V}(1) = 0$$

$$\bar{y}(0) = 0$$

$$\bar{y}(1) = \Delta \qquad (\Delta \text{ prescribed each time})$$

In addition

$$\frac{d\bar{x}}{ds} = -\sin\theta\,, \quad \bar{x}(1) = 0\,. \tag{2.3.22}$$

A separate program was written for equations (2.1). They were solved in exactly the same manner. The procedure for the complete collapse of the tube was as follows:

Using increments of Q (i.e., eqns. (2.3.17)), the pressure was taken up to point k (see fig. 2.17), a small distance below the limit point. The solution usually diverged at this point. The last converged solution (i.e., solution at point k) was used as initial guess for the next program where increments of displacement Δ were prescribed. Figure 2.17 shows in detail a typical example of the curve around the limit point. Increments of displacement were used until complete collapse of the ring. Figure 2.16 shows how the pressure displacement graphs change with the introduction of linear strain hardening. A distinct limit point is present in each case. The maximum pressure reached in each case is taken to be the buckling pressure. The post-buckling behavior is unstable. On

collapse some residual resistance to pressure remains in the tube. The minimum pressure always occurs for $\Delta < 2/\pi$ (collapse condition).

Figure 2.18 depicts a quadrant of the ring at different stages of collapse. The spread of plasticity along the length of the ring is also shown. The region of maximum moment, i.e., at s = 0 goes plastic first, followed by the region at s = 1. As the deformation continues the two regions spread inwards as shown in the figure. Fig. 2.19 shows a typical collapse sequence of a complete ring.

Figure 2.20 shows how the moment at s = 0 (point of maximum moment for all values of Δ) varies with displacement. It should be noted that no unloading occurs at any value of Δ. This is true everywhere along the ring. This fact helps simplify the numerical analysis considerably as no unloading capability had to be added to the program. The variation of forces at s = 0 and 1 with displacement are shown in fig. 2.21. Since these are the main reacting forces for the external pressure they follow the pattern of the pressure behavior with displacement Δ.

The moment distributions around the perimeter of a ring quadrant just before buckling and on final collapse are shown in fig. 2.22. Similar plots for the horizontal and vertical forces are shown in fig. 2.23.

(iii) Parametric Analysis

The purpose of carrying out the above analysis was two fold. First to find the dependence of the collapse load on the various parameters of the problem and second to find the buckling pressure of a tube with initial imperfection, as a function of the initial imperfection and D/t. The latter is needed for analyzing the the "Flip-Flop" mode of dynamic propagation described in chapter 4. It so happens that the buckling pressure is a direct by-product of the analysis required for the first problem.

Collapse pressure will be defined as the pressure at which the two points of maximum displacement finally touch. (See fig. 2.19). A parametric study of the collapse load has been carried out to determine its dependence to the various parameters of the problem.

For the inelastic case, buckling pressure is defined as the maximum value of pressure reached, or as the maximum pressure for which $\frac{dP}{d\Delta} = 0$. Figure 2.16 shows how the collapse behavior varies with different values of initial imperfection. Although the initial imperfection affects very much the buckling load, it has practically no effect on the post buckling behavior and absolutely no effect on the collapse load. It is of interest to compare this behavior with that of the elastic case, where of course the post buckling behavior is stable. Obviously the buckling load in this case is not imperfection sensitive. The initial imperfection has minimal effect on the collapse load. Varying

E changes the buckling load. As a result the prebuckling behavior is affected. The post buckling behavior very quickly converges to exactly the same values for all values of E. As a result the collapse load does not depend on E.

Figure 2.25 shows how the post buckling behavior is affected by the value of α. $\alpha = 1$ represents the elastic case and $\alpha = 10^4$ represents what is practically an elastic-perfectly plastic material behavior. It can be seen that the effect of strain hardening on the buckling load is insignificant. On the other hand the post buckling behavior, which after all takes place totally in the plastic regime (at least for the ring parameters considered), is critically affected by strain hardening. Figure 2.26 shows how the final collapse shape is affected by the same parameter.

For bigger values of α the radius of curvature at the pointed ends becomes smaller increasing the possibility of cracking at these points due to material failure. Such cracking leads to flooding of the pipe (Wet Buckle) which is highly undesirable. This subject obviously warrants further investigation.

The next parameter to be varied is D/t where the values of D/t from 26 to 100 were examined. This is the region of interest for pipeline application. Also for $D/t < 25$ the effect of membrane stresses cannot be ignored.

A study was done for four different values of α and the results are plotted on log-log scales in fig. 2.27. Straight line results are obtained indicating a power law dependence

of the collapse pressure on this parameter. The powers β of t/D were as shown below.

α	β
50	2.207
80	2.162
200	2.108
10000	2.05

It is important to note that although good agreement exists in the powers of these curves they are shifted in the log-log space giving quite different collapse load for the same D/t. Comparing these powers with those obtained from the experiments (from fig. 2.7) we find them a little smaller. (Steel β = 2.25; Aℓ β = 2.28.) It is important to keep in mind though that this analysis can only be considered as a strip theory representation of the full three-dimensional problem. Although the power of the (t/D) parameter is not exactly the same the shift in the curves observed in the experiments is repeated in the analytic results.

For the standard ring (D/t = 35.7, $\sigma_0/E = 4.2 \times 10^{-3}$) the value of α was varied further in order to see in detail its effect on the collapse pressure. For the imperfection considered ($w_0/R = 8 \times 10^{-3}$) the collapse process is always unstable if $\alpha > 1.2$. The value of P/P_c at collapse varies from 1.73 in the elastic case to 0.145 in the elastic-perfectly plastic case ($\alpha = 10^4$). The dependence of the collapse pressure P_{col} on α is shown in fig. 2.28. Clearly its effect

is substantial. Materials of interest (i.e., aluminum and steel alloys) have $\alpha\varepsilon(50,200)$ which as shown in fig. 2.28 is the region of most variation of the collapse pressure.

The next parameter to be varied was σ_0/E and the results are shown in fig. 2.29. Varying the yield stress changes the point of instability initiation along the elastic collapse curve. It is interesting to note that only a small increment in pressure is necessary for collapse to occur once the first (outside) fiber of the ring yields. The post buckling path is also affected and consequently the collapse pressure P is affected. The normalized collapse load is plotted vs. the normalized yield stress in fig. 2.30. Clearly the collapse load varies linearly with the yield stress parameter at least for the range of this parameter examined (range of interest for pipeline applications).

Summarizing some of the above results: It has been shown that the collapse pressure does not depend on E but on the other hand it is heavily affected by E/E' and σ_0/E. It can thus be concluded that the ring collapse pressure P has a parametric behavior as follows:

$$\frac{P_{col}}{\sigma_0} = f\left(\frac{E'}{\sigma_0}\right)\left(\frac{t}{R}\right)^{\beta} \qquad (2.3.24)$$

P_{col}/σ_0 is plotted vs. E'/σ_0 in figs. 2.31 (a) and (b) for two ranges of E'/σ_0. Approximating this curve with a straight line the following expression is obtained for the collapse pressure of the inelastic ring.

$$\frac{P}{\sigma_o} = \left[a + b\left(\frac{E'}{\sigma_o}\right)\right]\left(\frac{t}{R}\right)^{\beta} \qquad (2.3.25)$$

where $a \simeq 4.6$

$b \simeq 0.23$

$\beta \simeq 2.2$.

As already mentioned a one dimensional model such as the one presented above cannot by itself represent the behavior of the propagating Buckle. In particular, the profile through which the pipe transforms itself to a dogbone type of cross section undergoes bending and stretching deformations in the longitudinal sense; and these cannot be considered by a one-dimensional model. Even so, it is clear that the one-dimensional model represents by far the dominant effect. For this reason it is thought prudent to generalize conclusions about its behavior to the behavior of the complete problem. For instance, the one-dimensional problem predicts a linear dependence of the collapse load on the yield stress σ_o (actually σ_o/E but E does not affect the collapse load). This of course is in agreement with result (2.2.2) drawn from the experimental results. A second important conclusion is that the collapse load of the ring is strongly affected by the strain hardening parameter E'/σ_0. A third important conclusion is that due to the nature of the solution the unstable part of the load-displacement curve is practically independent of the value of E. In fact the collapse load is completely independent of E. In addition to the above, as expected, the magnitude of the initial imperfection has no effect on the collapse load.

2.3.2 A three-dimensional model

In section 2.3.1(a) a limit analysis on a one-dimensional ring model was carried out which gave upper and lower bounds to the collapse pressure of that model. In addition to the single dimension simplification an inextensionality condition was also used.

In this section the problem is examined through a more realistic geometry by considering the energy balance of a slowly propagating buckle front. The geometry of a typical buckle front is shown in fig. 1.5. The idealized geometry is shown in fig. C.1; this geometry represents a kinematically admissible one. The strain energy required by the material when the buckle moves forward a unit distance is calculated. The following assumptions are made

(a) The kinematically admissible geometry of fig. C.1 is assumed.

(b) The material is assumed to have a rigid perfectly plastic material behavior.

(c) Circumferential deformations are assumed to be inextensional.

(d) Strain energy going into bending and membrane deformations of longitudinal fibers are not neglected.

As shown in fig. C.1 the buckle front has a length a. It represents a transition region from a circular to a dogbone cross section of the pipe and is divided into regions A and B. Each region is assumed to undergo a uniform extension and the curvature does not vary in the circumferential direction. The longitudinal fibers of each region are assumed to have a cosine z dependence. This dependence was found to be realistic enough

when compared to real life buckle fronts. From these assumptions the total strain energy required for the buckle front to move a unit distance forward can be calculated as

$$U = U(\sigma_0,\ t,\ R,\ a)/\text{unit pipe length flattened}\ .$$

The above expression then includes contributions from circumferential and longitudinal bending strain energies as well as energy gone to longitudinal membrane deformations. The detailed calculations of U can be found in Appendix C.

The external work done can be calculated in the same way as the one dimensional problem and can be given by

$$W = W(P,\ R) = 2PR/\text{Unit pipe flattened}$$

From Appendix C

$$U = \frac{2}{3}\pi\sigma_0 t^2 + \frac{\sqrt{2}}{2}\,\pi\left(\frac{R}{a}\right)^2\sigma_0 t^2 + \left(1 - \frac{\sqrt{2}}{2}\right)\frac{\pi^3}{4}\left(\frac{R}{a}\right)^2\sigma_0 Rt$$

$$U = W \Rightarrow$$

$$P = \frac{\pi}{3}\,\sigma_0\left(\frac{t}{R}\right)^2\left[1 + \frac{3\sqrt{2}}{4}\left(\frac{R}{a}\right)^2 + \frac{3}{8}\,(1 - \sqrt{2})\pi^2\left(\frac{R}{a}\right)^2\left(\frac{R}{t}\right)\right] \qquad (2.3.26)$$

To find the dependence of P on R/t a relationship between R/t and R/a is necessary. It has not been possible to find such an expression theoretically; as a result the experimental values of fig. 4.3 are used in order to compare the values calculated from (2.3.26) with the experimental results for P_p.

It should be noted that the numerical values of this calculation are restricted to Aℓ-6061-T6 for which the measurements were made. The results are plotted in fig. 2.12. This provides a reasonably good upper bound for the value of P_p. The error is of the order of 15% and is bigger for bigger D/t's. The dominant term in

expression (2.3.26) is the first one (circumferential bending). The second and third terms increase the value of P/σ_0 by about 8%. Due to the fact that this is an upper bound neglecting the second and third terms brings the answer closer to the experimental results, especially for lower D/t's.

2.4 Conclusions

The value of the pipe propagation pressure (P_p) was found experimentally for both aluminum and steel alloys. Trying to find a parametric dependence for P_p it was noted that it is proportional to σ_0 and to some power of (t/R). However, describing the complete material σ-ε behavior of the pipe by only σ_0 was shown to be inadequate.

From limit plasticity analysis of a one-dimensional ring model, upper and lower bounds were found for the collapse pressure which can be associated -- as a first approximation -- to the propagation pressure. A more extensive three-dimensional model indicated that including longitudinal fiber bending and membrane deformations increased the predicted upper bound by 8%. However, these models suffer from the inherent problem of single parameter characterization of the pipe material behavior.

The above models, even though crude, have shown that the circumferential bending represents the dominant deformation mechanism. With this in mind the behavior of the ring model was considered using the nonlinear equations of equilibrium and large deformation kinematics (small strains). This was done for a class of pipe materials having elastic-linear

strain hardening material behavior. A parametric study of the collapse pressure was carried out and it was found that compared to the experimental results relatively good agreement was found as far as the parameters R/t and σ_0/E are concerned, but in addition the collapse pressure depends on E'/σ_0, in a simple algebraic form shown in (2.3.25). Based on the above results the Propagation Pressure is assumed to have the same dependence on E'/σ_0 as in (2.3.25). The values of (a) and (b) can be calculated by assuming that for the aluminum alloys used in the experiments $\alpha = 80$ and for the steel alloys $\alpha = 200$. The Propagation Pressure expression can then be approximated as:

$$\boxed{\frac{P_p}{\sigma_o} = \left[10.7 + 0.54\left(\frac{E'}{\sigma_o}\right)\right]\left(\frac{t}{D}\right)^{2.25}} \qquad (2.4.1)$$

3. DYNAMICS OF THE PROPAGATING BUCKLE

3.1 Introduction

In the preceding chapter buckle propagation under quasi-static conditions was discussed. Although that study is very important in establishing a criterion for the Propagation Pressure of the pipe, a physically more relevant examination of the problem cannot ignore the dynamics of the problem. It has already been stated that the Propagating Buckle phenomenon can only occur at pressures P such that

$$P_p \leq P \leq P_c \quad .$$

If a buckle is initiated at any pressure above P_p then it will propagate at a velocity U which is a function of the various parameters of the problem. It becomes clear then that quantifying the velocity is important in establishing the correct arrest conditions when trying to design arresting devices.

An attempt to quantify the velocity of propagation is given in ref. 3.1. An expression is presented which gives the velocity as a function of the parameters of the problem. This expression was derived (personal communication with T.G. Johns) by considering a steady state propagation of an elastic, small displacement axisymmetric disturbance in an infinitely long circular pipe. This model has two important drawbacks. First it does not take into account the inertial effects of the fluid and secondly it is restricted to elastic deformations. As established in chapter 2, the Propagating Buckle phenomenon is characterized above all by its dependence on the post yield stress-strain behavior of the pipe material.

Neglecting this in modeling the phenomenon is inappropriate.

In what follows, an effort is made to treat the problem in a more general manner by including important parameters neglected in ref. 3.1. The objective is to obtain empirical relations for the parametric dependence of the velocity. Again the experimental path of investigation is followed.

The main parameters of the problem are shown in fig. 3.1. In addition to those considered in the quasistatic case, structural as well as hydrodynamic inertial parameters are included. Some of the problems considered are for instance the variation of the buckle profile length with pressure the examination as to whether a steady state propagation condition is reached and the determination of the acceleration time to the steady state condition. High speed photography is used in order to observe the propagation and to investigate whether hydrodynamic phenomena such as separation or cavitation are present. With the guidance of these experimental results an effort is made to obtain a useful parametric relation with an energy balance type of approach.

3.2 Experimental Determination of the Velocity of Propagation

These experiments were the first to be carried out and the equipment used was not optimal. Most of the experiments were carried out in the high pressure test facility shown on fig. 3.2. It consists of a high pressure tank (3000 psi-207 bar-working pressure) having internal diameter of 22 in. (.56m) and height of 10.5 ft (3.2m). Access into the tank was provided by a 2.5 in (.064m) opening at the bottom end and two 1.25 in (.032m) openings

at the top end. These restricted the pipe dimensions to be tested to maximum length of 8 ft (2.44m) and maximum diameter of 1.5 in (0.038m). The system with its hydraulic connections was pressure tested to 2000 psi (138 bar).

The facility can operate with wet or dry pressurizing medium (air or water). For experiments in water the tank was filled with water but pressurized with compressed air. A sufficiently large air pocket was left to insure nearly constant pressure experiments. (Pressure drop from the beginning to the end of the experiment was 2-3%.) The pipe to be tested was placed into the tank through an opening in the floor. Lead weights were hung on the bottom of the pipe to keep it under the water surface at all times. The tank was filled with water to the necessary level and then pressurized with compressed air supplied from compressed air (or nitrogen) bottles (max. pressure 2200 psi (152 bar)). A pressure regulator kept the pressure at the required level. Pressure gages on the feed line provided pressure reading. In addition a pressure transducer, suitably calibrated, was connected to a digital voltmeter and a strip chart recorder provided continuous pressure reading.

For experiments in air the tank (capacity 25 cu ft (.7 cu m)) was pressurized solely by air supplied from pressurized air bottles. Depending on the specific operating pressure, up to four bottles were used to pressurize the tank and the pressurization process could take as long as one hour. At the latter stages of these experiments an air compressor was

added to the system but its maximum pressure was only 250 psi, (17.2 bar). The pressure monitoring system was the same as above.

The pipes were plugged at both ends. In some experiments the pipe was connected to the atmosphere to ensure (nearly) constant pressure experiments. Due to the tank construction it was practically impossible to inflict an imperfection externally in order to start the buckle; as a result an imperfection had to be machined on the pipe, providing a weaker section that could cause local buckling at a predetermined pressure. With careful machining this imperfection could be designed to buckle with an accuracy of $\pm$ 5%. The machined imperfection was usually about 4-5 diameters long (fig. 3.3b), placed about 5-6 diameters from one end. The buckling pressure of the imperfection was calculated using expression 17 from ref. 3.2. In cases where accuracy of more than $\pm$ 5% error was necessary the following technique was used. An 1 in. plug of a lower melting point alloy (melting point 150°F (66° C)) was molded inside the tube under the imperfection. A heating coil was placed around the imperfection as shown in fig. 3.3b. The pressure in the tank was taken up to the required level and kept constant. Current was passed through the heating coil. The plug melted removing the lateral support it was providing to the weakened pipe section, allowing it to locally buckle under the exact external pressure required, thus initiating a buckle. Considering that the process had to be carried out inside the tank with a wet environment it is easy to see that it was a very inefficient process. At the first opportunity the

facility described in section 2.2.1 was built. Due to the design of this facility, it was relatively easy to inflict a damage to the pipe at a specific pressure externally. The details of the design and operation of this facility are explained elsewhere. The experimental efficiency of the dynamic experiments was increased by a factor of 5 and all dynamic experiments apart from the ones described in this section were carried in this improved facility.

The velocity of propagation was measured by means of four strain gages attached externally to the tube at measured intervals. As the propagating buckle passed through the location of a strain gage a large response signal was obtained. In cases where the pipes were immersed in water, a special insulation had to be used to insulate the gages from the water (Micro-measurement M-Coat F). This insulation provided practically no resistance to bending or stretching and it did not affect the smooth propagation of the buckle in any significant way.

The signals were amplified (Astro DATA 810 DC differential amplifiers) and subsequently recorded on a four channel variable speed HP 3100 tape recorder. The recording procedure was as follows. When the pressure was within about 10% of the precalculated buckling pressure of the machined initiator, the instruments were switched on and the recorder started. The pressure was then allowed to rise slowly until buckling of the initiator occurred. This in turn caused a propagating buckle. The tape recorder and chart recorder

were switched off. The exact pressure at which the measurements were taken could be found from the pressure transducer which indicated a sudden drop in pressure in the tank. (When the tube collapses the volume it displaces becomes approximately 30% of its original volume.)

The recorded strain gage signals were played back at 15 times slower speed. The output of the recorder was displayed on a scope as well as on a high frequency response light pen galvanometer chart recorder (up to 80 in/sec paper feed). Through this procedure the time base of the signals could be stretched as much as necessary decreasing the measurement error. The period between two signals was measured and the average velocity between the two points could be calculated. Figure 3.4 shows a typical visicorder output and a schematic of the corresponding tube with the strain gages in place.

Typically, the first of the four strain gages was placed 6-8 diameters downstream of the initiator section. The second and third were at intervals of 2 ft (.15m) apart and the fourth was placed about 15 diameters from the other end plug. Thus, three values of velocity could usually be obtained although in some cases the elastic wave travelling ahead of the buckle, or the buckle itself could shear off one or two of the gages or break one of the electrical connections. In such a case fewer values of velocity were obtained. Usually the velocity obtained from the first two gage signals was taken to be the velocity of propagation. If the pipe interior

was connected to the atmosphere then the three values of velocity were usually within a 5% difference band with the first value being the biggest and the third the smallest (this was mainly due to the decrease in tank pressure caused by the decrease in displaced volume by the tube). In cases where the pipe was not connected to the atmosphere then the internal pressure at the moment the buckle reached the gage could be approximated by

$$P = P_{at}\left[\frac{\pi}{\pi - 2(L_g/L)}\right]^{\gamma}$$

where L = Length of Pipe

L_g = Distance of gage from point of buckle initiation

P_{at} = Atmospheric Pressure

γ = Specific gas constant

(Note: Adiabatic change of state is assumed.)

Thus the internal pressure when the buckle reaches the second gage can be calculated to be about 3 psi higher than the atmospheric pressure. The maximum error produced by this factor in the cases examined was about 3%. However, the error produced to the value of velocity obtained by the third and fourth gages was considerably higher, as a result whenever this value of velocity had to be used corrections had to be made to the pressure to compensate for the above error.

3.2.1 Velocity measurement -- results.

The characteristics of the pipes tested are tabulated in table 3-1. In the first series of experiments the velocity of

propagation was measured as a function of pressure for a constant D/t (= 35.7). This was carried out for both air and water to see the significance of the fluid structure interaction. Figure 3.5 shows the experimental results. The experiments covered the whole range of pressure between the propagation pressure (115.8 psi (10.7 bar)) and the buckling pressure (488 psi (33.7 bar)). Due to inadequacies of the facility used it was not possible to carry out experiments below $P/P_p = 1.05$. This was mainly due to the fact that near P_p, whether an initial dent propagates or not depends heavily on the type of dent inflicted on the pipe. Specifically it was found that diagonally opposite longitudinal dents tend to help the initiation of the buckle as opposed to transverse dents. At pressures above about 435 psi (30 bar) a new mode of propagation was discovered; this has been called the "Flip-Flop" mode of collapse and is discussed in detail in chapter 4.

By examining the time intervals between the different gages along the tube it was established that the buckle, in a relatively short time (6-8 diameters), accelerates to steady state. Provided that all other variables are kept constant, it continues travelling at a constant velocity.

As the results indicate, the velocity is dependent on pressure as well as on the density of the pressurizing medium. The velocity of the propagating buckle in water is less than half of that in air, indicating the considerable importance of the fluid structure interaction problem. The same data have also been plotted against a pressure parameter stemming

from the energy balance calculations that follow. Using this parameter the data fall on a straight line (see fig. 3.6), but the experimental lines fail to go through the origin. The reason for this is still unexplained. Reference 3.1 makes an attempt to calculate the velocity of propagation (details are not presented). The prediction of this reference is plotted on fig. 3.6. Comparing this analysis with the experimental results, the theory is inadequate as it neither predicts the correct pressure dependence nor is it sensitive to pressurizing medium density changes.

Additional results for different D/t are shown in fig. 3.7. It is of interest to note that for thicker pipes the buckle travels faster in both air and water. Note also that the various straight lines are parallel to each other. The dependence of velocity on D/t for constant P/P_p (= 1.7) is shown in fig. 3.8.

During the course of this investigation it was noticed that the length of the strain gage signals varied substantially with velocity. For one series of experiments (specimen 2 of table 3-1) careful measurement of the signal lengths was carried out and the length of the buckle profile was calculated as follows. Referring to fig. 3.4, let the length of a typical signal (usually the average value of the first two gages was taken) be $\hat{T}$ sec. It is known that in T_1 sec. a distance X_1 ft is traveled by the buckle. Thus the length of the profile is given by

$$a = \frac{\hat{T}}{T_1} X_1 \ .$$

It should be noted that the length of the signal depends on the orientation of the buckle with respect to the gage position. Since in these early series of experiments no control was available as to the orientation of the buckle, some of the results had to be disregarded. Figure 3.9 shows a plot of the profile length as calculated vs. a pressure parameter. This pressure parameter is proportional to the velocity (different constants of proportionality for air and water). Although the quantitative value of these results is questionable, qualitatively they indicate that the profile "sharpens" with higher velocity. This conclusion is tested in the next section.

3.3 High Speed Photographic Observation of a Propagating Buckle

Although quasistatic observation of the propagating buckle had been observed both by the author as well as other investigators, no effort had been made to observe a buckle propagating under dynamic conditions. Such an endeavor was worthwhile for a number of reasons. For instance, nothing was really known about the fluid behavior at the buckle front. The possibility of cavitation or other fluid effects required direct observation. The problem of the "flip-flop" mode of collapse needed direct observation in order to verify a theory as to its mechanism. Another problem requiring further experimental examination was the velocity dependance of the length of the profile of the propagating buckle.

For these reasons and others the transparent test facility described earlier was designed and fabricated.

Figure 3.10 represents a schematic of the circuit used to initiate and photograph a propagating buckle. With switches **a** and **b** closed and the knife edge retracted the camera was started. At a prearranged time, t_o, after the camera was started, the microswitch would automatically close, activating the solenoid valve which operated the piston and the knife edge would move down, locally crushing the tube. Thus a buckle would be initiated. The buckle very quickly would accelerate to its steady state condition and enter the camera viewing field at a constant velocity. By this time the camera would be running at the required speed capturing the phenomenon.

From the above description it can be seen that the process required reasonably good timing for a successful experiment. As a result some side experiments had to be carried out to determine the order of magnitude of the time elapsed from the moment of triggering to the moment the buckle entered the camera viewing field. This was done as follows. A microswitch was connected to the pneumatic cylinder and arranged to open when the piston moved 1mm down. This microswitch triggered a scope as well as a counter. A strain gage placed on the pipe in the middle of the camera viewing field gave a signal when the buckle reached that point. This amplified signal was recorded on the scope and triggered off the counter. Thus two measures of the necessary period were obtained. This time was found to be about 40 msec for the specified tube used in the experiments. (Pressure was 180 psi (12.4 bar)). This

time transformed into feet of film had to be taken into consideration when arranging the delay system of the camera in order to obtain the correct framing rate in the period of interest.

Numerous tests were also carried out in order to test the uniformity as well as the amount of light necessary for the photography.

3.3.1 Experimental results.

A total of three films of the propagating buckle were obtained. The main parameters of each experiment are listed in table 3.2, below.

	Pres. Medium	$\frac{P}{P_c}$	$\frac{D}{t}$	Frames/ sec	U ft/sec (m/sec)	$\frac{a}{D}$
1	Water	.878	50	3,250	350 (107)	5
2	Water	.902	50	4,500	372 (113)	5
3	Air	.890	50	11,500	726 (221)	4

TABLE 3.2. EXPERIMENTAL PARAMETERS OF PHOTOGRAPHIC EXPERIMENTS

Two experiments were run with water as a pressurizing medium in order to investigate the possibility of cavitation. Figure 3.11 shows the results of experiment 2. No cavitation is visible. The velocity of propagation was calculated by knowing the width of the viewing field and the frame rate. It should be noted that in the cases where the tank was filled

with water, due to its cylindrical construction the ratio of the two principal magnifications was about 1.5. As a result the linear dimensions of the pipe are disproportionate.

The velocities calculated here are in good agreement with those of fig. 3.7, where direct measurements were made by the strain gage signal method. As far as can be told from such a small viewing section (16 in. wide) the velocity of propagation does not change during the experiment, reinforcing previous results. By carefully looking at the pictures it can be seen that somewhere ahead of the profile the diameter of the pipe is bigger than the undisturbed diameter at the right hand side. This indicates ovalization with major axis perpendicular to that of the buckle. More will be mentioned about this in the next chapter. The film from experiment 1 has nothing to add to the above and is not included.

Figure 3.12 shows the film obtained from experiment 3. This experiment was carried out in air, as a result the velocity is much higher. Again the value of velocity is in good agreement with the value calculated from fig. 3.7. The major axis of the buckle in this case is in the viewing plane. As a result this picture complements the previous one. As can be seen from the figure the profile is much sharper than the one from a quasi-static buckle (see fig. 3.13). The lengths of the profiles are measured in both cases and are tabulated in table 3.2. A difference is noted from air to water. From fig. 4.3 the value of the a/D for the quasi-static case is found to be 7.75. This indicates that the profile length

decreases with velocity. No effort to further quantify this was made.

3.4 Parametric Dependence of the Velocity of Propagation

As established in the experiments a buckle propagating in a constant pressure environment achieves steady state conditions (velocity, U) rather quickly (6 - 8 diameters). It would be useful if the parametric dependence of the velocity could be found. The complete problem involves all the non-linear effects described earlier. An energy balance type of analysis is attempted with the objective of obtaining some useful parametric relationships.

For the purpose of this analysis consider a buckle propagating at velocity U (fig. 3.1). The pipe has a diameter D, a thickness t and is made of a material with a stress-strain behavior that can be approximated by a bilinear one with parameters E, E' and σ_0, these having their usual meaning. The pipe material density is ρ. The surrounding medium is assumed to be inviscid, incompressible and of density ρ_f.

As the buckle propagates with a velocity U, the structure absorbs a certain amount of energy in a given time interval ΔT. During this time the buckle moves forward a distance $U\Delta T$. The energy absorbed by the structure is produced by the work done by the external pressure. In addition to the strain energy going into deforming the structure kinetic energy is important to the structure as well as the surrounding fluid. As energy balance gives a relation between velocity and the other parameters of the problem. The various terms of this

energy balance are discussed below.

As the buckle passes through a given location, the pipe deforms from a circular to a collapsed state (dogbone). If the material is assumed to be rigid-perfectly plastic, then the only characteristic material property is the yield stress σ_0. Assuming that only plastic bending deformations occur, a four hinge mechanism analysis as in section 2.3.1 gives the plastic strain energy absorbed to be

$$W_{PL} \sim \sigma_0 t^2 U\Delta T \quad .$$

This term is appropriate provided that the pipe goes from its original circular shape to a developable shape without stretching and plastic work is confined to the yield hinges. In actuality, stretching and bending of the longitudinal fibers do occur. As a result the plastic work is a function of the length (a) of the buckle profile and the pipe diameter (D). In addition, as shown for the quasistatic case in (2.3.25), the strain energy is also a function of E'/σ_0. The expression can then be written as

$$W_{PL} = \sigma_0 t^2 F_{PL}\left(\frac{D}{t}, \frac{a}{D}, \frac{E'}{\sigma_0}\right) U\Delta T \quad . \qquad (3.1)$$

The pipe wall will be accelerated as the buckle progresses. This imparts a kinetic energy to the pipe which is assumed to be dissipated when the pipe collapses and impacts the other side. The amount of kinetic energy depends upon the shape of the buckle, however the parametric dependence can be expressed as follows:

$$W_{KP} = \rho t^2 U^2 F_{KP}\left(\frac{D}{t}, \frac{a}{D}\right) U\Delta T \quad . \tag{3.2}$$

where ρ is the pipe mass density.

Likewise, energy goes into accelerating the surrounding fluid medium, which is assumed to follow the pipe deformations at all times. It is assumed that the kinetic energy imparted to the fluid is subsequently dissipated. The fluid kinetic energy term then can be written as

$$W_{KF} = \rho_f D^2 U^2 F_{KF}\left(\frac{a}{D}\right) U\Delta T \quad . \tag{3.3}$$

The work done by the surrounding medium consists of the pressure times the change in volume that occurs when the buckle moves $U\Delta T$ forward. This is given by

$$W_{PR} = \tfrac{1}{2} P D^2 U\Delta T \quad . \tag{3.4}$$

The energy balance is then given by:

$$W_{PR} = W_{KF} + W_{KP} + W_{PL} \tag{3.5}$$

(3.1 - 3.4) $\rightarrow$ (3.5) $\Rightarrow$

$$-\sigma_0 t^2 F_{PL} + \tfrac{1}{2} P D^2 = U^2\ \rho t^2 F_{KP} + \rho_f D^2 F_{KP} \quad . \tag{3.6}$$

If the propagation velocity is zero then the pressure is equal to the propagation pressure (P_p).

i.e. $$P_p = 2\sigma_0 F_{PL}\left(\frac{D}{t}, \frac{a}{D}, \frac{E'}{\sigma_0}\right)\left(\frac{t}{D}\right)^2 \quad . \tag{3.7}$$

If the complicating effect of the profile length dependence on velocity is neglected then $\frac{a}{D} = f\left(\frac{D}{t}\right)$. Then from (2.4.1)

and (3.7)

$$F_{PL}\left(\frac{D}{t},\ \frac{a}{D}\left(\frac{D}{t}\right),\ \frac{E'}{\sigma_0}\right) = \tfrac{1}{2}\left[10.7 + 0.54\left(\frac{E'}{\sigma_0}\right)\right]\left(\frac{t}{D}\right)^{2.5} . \quad (3.8)$$

(3.7) → (3.6) ⇒

$$\frac{U}{\sqrt{\frac{\sigma_0}{\rho}}} = \sqrt{\frac{P}{P_p} - 1}\left[\frac{F_{PL}\left(\frac{D}{t},\ \frac{E'}{\sigma_0}\right)}{F_{KP}\left(\frac{D}{t}\right) + \frac{\rho_f}{\rho}\left(\frac{D}{t}\right)^2 F_{KF}\left(\frac{D}{t}\right)}\right]^{\frac{1}{2}} \quad (3.9)$$

The general parametric dependence of the velocity can be seen in (3.9). F_{PL} is given by (3.8). In the case where experiments are carried out in air $\frac{\rho_f}{\rho} \sim 0(10^{-4})$, thus the second term in the denominator can be neglected. In that case an expression for F_{KP} can be obtained by using (3.8) and fig. 3.8.

The proportionality of the velocity to $\sqrt{\frac{P}{P_p} - 1}$ was shown in fig. 3.7, where the experimental results are shown to behave in the predicted way. However, in all cases tested the straight lines failed to pass through the origin, indicating a different behavior for buckles propagating at pressures close to the propagation pressure. Both expression (3.9) as well as the experimental results in fig. 3.7 show the dependence of velocity on the pressurizing medium properties.

3.5 Conclusions

Experiments have shown that a buckle propagating in a constant pressure environment rapidly reaches a constant velocity. The acceleration distance to this steady state was

found to be of the order of 6 - 8 diameters. The parametric dependence of this velocity has been discussed through an energy balance. The velocity has been shown to be proportional to $\sqrt{\frac{P}{p_p} - 1}$. The experimental results showed this proportionality satisfactory over the range of pressure and in the experiment. However, this dependence could not be tested for buckles propagating very close to the propagation pressure. The velocity of propagation has also been shown experimentally to be influenced by the density of the pressurizing medium. For instance, differences of more than a factor of 2 were noticed in velocities of buckles propagating in water and air.

High speed filming of the propagation in water did not reveal (at least for the cases tested) any cavitation occurring during propagation of the buckle. However, it was noticed that the length of the profile of the propagating buckle was velocity dependent.

For buckles initiated at pressures close to the pipe buckling pressure a new mode of collapse and propagation was observed. This is described in detail in the next chapter.

While the analysis and experiments described above do not lead to a conclusive solution of the dynamic problem, they do give the important parametric relations which should help in formulating an analysis of the problem. The completion of this analysis will probably dictate a numerical approach.

4. THE "FLIP-FLOP" MODE OF COLLAPSE

4.1 Introduction

"Flip-Flop" is the name given to a new mode of collapse discovered in the process of carrying out the dynamic propagation experiments described previously. A picture of a pipe which suffered this collapse is shown in fig. 4.1. As can be seen from the figure the pipe underwent a number of changes in the orientation of the collapse mode. The buckle was always initiated by some means at one end of the pipe. Since the pipe was initially undisturbed, the phenomenon was always considered as a change in the mode of propagation. In other words the buckle once initiated starts travelling down the tube until after some distance it changes the orientation of collapse by exactly 90^{o}. It again propagates a certain distance and repeats the change in collapse orientation returning to the mode in which it was originally travelling. The process is repeated a number of times until the end of the pipe is reached.

Early in this investigation Dr. Martin Mikulas* pointed out that when a circular pipe is flattened locally, some distance away from the damaged point ovalization occurs with major axis perpendicular to the major axis of the flattened area. The same effect was noted in a series of papers on the collapse of short tubes under point loads by Reid, Johnson and others (ref. 4.1). Yuan obtained the same effect when examining the problem of point load on an infinitely long

*Visiting Associate in Aeronautics, 1977-78

pipe [4.2, 4.3]. Although Yuan's problem was restricted to small displacement linearized shell theory, ovalization was observed some distance away from the point of load application. The reason for this kind of behavior is thought to be the fact that through such a deformation the local stretching in the tube is minimized.

To examine the magnitude of this ovalization in the plastic deformation regime a series of experiments were carried out, where long tubes were subjected to local deformations by knife edge indentors as shown in fig. 4.2. The deformation of the cylinder along its principal axes was measured carefully for different values of indentation. The procedure was repeated until the two pipe walls were touching at the point of maximum indentation. The results from one of these experiments are shown in exaggerated form in fig. 4.2. At a distance of about four diameters away from the point of indentation, the pipe ovalized with the major axis perpendicular to that of the indentation deformation. The region of ovalization was about five diameters in length with the maximum ovalization occurring about five diameters away from the point of indentation. From the analysis of ref. 4.2 it was found that the length to which ovalization extends, in the elastic, small deformation analysis was much bigger, however, the point of maximum ovalization was almost exactly the same as in the experiment. In light of this and the results of fig. 4.2 it was concluded that the position of maximum ovalization is not highly dependent on the magnitude of deformation.

The same experiments were repeated using an indentor with a different contact diameter. It was found that although the area close to the indentor exhibited different deformations the dimensions of the ovalized region remained unaffected. It was thus concluded that some of these results could be transferred to the case of the Propagating Buckle. A series of experiments were carried out where a buckle was allowed to propagate quasistatically halfway down the pipe and then was stopped. The profiles of the buckles were subsequently measured along the two principal directions. The dimensions of the pipes and the measured results are given in table 4-1. The nominal length of the profile as defined in table 4-1 is plotted vs. D/t in fig. 4.3. These results were be used in calculating the plastic work done during propagation. The maximum imperfection resulting in the ovalized region is plotted against D/t in fig. 4.4. The mean ovalization over the same region is also given in this figure.

As previously mentioned the profile of propagation becomes sharper as the velocity increases. From the simple tests with the different radii indentors it was found that the magnitude of ovalization was independent of the indentor radius. As a result it is assumed that the magnitude of the ovalized region measured from the static experiments is approximately the same as that which occurs in the dynamic case. The mean size of the imperfection induced by the buckle, calculated over a length of three diameters of the affected region, is given in table 4-1 and can be found as a function

of D/t in fig. 4.4. As previously discussed, Timoshenko's simple formula (ref. 4.4) for calculating the buckling pressure of an imperfect ring compares very well with more accurate analysis. Using this criterion for buckling and assuming that the imperfection measured above is of the type $R = R_0 + w_0 \cos 2\theta$ the pressure at which the imperfect section in front of the Propagating Buckle collapses can be calculated. This calculated value is then assumed to be the lowest pressure at which the "Flip-Flop" mode can occur.

"Flip-Flops" were obtained in a number of experiments with two different pipes. The geometric and material parameters of the pipes used are tabulated in table 4.2. The calculated values for the minimum pressure at which flip-flop is predicted to occur (P_{ff}) and pressures at which flip-flops occurred(P^*_{ff}) experimentally are given in the table. All the observed pressures are above the calculated minimum pressure. This criterion was used in order to establish the operating pressure of the experiments that are described next.

4.2 High Speed Photographic Observation of the Formation of a "Flip-Flop"

A theory as to the mechanism of the "Flip-Flop" was described in the preceding section. What follows is an experimental verification of this theory. This was done through high speed photographic observation of a buckle at the instant of "Flip-Flop". The transparent test facility and the photographic technique described in the dynamic experiments were used to observe the phenomenon. In addition to the timing problems described in the dynamic propagation

experiments the problem of calculating the position where a "Flip-Flop" node would occur, a priori, had to be faced. The simple theory described above and the repeatability of experiments made the correct determination of the node position possible.

The same tube used for the other dynamic experiments was used in this case. After initiation the buckle would propagate down the tube, undergo one "Flip-Flop" and then enter the camera viewing field where it would undergo another flip-over. By this time the camera would be running at the required speed, capturing the phenomenon.

Three different successful experiments were carried out where the "Flip-Flop" was photographed. Each has a different framing rate and different degree of clarity and detail.

Figure 4.5 shows a series of pictures obtained at 192 psi and 4000 fr/sec. The pictures were originally 16mm but were cut down and rearranged as shown. The film used was Kodak 2476 with an ASA rating of 200. The quality of the pictures is satisfactory, although some light nonuniformity is present in the pictures. As can be seen, the buckle entered the camera viewing field from left to right. The total width of the viewing field was .4m (16 in). The velocity of the incoming buckle was calculated to be about 241m/s (790 ft/sec). from the first to the fifth frames the severe ovalization in front of the buckle can be observed. The point of maximum ovalization travelled at the same speed as the buckle front and remained in all frames about 5 diameters in front. In the fifth frame the ovalized section became unstable and in the sixth and

seventh frames the collapse of the ovalized region is shown.

The incoming buckle is thus stopped and a new one having its major axis at 90^{o} to the old one starts propagating. Although the phenomenon can be seen clearly from these pictures it was felt necessary to increase the frame rate in order to observe the phenomenon in more detail.

Figure 4.6 shows a more elaborate sequence of pictures obtained in the second experiment. This film was taken at 15,000 fr/sec. The frames were 8mm. The film used was Kodak PAN 2484 with an ASA rating of 800. In spite of the film sensitivity, the light requirement was too high for the sources available. The pipe was coated with a special illuminating coating to help the situation. The light uniformity was carefully checked with a lightmeter but the right hand side of the picture still is under-illuminated. Due to the high film speed the pictures are more grainy. In spite of its imperfections, this sequence of pictures provides far more detail of the event than the previous one. It can, for instance, be seen that the buckle ahead of the node takes some time to accelerate and develop itself into the usual profile of propagation. The velocity of the incoming buckle was calculated to be 259m/s (850 ft/sec). This compares well with that given in fig. 3.7. Due to the more frames available this value of the velocity is more acceptable than the one calculated from fig. 4.5. The mean pressure for this experiment was 192 psi (13.2 bar).

The third picture was taken at 190 psi and 13,000 fr/sec

per second. The film in this case was Eastman 4-X Neg 7224, ASA 400. This film was originally underexposed. An effort was made through photographic tricks to salvage it. The results can be seen in fig. 4.7. The incoming buckle cannot be seen very clearly but a better description of what happens after the ovalized section collapses is shown. The initiation of the new buckle and its development can be seen in a sequence of frames. The time taken for the ovalized section to collapse and for the buckle to progress to its steady state propagation profile can be calculated to be about 400 μsecs or 6-8 diameters distance. After this distance the buckle profile has completely developed and a new section of pipe ovalizes in the opposite direction. This ovalized section is about 4-6 diameters away from the buckle front. Thus it can be concluded that a node will occur every 12-16 diameters. This was indeed the case in as many as six experiments on the same tube, out of which only three were photographically recorded. Figure 4.8 shows a static picture of one of the nodes after the dynamic filming was completed. It can be clearly seen that the two buckles are circumferentially exactly 90^{o} out of phase.

In a separate experiment four strain gages were placed at distances of 6, 7, 8 and 9 diameters away from the knife edge. The knife edge triggered a microswitch with the slightest downward movement. All five signals were recorded. From the gage signals it was found that the velocity of propagation reached a maximum value after about seven

diameters. It was thus confirmed that the profile takes 6-8 diameters to accelerate to its maximum velocity. Although pictures were obtained only for pipes of D/t = 50, the above conclusions can be carried over, with reasonable success, to D/t = 35.7 (the second pipe for which the "Flip-Flop" was obtained).

5. BUCKLE ARREST

5.1 Introduction

In the preceding chapters the emphasis was concentrated in better understanding the problem of the Propagating Buckle and its mechanics. In this chapter an effort is made to look at the problem from a more practical angle. With the results established so far, in mind, it is clear that one way of avoiding the problem completely is to base the design of a pipeline on its propagation pressure (2.4.1). However this is considered wasteful due to the substantial increase in thickness that is required (factor of 2-3). A second way of dealing with the problem is to accept the fact that buckles will always somehow be initiated and look for a method of restricting the damage, that the pipeline suffers, to a minimum. This requires the use of some kind of a buckle arresting device.

Buckle arrestor is the name given to any device which locally reinforces the pipe and prevents the buckle from propagating any further. In their most common design, these devices are installed at regular intervals along the pipeline and if properly designed they restrict the damage to the length ℓ, of pipe, between two arrestors (fig. 5.1). A designer then has to choose a balance between a more economical pipeline and the possibility of damage occurring to a length of pipe ℓ.

Some of the factors that should be considered in deciding the value of ℓ are the total length of the pipe-

line, the diameter, thickness and unit length cost of the pipe, the water depth at which the pipeline is laid, as well as the cost of retraction and replacement of a unit length of damaged pipeline. Table 5.1 gives an example where arrestors were used every 150 m (490 ft.) [5.1].

A number of types of arresting devices have been suggested to date [5.2, 5.3, 5.4]. They vary in shape, cost, ease of application, etc. Reference 5.2 describes a device which is temporarily placed on the inside of the pipe to prevent any local deformation. The device, which operates in a similar way as a "pig", is always kept at a critical distance away from the ship so that it protects the pipeline downstream from its position. The main disadvantage of this device is that it only gives temporary protection to the pipeline as it cannot be left in place during the operation of the pipeline. It is also difficult to use in the case of pipelaying off a reel lay barge, References 5.3 and 5.4 describe devices which are permanently placed on the outside of the pipe. They have the purpose of locally strengthening the pipe by increasing its section modulus so as to prevent a propagating buckle from crossing over the arrestor. Some of these devices are schematically shown in fig. 5.2 (a-d).

The "Slip-On" arrestor is a close fitting ring slipped on the pipe as shown in fig. 5.2-a. The "Grouted" arrestor (fig. 5.2-b) is a similar device but with a gap between the pipe and the arrestor; this is filled with grout--usually

cement. Figure 2-c represents another version of the Slip-On but in this case the ends of the ring are welded to the pipe either all around or in "stitch" form. The "Heavy walled cylinder" arrestor (fig. 5.2-d) consists of a length of pipe having usually the same internal diameter as the pipe but having a thicker section. This is welded between two sections of pipe.

Each of these devices has relative merits and problems associated with its use (ease of application, cost of installation, etc.). However, one common disadvantage of these arrestors is the fact that they are difficult to use in the case of a continuous pipelaying process such as one where the pipe is laid from a shipboard reel onto which the pipeline has been prewound (see fig. 5.1). This is because in such a case no end exists over which the sleeves can be slipped on or to which the heavier sections can be welded. Another disadvantage with these arrestors is that due to their construction, bending stress concentration points can be created during the laying process due to the thickness discontinuity at the end of the arrestor. This can be designed against but at the expense of rather extensive machining.

Figure 5.2-e shows a new arresting device suggested by the authors which due to its design does not have these disadvantages. It is called the "Spiral" arrestor and it can be simply described as a rod closely wound to the pipe for a number of turns and welded at the ends to keep it in

place and prevent it from expanding while a buckle propagating in the pipe is arrested. It can be wound onto the pipe at any stage of the operation (before the pipe is wound onto the reel, during laying before the tensioner and straightener, or after these devices). Due to the relative ease of application it can also be used in laying by traditional lay barges as well as in cases where the pipeline is coated with concrete.

Although arresting devices have been in use for some time now, their design was based on very limited tests. A number of tests have been carried out by investigators at Battelle [Ref. 54] but the parametric dependence of arrestor performance may not have been explored. In what follows an effort is made to improve this situation by putting the problem on the correct basis through dimensional analysis and establishing an experimental methodology for studying the arrestor efficiency. The slip-on and spiral arrestors are studied through this method both under quasistatic as well as dynamic conditions. Empirical expressions for the arrestor efficiency are derived in each case, and these can be used for designing the device.

5.2 The Problem Parameters

The objective of this study is to find the parametric dependence of the arrestor efficiency. The slip-on arrestor will be used as an example for developing the methodology for tackling the problem but the arguments hold true for any arrestor, with the appropriate changes in the parameter in

expression (5.2.4).

A slip-on arrester is a close fitting ring slipped over the pipe with the purpose of arresting an incoming propagating buckle. The goal is to design this ring in an efficient and effective way, given a set of field conditions. Figure 5.3 schematically shows the various parameters of the problem. The pipe is characterized by two critical pressures:

(a) *Propagation Pressure* (P_p): This is defined as the lowest pressure at which an initiated buckle will propagate. From (2.4.1) this expression is given by

$$P_p = \left[10.7 + 0.54 \left(\frac{E'}{\sigma_0}\right)\right] \left(\frac{t}{D}\right)^{2.25} \qquad (5.2.1)$$

(b) *Buckling Pressure* (P_c): This is the pressure at which a long pipe under external pressure becomes unstable (buckles). A classical result for this pressure (for elastic buckling) is

$$P_c = \frac{2E}{(1-\nu^2)} \left(\frac{t}{D}\right)^3 \quad . \qquad (5.2.2)$$

The assembly of pipe and arrestor are characterized by one critical pressure known as the *Crossover Pressure* (P_o). This is defined as the pressure at which an incoming propagating buckle penetrates the arrestor and continues propagating.

An arrestor efficiency is defined and can be used as a basis for comparing the merits of various arrestor designs; it is given by

$$\eta = \frac{P_o/P_p - 1}{P_c/P_p - 1} \quad . \tag{5.2.3}$$

Clearly an arrestor which allows a buckle, propagating at P_p, to go through has an efficiency of zero. On the other hand, one that has a crossover pressure equal to P_c has an efficiency of 1.

It is required that the crossover pressure (and the efficiency) be found as a function of the various parameters of the problem. The problem again involves large deformations in the plastic regime, post-buckling considerations as well as contact area problems. Due to these formidable complications an experimental path was again chosen for analyzing the problem.

If the study is restricted to the quasistatic problem, then all intertial parameters can be neglected, which simplifies the problem. The crossover pressure can then be expressed as

$$P_o = F(P_p, E, \sigma_0, \sigma_0', t, D, L, h),$$

where the parameters in f( ) are considered to be the main parameters of the problem. From Buckingham's π theorem this can be expressed as

$$\frac{P_o}{P_p} = f\left(\frac{E}{\sigma_0}, \frac{\sigma_0'}{\sigma_0}, \frac{D}{t}, \frac{L}{t}, \frac{h}{t}\right) \quad . \tag{5.2.4}$$

If it is assumed that this can be expressed in the form of an infinite power series then,

$$\frac{P_o}{P_p} = \sum_{n=0}^{\infty} A_n \left[\left(\frac{E}{\sigma_0}\right)^{\alpha_1} \left(\frac{\sigma_0'}{\sigma_0}\right)^{\alpha_2} \left(\frac{D}{t}\right)^{\alpha_3} \left(\frac{L}{t}\right)^{\alpha_4} \left(\frac{h}{t}\right)^{\alpha_5} \right]^n . \qquad (5.2.5)$$

From physical considerations $\frac{P_o}{P} \geq 1$, thus $A_o = 1$. If powers of $n \geq 1$ are neglected* then (5.2.5) becomes

$$\frac{P_o}{P_p} = 1 + A_1 \left(\frac{E}{\sigma_0}\right)^{\alpha_1} \left(\frac{\sigma_0'}{\sigma_0}\right)^{\alpha_2} \left(\frac{D}{t}\right)^{\alpha_3} \left(\frac{L}{t}\right)^{\alpha_4} \left(\frac{h}{t}\right)^{\alpha_5} \qquad (5.2.6)$$

(5.2.3), (5.2.6) ⇒

$$\eta = A_1 \left(\frac{E}{\sigma_0}\right)^{\alpha_1} \left(\frac{\sigma_0'}{\sigma_0}\right)^{\alpha_2} \left(\frac{D}{t}\right)^{\alpha_3} \left(\frac{L}{t}\right)^{\alpha_4} \left(\frac{h}{t}\right)^{\alpha_5} \Big/ \left(\frac{P_c}{P_p} - 1\right) \qquad (5.2.7)$$

A series of experiments have been carried out to find the unknown α_i for efficiencies ranging from 0 to 1.

5.3 Experimental Procedure

The experiments were conducted in the same facility described earlier (2.2.1) and shown in fig. 2.1. The transparent section of this facility was also used in order to observe the engagement of the buckle to the arrestor by photographic means.

(a) Quasistatic Experiments

In the case of the quasistatic buckle arrest, control over the speed of propagation was required so the tank was completely filled with water. An air driven piston water pump was used for pressurizing the tank. A buckle was initiated at one end of the pipe and allowed to propagate at

---

*The validity of this assumption will be shown later.

a controlled speed (very small) by monitoring the amount of water pumped into the tank.

For the quasistatic experiments a number of arrestors (4-6) were arranged on 3.66 m (12 ft.) long pipe specimens. Enough distance was allowed between arrestors to avoid interference between them (usually 15-20 diameters). A pressure transducer provided continuous readings of the pressure in the tank. Figure 5.4 shows schematically the output from the transducer for a typical experiment. In order to initiate the propagating buckle the pressure was slowly increase until propagation started from the damaged section of the pipe. The pressure then dropped back to the propagation pressure. On reaching the first arrestor, the buckle was stopped and the pressure increased. At some pressure the buckle suddenly (usually) penetrated the arrestor and continued propagating on the other side of the arrestor at the propagation pressure of the pipe. This continued until the buckle encountered another arrestor. *The highest value of pressure reached in each case was taken to be the Crossover Pressure of the arrestor.* The propagation pressure of each pipe was also recorded.

In the case of the slip-on arrestors, these were machined from solid stock to tolerances of 0.013 mm (0.0005 in.) in the thickness and 0.025 mm (0.001 in.) in the length. Stress-strain curves were obtained for both the pipe and arrestor materials used. The inside diameter of the arrestor was always kept less than 0.051 mm (0.002 in.) larger than

the maximum diameter of the cross section of the pipe. The pipes had typical imperfections in the radius of the order of $\Delta R/R = .006$. Thickness imperfections in the pipe could only be measured in the mean and were taken into consideration. The nominal dimensions of the pipes used are listed in Table 5.2.

(b) Dynamic Experiments

As already shown in Chapter 3, for pressures above the propagation pressure, the buckle travels at substantial velocities. It therefore becomes imperative to examine the influence of the dynamics on the crossover pressure.

The static efficiency of the arrestor was first measured and subsequently tests were carried out to find the efficiency under dynamic conditions. Experiments were carried out both with water and air as the pressurizing medium. In the case of water, the tank was filled with water so the pipe was completely covered. An air gap was left in the tank and the system was pressurized with compressed air. The air gap ensured nearly constant pressure conditions during the experiment (pressure drop from the beginning to the end of the experiment was 2-3%). In the case of the tank being completely filled with air, the drop in the pressure was less than 1%.

In each case a number of pipes were fitted with the same arrestor and tested one by one starting from the static crossover pressure and increasing (or decreasing) the pressure in each case by 0.34-0.69 bar (5-10 psi). At the

desired pressure a buckle was initiated at one end of the pipe and it was observed whether the propagating buckle penetrated the arrestor. The arrestor was placed far enough from the initiation point (20-30 diameters) to ensure that the buckle reach steady state conditions before engaging the arrestor. If the buckle was arrested, a new experiment was conducted with higher pressure. This was repeated until the buckle finally penetrated the arrestor. The dynamic crossover pressure was taken to be the mean between the last pressure at which the buckle was stopped and the pressure at which it penetrated. Thus an error of 0.14-0.34 bar (2-5 psi) or 1-2% is possible in all the recorded dynamic crossover pressures.

5.4 Experimental Results

(a) Quasistatic Results

The first series of experiments was conducted varying the thickness of the arrestor and keeping all other parameters constant. The crossover pressure normalized by the propagation pressure is given as a function of the arrestor thickness normalized by the pipe thickness in fig. 5.5 for the range of pressures from P_p to P_c. It should be noted that once the buckling pressure is reached, the pipe ahead of the arrestor buckles independently, no further increase in the crossover pressure is possible. For this set of experiments an arrestor having a thickness of 3.5 times that of the pipe takes the crossover pressure up to the buckling pressure. Plotting these results on log-

log scales, the power of this parameter is found to be 3. The same results are plotted vs. $(h/t)^3$ in fig. 5.6 and direct proportionality is observed.

A similar set of tests was conducted for arrestors of different yield stresses. Four different values of σ_0'/σ_0 were used. The results are shown in fig. 5.7, vs. $(h/t)^3$. If the same results are plotted vs. the parameters $(\sigma_0'/\sigma_0)\ (h/t)^3$ then the data coalesce to one straight line indicating direct proportionality with the (σ_0'/σ_0) parameter (fig. 5.8).

In another set of experiments, the arrestor length was varied keeping all other parameters constant. Going through the same procedure as above it is found that the unknown power for the (L/t) parameter is 1.5. These results are shown in fig. 5.9.

This set of experiments was repeated for different (D/t). The results are plotted vs. $(L/t)^{1.5}$ in fig. 5.10. Note that if D/t is varied then the maximum crossover pressure (buckling pressure) of each pipe changes. If the ordinate is changed to the arrestor efficiency η and the abscissa to $(t/D)\ (L/t)^{1.5}$ then the results coalesce.

A final set of experiments in this series was carried out with E/σ_0 varied. Tests were carried out with pipes made from:

Al - 6061-T6 ($\sigma_0 = 42.0 \times 10^3$ psi, $E = 10.0 \times 10^6$ psi)

Al - 2024-T3 ($\sigma_0 = 55.0 \times 10^3$ psi, $E = 10.2 \times 10^6$ psi)

SS - 304 ($\sigma_0 = 49.5 \times 10^3$ psi, $E = 27.6 \times 10^6$ psi)

Figure 5.11 shows the results. Since no appreciable difference was observed, it is concluded that the crossover pressure is insensitive to this parameter.

Using the above empirical results the efficiency of a slip-on arrestor can be expressed as

$$\eta = A_1 \left(\frac{\sigma_0'}{\sigma_0}\right) \left(\frac{Lh^3}{Dt^3}\right) \left(\frac{L}{t}\right)^{0.5} \Big/ \left(\frac{P_c}{P_p} - 1\right) \qquad (5.4.1)$$

The results of fig. 5.8 and fig. 5.10 are plotted in fig. 5.12 as a function of this parameter. There exists some scatter in the results which can be attributed to inadequate parametrization, experimental error or other uncontrolled factors. But the proportionality of this parameter to η is quite obvious, indicating that neglecting higher powers of this parameter is acceptable. The results given in ref. 5.4 are within this scatter band for $\eta \leq 0.5$ but show considerable disparity for higher efficiencies.

(b) Dynamic Results

The results from these sets of experiments are tabulated in Table 5.3. For each pipe (D/t = 35.7 and 50.0) arrestors of three different static crossover pressures were tested. Each one was tested both in air and in water. The normalized static and dynamic crossover pressures as well as the static and dynamic arrestor efficiencies are tabulated. The velocity at which the buckle was travelling on engaging the arrestor was found from fig. 3.7. For both the air and water experiments, the dynamic crossover pressure was higher than the static one. (As a result $\eta_{Dy} > \eta_{St}$.) The dynamic

vs. the static arrestor efficiencies are plotted on fig. 5.13, for both air and water. Comparing the results for the same arrestor in air and in water, one notes that the increase in efficiency is higher for buckles travelling in air; this difference being quite substantial in some cases. It should be noted that buckles travel much faster in air than in water. The increase in arrestor efficiency is much higher for the higher arrestor efficiencies. For low efficiency arrestors ($\eta_{St} < 0.4$) very small difference was noted.

In previous work on dynamic arrest (ref. 5.4) it was reported that there was very small difference between the dynamic and static crossover pressures. Since the work of ref. 5.4 was carried out with low efficiency arrestors, this is consistent with the present results. However, for high efficiency arrestors, considerable difference exists between dynamic and static crossover pressures for the slip-on arrestor.

Figure 5.14 shows a statically and a dynamically arrested buckle. In the dynamic case, the buckle, which propagates in a dogbone cross section if unrestricted, penetrated the arrestor much further and tried to push its way through the arrestor in a doubly symmetric mode. Figure 5.15 shows buckles that penetrated the arrestors statically and dynamically. Without the inertial effects the buckle usually penetrates in a U-shaped mode (single symmetry mode). In the dynamic case this becomes impossible due to the deep penetration of the doubly symmetric mode and a completely

different mode results for which a higher pressure is necessary. These observations are restricted to the slip-on arrestor. Whether inertial effects have the same effect on other arrestor configurations has not been investigated.

It should be noted that for both the quasistatic and dynamic cases a second mode of penetration exists. It is shown on fig. 5.15c. It has been called the Flip-Flop mode of penetration due to its resemblance to the Flip-Flop mode of collapse. Like the Flip-Flop mode of collapse it occurs for pressures very close to the buckling pressure of the pipe. In such a case a small ovalization occurs ahead of the arrestor once the buckle is arrested. The axis of ovalization is at 90^{o} to the axis of propagation and if the pressure is high enough this is enough imperfection to cause the pipe to buckle locally.

(c) Gap Effects

In comparing some of the results of ref. 5.4 with the ones presented above, it was found that considerable difference existed in the case of arrestors of efficiency larger than 0.75. Although some relatively large sized arrestors (which relative to the pipe could almost be considered rigid) were used, no arrestor reported in this reference had an efficiency of 1.0. This indicated that there existed an upper limit to the arrestor efficiency which was completely independent of the arrestor dimensions. This is contrary to the results presented above. In an effort to investigate the reason for this disagreement, an additional

series of experiments were carried out which included a gap between the arrestor and the pipe. In each case the bending rigidity of the arrestors was kept constant (EI = const.) but the gap was varied. The results of these experiments are shown in fig. 5.16. Five different arrestor sizes were tested. In all cases the gap size affected the crossover pressure. The effect was more pronounced in the cases of arrestors with higher efficiency. Cross plotting from fig. 5.16 the effect of gap size on the crossover pressure can be obtained (fig. 5.17). Please note that these results hold only in the case examined and should not be used for design purposes. In the light of these results it is thought that the gap size may be the main reason for disagreement between the results presented here and in ref. 5.4.

It should be pointed out that as pipes are inherently imperfect gaps will always exist for this type of arrestor. Careful manufacturing of the arrestor can minimize the problems but this will remain a definite disadvantage for this arrestor.

5.5 The "Spiral" Buckle Arrestor

As already mentioned, the spiral arrestor consists of a rod wound tightly and closely onto the pipe to form a number of turns. The ends of the rod are secured, as by welding, to the pipe (fig. 5.18a) to the rod itself (fig. 5.18b) or to the rod and pipe simultaneously, thus forming an obstacle which a propagating buckle must overcome. The turns may also be individual and unconnected (fig. 5.18c). Due to

the relatively small bending rigidity the device has, in the pipe's longitudinal direction, the pipe can be bent to relatively small radii without any arrestor induced restriction. Thus the arrestor can be applied before the pipe is wound onto the reel or at any stage during the laying operation. The latter can be achieved since this device does not require a free pipeline end for installation. In the case of the traditional section by section laying process, the arrestor can be prewound on some of these sections which can be welded in place at the required intervals. If the pipe has to be coated with concrete then the arrestor can be placed underneath the concrete as shown in fig. 5.19, thus providing a smooth outside surface which can be important for the tensioner. If the pipe does not have a concrete coating but some kind of corrosion coating instead, then the arrestor can be placed after the coating and it can also be coated.

The arrestor rod can be of any cross sectional shape although shapes maximizing the bending rigidity of the cross section of the rod should be preferred as they are more efficient. Some possible cross sectional configurations are shown in fig. 5.20. Of these, the circular cross section is considered the easiest and most economical to use. This was therefore chosen to carry out a series of experiments to verify the effectiveness of the arrestor and obtain some design specifications.

5.5.1 Parametric Study of the Spiral Arrestor Efficiency

As in the case of the slip-on arrestor, the experimental path is again followed in order to parametrize the arrestor efficiency. The methodology established in Section 5.2 will be used here as well. The crossover pressure can be written as

$$\frac{P_o}{P_p} = \left(\frac{E}{\sigma_0}, \frac{\sigma_0'}{\sigma_0}, \frac{D}{t}, \frac{h}{t}, \frac{L}{t}, N \right) , \qquad (5.5.1)$$

where the symbols are as defined in fig. 5.2.1. According to 5.2.5-5.2.7 the efficiency can then be approximated by

$$\eta = A_1 \left(\frac{E}{\sigma_0}\right)^{\alpha_1} \left(\frac{\sigma_0'}{\sigma_0}\right)^{\alpha_2} \left(\frac{D}{t}\right)^{\alpha_3} \left(\frac{L}{t}\right)^{\alpha_4} \left(N\right)^{\alpha_5} \left(\frac{h}{t}\right)^{\alpha_6} \Big/ \left[\frac{P_c}{P_p} - 1\right] . \qquad (5.5.2)$$

A_1 (a constant) together with the unknown powers α_i have to be found experimentally.

The experimental procedure was the same as for the slip-on arrestor. One of the parameters shown to be important in the case of the slip-on arrestor was the gap between the arrestor and the pipe. Care was taken to avoid this by applying some tension to the rod during the winding process, thus making sure of good contact. From preliminary experiments it was found that the way the end of the rod was welded did not have an effect on the crossover pressure. On the other hand welding it to the pipe sometimes caused breakage of the weld when it was forced to follow the large deformation through which the pipe undergoes as it buckles. Because of these reasons the ends of the rod were usually welded to the

last complete turn of the spiral. This technique was used in all experiments.

All the pipes used were Aℓ-D-6061-T6. Four different thicknesses of drawn rod were specially made and used, having the same material properties (same grade and heat treatment).

For the slip-on arrestor it has been shown that the quasistatic efficiency underestimates the efficiency under dynamic conditions. A number of tests were conducted in order to test the validity of such an assumption as far as the spiral arrestor is concerned. Exactly the same behavior was observed for all experiments. As a result, further work on the subject was not considered necessary and the quasistatic crossover pressures for the spiral arrestor are considered to be conservative for the dynamic conditions.

5.5.2 Experimental Results

Figure 5.22 shows a spiral arrestor stopping a buckle and fig. 5.33 shows a buckle that was forced through the arrestor. As in the case of the slip-on arrestor, the mode of penetration is usually the U-type mode. For low efficiency arrestors the arrestor usually follows the contour of the flattened pipe and for arrestors with efficiency close to 1 the flip-flop mode of penetration described in chapter 4 was observed.

In the first series of experiments all the parameters were kept constant and the pitch of the arrestor winding was varied. It was found that the closer the winding, the

greater the efficiency. As a result, all further experiments were wound with no spacing between each turn. In this case the arrestor length L is equal to Nh and the fifth parameter in 5.5.1 is a product of the fourth and sixth, i.e., it is no longer an independent quantity; it can thus be dropped from 5.5.2. Figure 5.24 shows how the crossover pressure of a specific arrestor was affected by the arrestor's pitch. It is considered safe to generalize the result and say that the drop in efficiency is small (less than 10%) if the pitch is kept less than half of the rod diameter.

In the next experiment the number of turns (N) in an arrestor was varied with all other parameters constant. The results are shown in fig. 5.25, from which the crossover pressure (and the efficiency) is shown to be directly proportional to N (thus $\alpha_5 = 1$).

In another experiment the rod diameter (h) was varied. The results appropriately plotted in fig. 5.26 indicate that $\alpha_6 = 3$. It should be noted that this value is in agreement with that found for the power of the corresponding thickness parameter (h/t) of the slip-on arrestor.

From the tests discussed so far it is clear that a great similarity exists between the behavior of the slip-on and the spiral arrestors. The method of resisting penetration and the mechanism of the crossover are much the same. In fact the spiral arrestor can be considered as a series of narrow slip-on rings slipped onto the pipe with no spacing between them (in our case). Due to these similarities between the

two arrestors it was considered reasonable to expect the dependence of the efficiency D/t, E/σ_0 and σ_0'/σ_0 expression (5.5.2) to be the same as in the corresponding expression for the slip-on arrestor (5.2.7). With this assumption $\alpha_1 = 0$, $\alpha_2 = 1$ and $\alpha_3 = -1$.

Accepting the above values of α_i all the experimental results are plotted on an efficiency vs. parameter plot in fig. 5.27. The results thus plotted exhibit a linear behavior indicating that the assumptions made in the dimensional analysis in (5.2.6) were reasonable. Some scatter in the results is present and can be attributed to possible small differences in the material behavior of each tube, differences in the tension that was applied in winding the different arrestors and differences in the size and orientation, with respect to the buckle direction, of the end welds. However the scatter is acceptable for design purposes.

Like the slip-on arrestor, this arrestor's performance exhibits a bifurcation behavior when the crossover pressure reaches the buckling pressure. Any further reinforcement of the arrestor above this pressure does not help because the pipe buckles in front of the arrestor independently.

5.6 Conclusions

A relatively extensive parametric study of the crossover pressure and efficiency of the slip-on arrestor has been carried out. A new arrestor design termed the spiral arrestor has been suggested and was shown to behave in very

much the same way as the slip-on arrestor. It has the advantage of not restricting the pipe in longitudinal bending. In addition, this device can be used in continuous pipelaying operations such as the case of pipelaying off a reel.

Empirical design formulas have been derived for both these devices. The empirical method established can very easily be used for testing other arrestor designs as well. It has been shown that with careful design arrestor efficiency of 100% can be achieved. Any gap between the arrestor and the pipe was shown to decrease the arrestor efficiency. Finally, for these two types of arrestors, quasistatic design criteria always underestimate the arrestor efficiencies under dynamic conditions.

It should be noted that for each pipe a limit pressure exists above which a buckle will always penetrate a rigid infinitely long arrestor. For the materials considered this pressure was always higher than the pipe buckling pressure. However, it is possible that with the right choice of pipe material this maximum efficiency pressure may be lower than the buckling pressure. In such a case arrestors cannot achieve an efficiency, as defined by (5.2.3), of 100%. The parametric dependence of this limit pressure still remains to be found.

REFERENCES

1.1 Brown, R.J. "New Technology Reduces Deepwater Construction Cost", Pipe Line Industry, July 1979, pp. 39-42.

1.2 Powers, J.T. and Finn, L.D. "Stress Analysis of Offshore Pipelines During Installation". Proceedings Offshore Technology Conference, OTC 1071, 1969.

1.3 Palmer A.C., Hutchinson, G. and Ells, J.W. "Configuration of Submarine Pipelines During Laying Operations", Journal of Engineering for Industry, TASME, 1974.

1.4 Palmer A.C. "Analysis and Behavior of Pipelines During Installation", BOSS, 1976.

1.5 Pedersen, P.T. "Equilibrium of Offshore Cables and Pipelines During Laying", The Danish Center of Applied Mathematics and Mechanics, Re. No. 80, February 1975.

1.6 Azar, J.J. and Randolph, V. "Deep Water Pipe-Lay Stresses". Presented at the Pressure Venel and Piping Conference (ASME), Mexico City, September 1976.

1.7 Kunzi, R.E. and Uyeda, S. "Apache: First Dynamically Positioned Vertical Reel Pipelay Ship", Ocean Industry, August 1979, pp. 47-49.

1.8 Meyer, R.A. "Ocean Thermal Energy Conversion Will Be Tested Off Hawaii", Ocean Industry, November 1978, pp. 40-44.

1.9 Mayer, A.J. "Proper Sizing Prevents Ice From Squeezing Off Plastic Inserts", Pipe Line Industry, December 1977, pp. 51-54.

1.10 Mesloh, R.E., Sorenson, J.E. and Atterbury, T.J. Battelle-Columbus Laboratories "Buckling and Offshore Pipelines", Gas Magazine, July 1973, Vol. 7, pp. 40-43.

1.11 "Battelle to Research Problems of Laying Offshore Gas, Oil Lines", Pipe Line Industry, December 1979, p. 59.

1.12 Palmer, A.C. "Buckle Propagation in Submarine Pipelines", Nature, Vol. 254, No. 5495, pp. 46-48, March 6, 1975.

1.13 Mesloh, R., Johns, T.G. and Sorenson, J.E. Battelle-Columbus Laboratories "The Propagating Buckle", BOSS 76, Proceedings, Vol. 1, pp. 787-797.

1.14 "Diver Operated Dredging Unit", Ocean Industry, July 1979, p. 75.

1.15 "Pipeline Trenching Burial Tool", Ocean Industry, December 1978, p. 63.

1.16 Mousselli, A.H. "Pipe Stresses at the Seabed During Installation and Trenching Operations", OTC 2965, Proceedings 1977, pp. 55-62.

1.17 Brown, R.J. "Pipelines Can be Designed to Resist Impact From Dragging Anchors and Fishing Boards", OTC 1570, Proceedings 1972, pp. 579-86.

1.18 Gerard, G. "Plastic Stability Theory of Thin Shells", J. of Aeronautical Sciences, April 1957, Vol. 24, pp. 269-274.

2.1 Mesloh, R., Johns, T.E., Sorenson, J.E. "The Propagating Buckle", BOSS, 1976.

2.2 Remseth, S.N., Holthe, K., Bergan, P.G. and Holland, I. "Tube Buckling Analysis by the Finite Element Method", Finite Elements in Nonlinear Mechanics TAPIR, TRONDHEIM, 1978, pp. 676-694.

2.3 Greenberg, H.J. and Prager, W. "Limit Design of Beams and Frames", Trans. ASCE, Vol. 117, p. 447, 1952.

2.4 Prager, W. "An Introduction to Plasticity", Addison-Wesley, 1959.

2.5 Drucker, D.C., Prager, W. and Greenberg, H.J. "Extended Limit Design Theorems for Continuous Media", Quart. of Appl. Math., Vol. IX, 1951, p. 381.

2.6 Lentini, M. and Pereyra, V. "An Adaptive Finite Difference Solver for Nonlinear Two-Point Boundary Value Problems with Mild Boundary Layers", SIAM, J. Numerical Analysis, 14, pp. 91-111, 1977.

2.7 Timoshenko, S. "Working Stresses for Column and Thin-Walled Structures", Trans. ASME, Applied Mechanics Division, Vol. 1, pp. 173-183, 1933.

2.8 Tadjbakhsh, I. and Odeh, F. "Equilibrium States of Elastic Rings", Journal of Mathematical Analysis and Application, 18, pp. 59-74, 1967.

2.9 Sills, L.B. and Budiansky, B. "Postbuckling Ring Analysis". Brief Notes. Transactions of the ASME Journal of Applied Mechanics, Vol. 45, March 1979, p. 208.

2.10 Rehfield, L.W. "Initial Post Buckling of Circular Rings Under Pressure Loads", AIAA Journal, Vol. 10, 1975, pp. 1358-1359.

2.11 Arbocz, J. "On the Problem of Limit Point Calculations",

3.1 Mesloh, R., Johns, T.G., Sorenson, J.E. "The Propagating Buckle", Battelle, Columbus, Ohio. BOSS 76, Proceedings, Vol. 1.

3.2 NASA SP-8007. "Buckling of Thin-Walled Circular Cylinders", Sept. 1965, Revised Aug. 1968.

4.1 Reid, S.R., Johnson, W., Watson, A.R. "Large Deformations of Thin-Walled Circular Tubes Under Transverse Loading", I, II, III, Intern. Journal of Mech. Science, 1976.

4.2 Yuan, Shau Wen, "Thin Cylindrical Shells Subjected to Concentrated Loads", Quarterly of Applied Mathematics, Vol. 4, No. 1, 1946, pp. 13-26.

4.3 Yuan, S.W. and Ting, L. "On Radial Deflections of a Cylinder Subjected to Equal and Opposite Concentrated Radial Loads", J. of Appl. Mech., Vol. , 1957, pp. 278-282.

4.4 Timoshenko, S. "Working Stresses for Columns and Thin Walled Structures", Trans. ASME, Applied Mechanics Division, Vol. 1, pp. 173-183, 1933.

5.1 Hayes, D.J. and Lux, M.D. "Full Scale Crack Arrest Test and Arrestor Device Performance for the Flags Gas Line", SPE 8220, 54th Annual Fall Technical Conference and Exhibition of the SPE of AIME, Sept. 1979.

5.2 Lochridge, J.C. and Gibson, T.L. "Method of Arresting the Propagation of a Buckle in a Pipeline", U.S. Patent

3,747,356, July 24, 1973.

5.3 Broussard, D.E., Ayers, R.R. and Walker, Jr., G.E. "Mitigation of Propagating Collapse Failures in Pipelines due to External Load", U.S. Patent 3,768,269, Oct. 30, 1973.

5.4 Johns, T.G., Mesloh, R.E. and Sorenson, J.E. "Propagating Buckle Arrestors for Offshore Pipelines", OTC 2680, May 1976.

5.5 Ives, Jr., G., Construction Editor, Pipe Line Industry, "Loop Construction Program on Schedule for 1980 Start-up", Pipe Line Industry, Oct. 1979, pp. 35-37.

5.6 "Mediterranean Sea Gas Line Crossing Under Construction", Pipeline Industry, Nov. 1979, pp. 80-87.

5.7 Lallier, L. and Tegon, A. Total Oil Marine, "A Technical Review of the Frigg Pipelines Construction", OTC 2915, 1976, pp. 303-314.

5.8 Walker D.B.L., B.P. "A Technical Review of the Forties Field Submarine Pipeline", OTC 2603, 1976, pp. 819-829.

APPENDIX A

Moment-Curvature Relationship

Thin Inextentional Ring

The stress-strain curve assumed is shown in fig. A.1. Consider a section of a curved ring as shown below. The ring is assumed to have unit length.

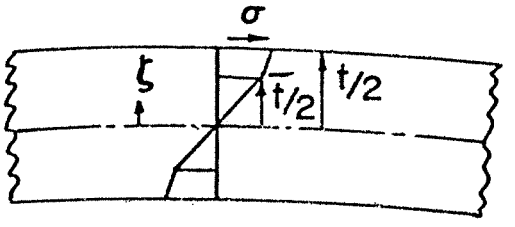

FIG. A.1 RING SECTION

Strain-displacement

$$\varepsilon = \zeta\left(\frac{d\theta_0}{ds} - \frac{d\theta}{ds}\right) = \zeta\kappa \qquad \kappa = \frac{d\theta_0}{ds} - \frac{d\theta}{ds} \tag{A.1}$$

θ and s are as defined in fig. 2.14.

Stress-strain

Only one stress and one strain are present in the problem.

For $|\zeta| \leq \bar{t}/2$ $\qquad \sigma = \zeta E\kappa$

(A.2)

$$\bar{t}/2 \leq |\bar{\zeta}| \leq t/2 \qquad \sigma = \sigma_0 + E'(\varepsilon - \varepsilon_0) = \alpha\left(1 - \frac{1}{\alpha}\right) + \frac{E}{\alpha}\zeta\kappa$$

Moment-curvature

$$M = 2\left\{\int_0^{\bar{t}/2} E\zeta\kappa\, d\zeta + \int_{\bar{t}/2}^{t/2}\left[\sigma_0\left(1 - \frac{1}{\alpha}\right)\zeta + \frac{E}{\alpha}\zeta^2\kappa\right] d\zeta\right\} \tag{A.3}$$

Define $\qquad \kappa_0 = \frac{2\sigma_0}{Et} \qquad \kappa = \frac{2\sigma_0}{E\bar{t}} \qquad \Rightarrow \qquad \frac{\bar{t}}{t} = \frac{\kappa_0}{\kappa}$ (A.4)

$$(A.4) \rightarrow (A.3) \Rightarrow M = \frac{\sigma_0 t^2}{6}\left[\frac{1}{\alpha}\left(\frac{\kappa}{\kappa_0}\right) - \frac{1}{2}\left(1 - \frac{1}{\alpha}\right)\left(\frac{\kappa_0}{\kappa}\right)^2 + \frac{3}{2}\left(1 - \frac{1}{\alpha}\right)\right]$$

APPENDIX B

Calculation of Initial Vector $\underline{u}^{(0)}$

The problem of the response of a circular ring with an initial imperfection under external pressure was solved by Timoshenko in ref. 2.7. His analysis of course is restricted to small deflections and linearly elastic solids. In the notation of chapter 2 for the elastic case the moment at any point is given by

$$\overline{M} = - \frac{4}{\pi^2} Q \left(\frac{w_0}{R}\right) \left(\frac{1}{1 - P/P_c}\right) \cos \pi s \quad . \qquad (B.1)$$

Looking at the equilibrium of a quadrant of the ring the forces H and V can be derived as follows:

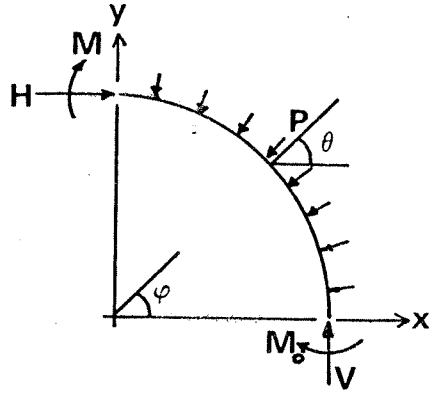

For small deflections $\theta \simeq \phi$ and

$$\left.\begin{aligned} H &= - PR \sin \theta \\ V &= PR \cos \theta \end{aligned}\right\} \qquad (B.2)$$

or

$$\left.\begin{aligned} \overline{H} &= - \frac{2}{\pi} Q \sin \frac{\pi}{2} s \\ \overline{V} &= \frac{2}{\pi} Q \cos \frac{\pi}{2} s \end{aligned}\right\} \qquad (B.3)$$

Thus, the inital guess $\underline{u}^{(0)}$ is given by:

$$\underline{u}^{(0)} = \begin{Bmatrix} \overline{H}^{(0)} \\ \overline{N}^{(0)} \\ \overline{M}^{(0)} \\ \theta^{(0)} \end{Bmatrix} = \begin{Bmatrix} -\frac{2}{\pi} Q \sin \frac{\pi}{2} s \\ \frac{2}{\pi} Q \cos \frac{\pi}{2} s \\ \frac{\pi}{2} s \\ -\frac{4}{\pi^2} Q \left(\frac{w_0}{R}\right) \left(\frac{1}{1 - P/P_c}\right) \cos \pi s \end{Bmatrix} \quad \text{(B.4)}$$

$0 \leq s \leq 1$

APPENDIX C

Calculation of Strain Energy in Buckle Profile

Consider the kinematically admissible assumed geometry for the buckle front shown in fig. C.1. The strain energy required (gone to plastically deform the pipe) for the buckle to move a unit length forward can be separated into three categories as follows:

(I) Strain energy due to circumferential bending.

Four hinges are placed on the pipe's circumference as shown below. The ring quadrants between the hinges are made rigid. The moment in the hinges is assumed to be

$$M_0 = \frac{\sigma_0 t^2}{4} \frac{1}{(1 - \nu'^2)} \qquad \text{(C-1)}$$

For perfectly plastic material $\nu' = 1/2$, thus (1) $\Rightarrow$

$$M = \frac{\sigma_0 t^2}{3} \qquad \text{(C-2)}$$

The strain energy required to take a unit length of the pipe from the undisturbed to the collapsed configuration can be found to be

$$U_{BC} = 8M_0\frac{\pi}{4} = \frac{2}{3}\pi\sigma_0 t^2 \qquad \text{(C-3)}$$

(II) Strain energy due to longitudinal fiber bending.

(a) Region A

Consider first region A as shown in fig. C.2 (note that there are two of these). Assume that its geometry is given by:

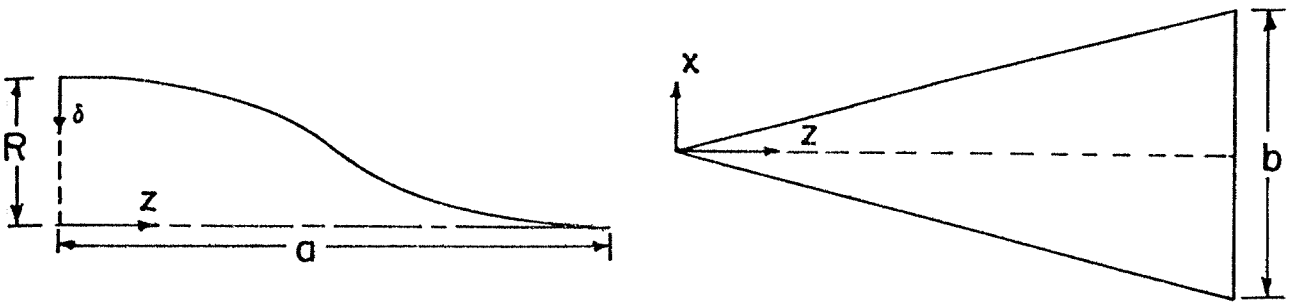

FIG. C.2 ASSUMED GEOMETRY OF REGION A.

where $$\frac{\delta}{\delta_0} = \frac{1}{2}\left(\cos\frac{z\pi}{a} - 1\right) \qquad \text{(C-4)}$$

Then the elemental longitudinal bending strain energy, ΔU_{BLA} is given by

$$\Delta U_{BLA} = M_0 \frac{d^2\delta}{dz^2}\, dz \quad .$$

Thus

$$U_{BLA} = \int_{-\frac{bz}{2a}}^{\frac{bz}{2a}} \int_{o}^{a} dx\, M_0 \frac{d^2\delta}{dz}\, dz = \frac{b\delta_0}{a} M \quad . \qquad \text{(C-5)}$$

But

$$\delta_0 = R \;,\quad b = \pi R \;,\quad M_0 = \frac{\sigma_0 t^2}{4} \quad . \qquad \text{(C-6)}$$

Thus, strain energy per unit length is given by

$$U_{BLA} = \frac{\pi}{2}\left(\frac{R}{a}\right)^2 t^2 / \text{ unit pipe length} \qquad \text{(C-7)}$$

(b) Region B.

Let the geometry of region B be as follows:

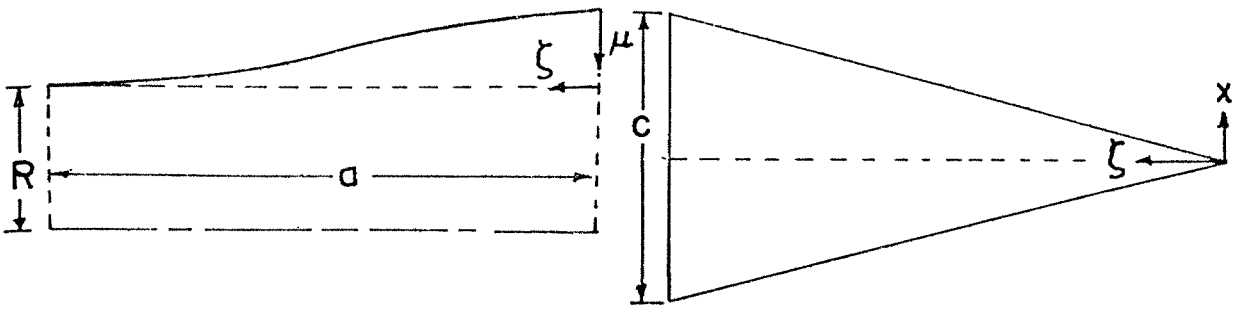

FIG. C.3 ASSUMED GEOMETRY OF REGION B

where $\frac{\mu}{\mu_0} = \frac{1}{2}\left(\cos\frac{\zeta\pi}{a} - 1\right)$

In a similar manner as region A the bending strain energy is given by

$$U_{BLB} = \int_{-\frac{C\zeta}{2a}}^{\frac{C\zeta}{2a}} dx \int_0^a M_0 \frac{d^2\zeta}{d\zeta^2}\, d\zeta = \frac{CM_0}{a} M_0 \quad , \qquad \text{(C-9)}$$

Where $\zeta_0 = (\sqrt{2}-1)\, R \equiv \gamma R$, $M_0 = \frac{\sigma_0 t^2}{4}$, $C = \pi R$. (C-10)

Thus the strain energy is given by

$$U_{BLB} = \frac{\pi\gamma}{2}\frac{R^2}{a}\sigma_0 t^2 / \text{ unit pipe length} \qquad \text{(C-10)}$$

(III) Strain energy due to longitudinal membrane stretching.

Again assume that the strain in each region is equal to that of the longest fiber of that region.

(a) Region A

Let the deformed length of the biggest longitudinal fiber be a' then from fig. C.2.

$$a' = \int_0^a 1 + \frac{1}{2}\left(\frac{d\delta}{dz}\right)^2 dz \qquad \text{(C-12)}$$

(C-4) → (C-12) ⇒

$$\varepsilon_A = \frac{a' - a}{a} = \frac{1}{4}\left(\frac{\delta_0 \pi}{2a}\right)^2 \qquad \text{(C-13)}$$

Thus the stretching energy/unit pipe length is given by

$$U_{SLA} = \frac{2}{a}\left[\mathscr{A}_A \sigma_0 \varepsilon_A t\right]$$

$$\mathscr{A}_A = \frac{\pi R a}{2} \quad , \quad \delta_0 = R \qquad \text{(C-14)}$$

$$U_{SLA} = \frac{\pi^3}{16}\left(\frac{R}{a}\right)^2 \sigma_0 R t/\text{unit pipe length}. \qquad \text{(C-15)}$$

(b) Region B

In a similar manner

$$U_{SLB} = \frac{2}{a}\left[\mathscr{A}_B \sigma_0 \varepsilon_B t\right] \qquad \text{(C-16)}$$

Where $\mathscr{A}_B = \pi R a$, $\varepsilon_B = \frac{1}{4}\left(\frac{\zeta_0 \pi}{2a}\right)^2$, $\zeta_0 = (\sqrt{2}-1)\, R \equiv \gamma R$ (C-17)

(C-17) → (C-16) ⇒

$$U_{SLB} = \frac{\pi^3}{16}\gamma^2\left(\frac{R}{a}\right)^2 \sigma_0 R t/\text{unit pipe length}. \qquad \text{(C-18)}$$

Thus the total strain energy per unit length of pipe flattened is given by

$$U = U_{BC} + \left[U_{BLA} + U_{BLB}\right] + \left[U_{SLA} + U_{SLB}\right]$$

(C-3), (C-7), (C-11), (C-15), (C-18) → (C-19) ⇒

$$\boxed{U = \frac{2}{3}\pi\sigma_0 t^2 + (1+\gamma)\frac{\pi}{2}\left(\frac{R}{a}\right)^2 \sigma_0 t^2 + (1+\gamma^2)\frac{\pi^3}{16}\left(\frac{R}{a}\right)^2 \sigma_0 R t}$$

$$\gamma = \sqrt{2} - 1 \qquad \text{(C-20)}$$

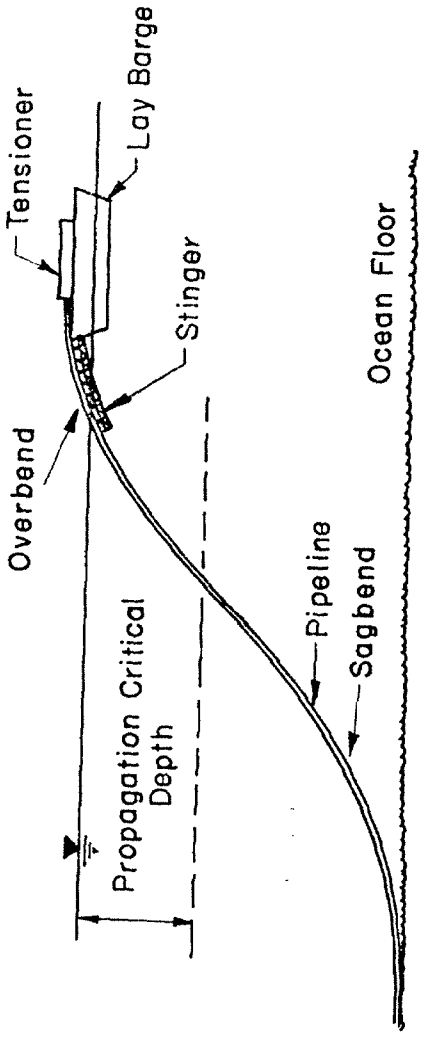

FIG.1.1 PIPELINE LAYING OPERATION

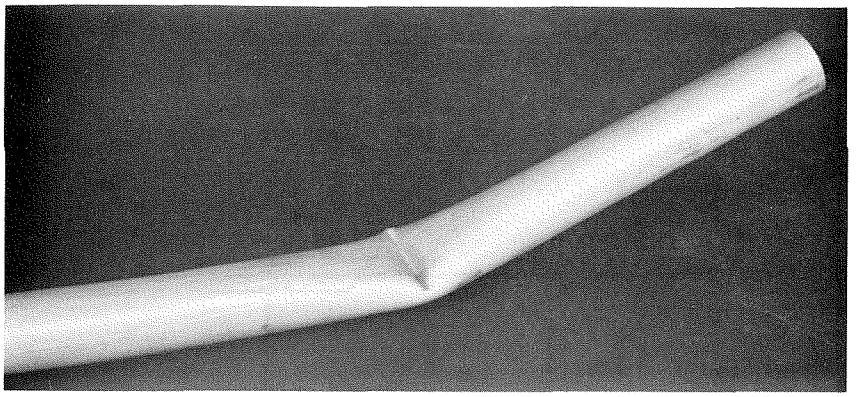

(a) Bending buckle on pipe (Aℓ) with D/t=35.7.

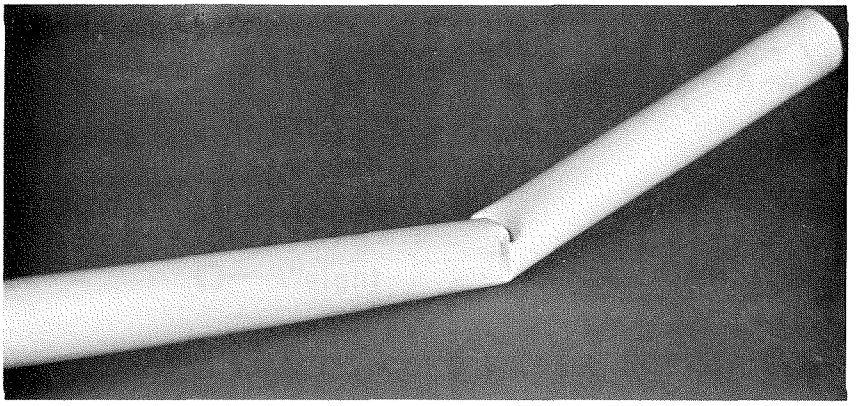

(b) Diamond bending buckle on pipe (Aℓ) with D/t=39.3

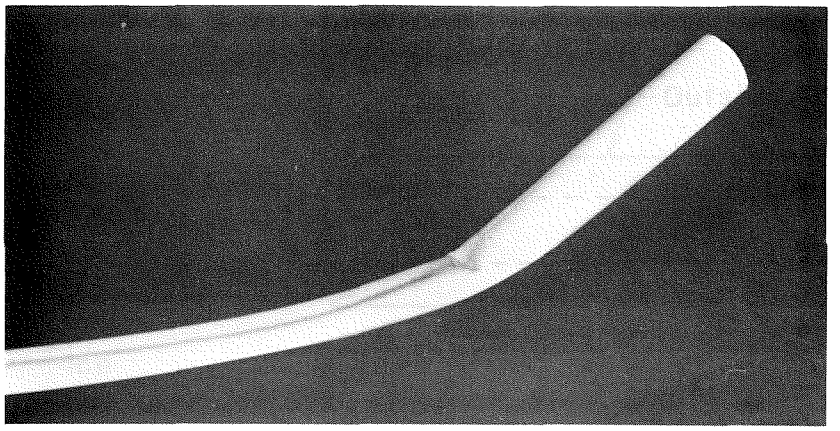

(c) Bending buckle initiated a propagating one.

FIG. 1.2 BENDING BUCKLES.

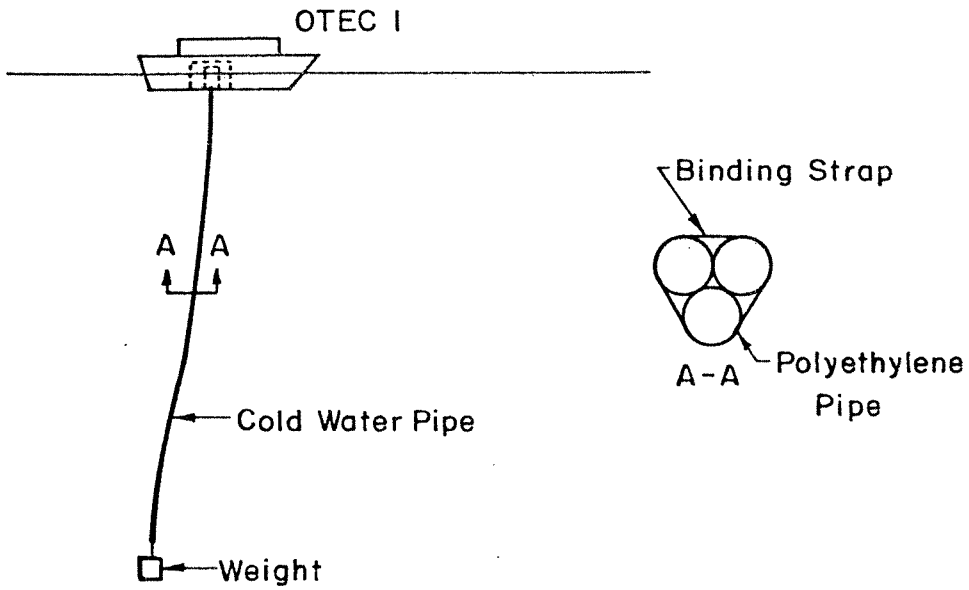

FIG. I.3 OTEC COLD WATER SUPPLY SYSTEM

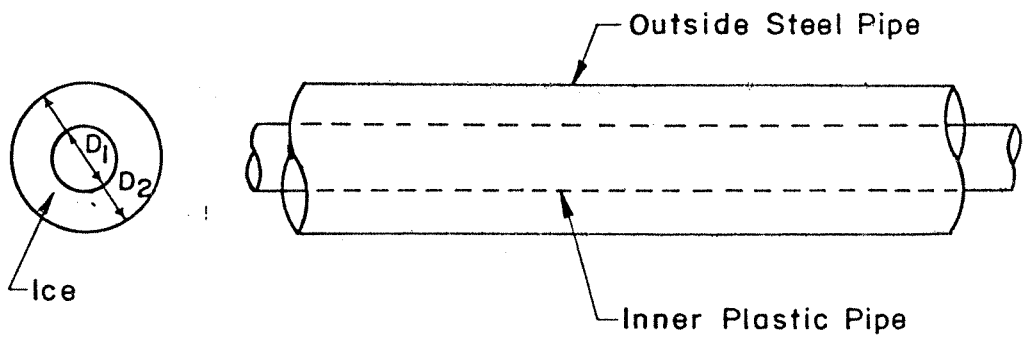

FIG. I.4 GAS LINE ARRANGEMENT PRONE TO BUCKLING

(a) Propagating buckle on a 12 in. pipe.

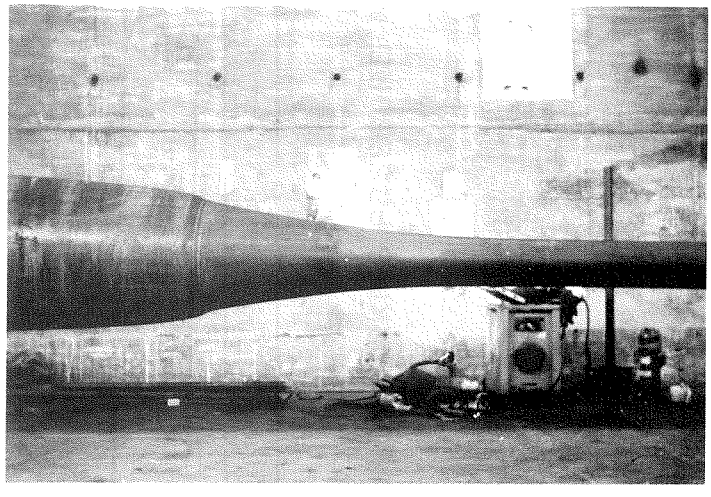

(b) Propagating buckle on a 32 in. diameter pipe.

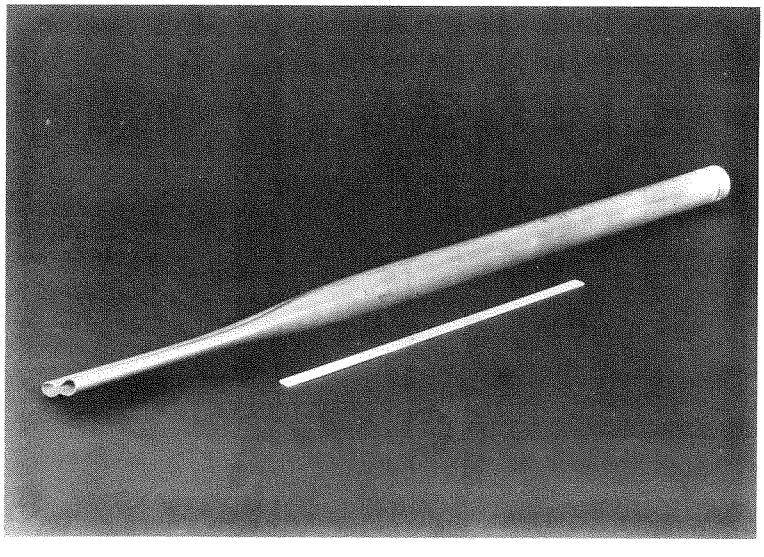

(c) Propagating buckle on model pipe (1.25 in. diameter)

FIG. 1.5 PROPAGATING BUCKLES ON DIFFERENT SIZE PIPES.

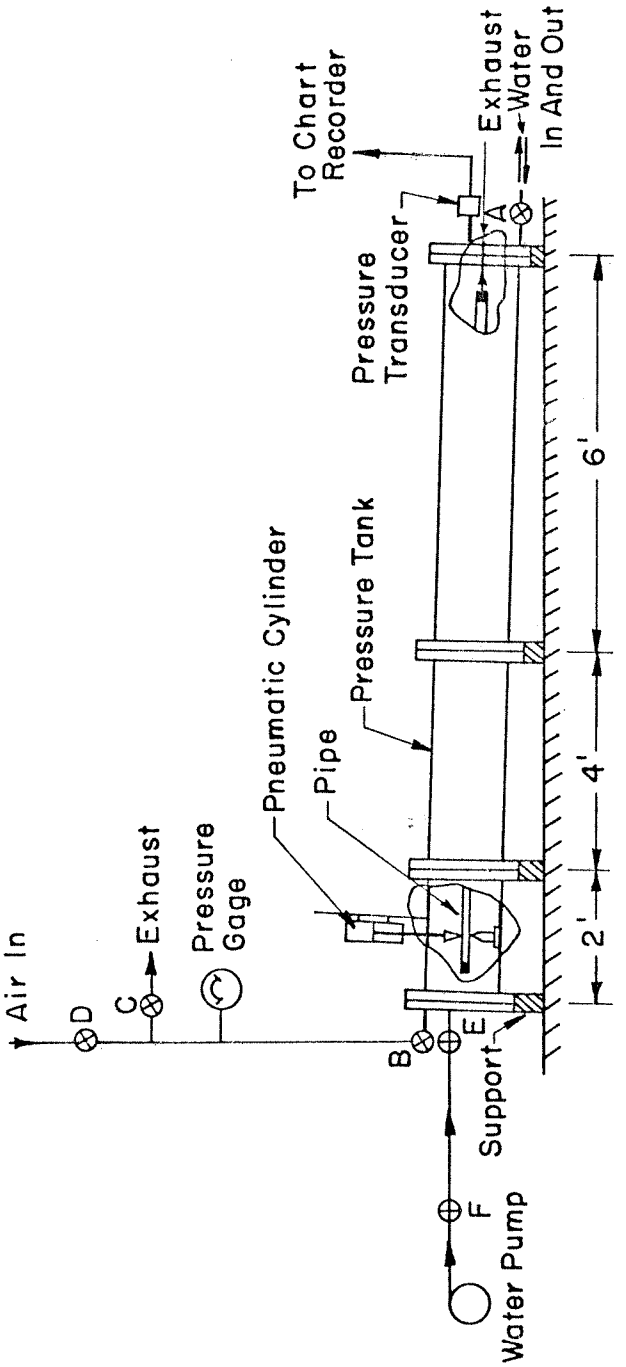

FIG.2.1 PRESSURE TANK ASSEMBLY (WORKING PRESSURE 800 PSI)

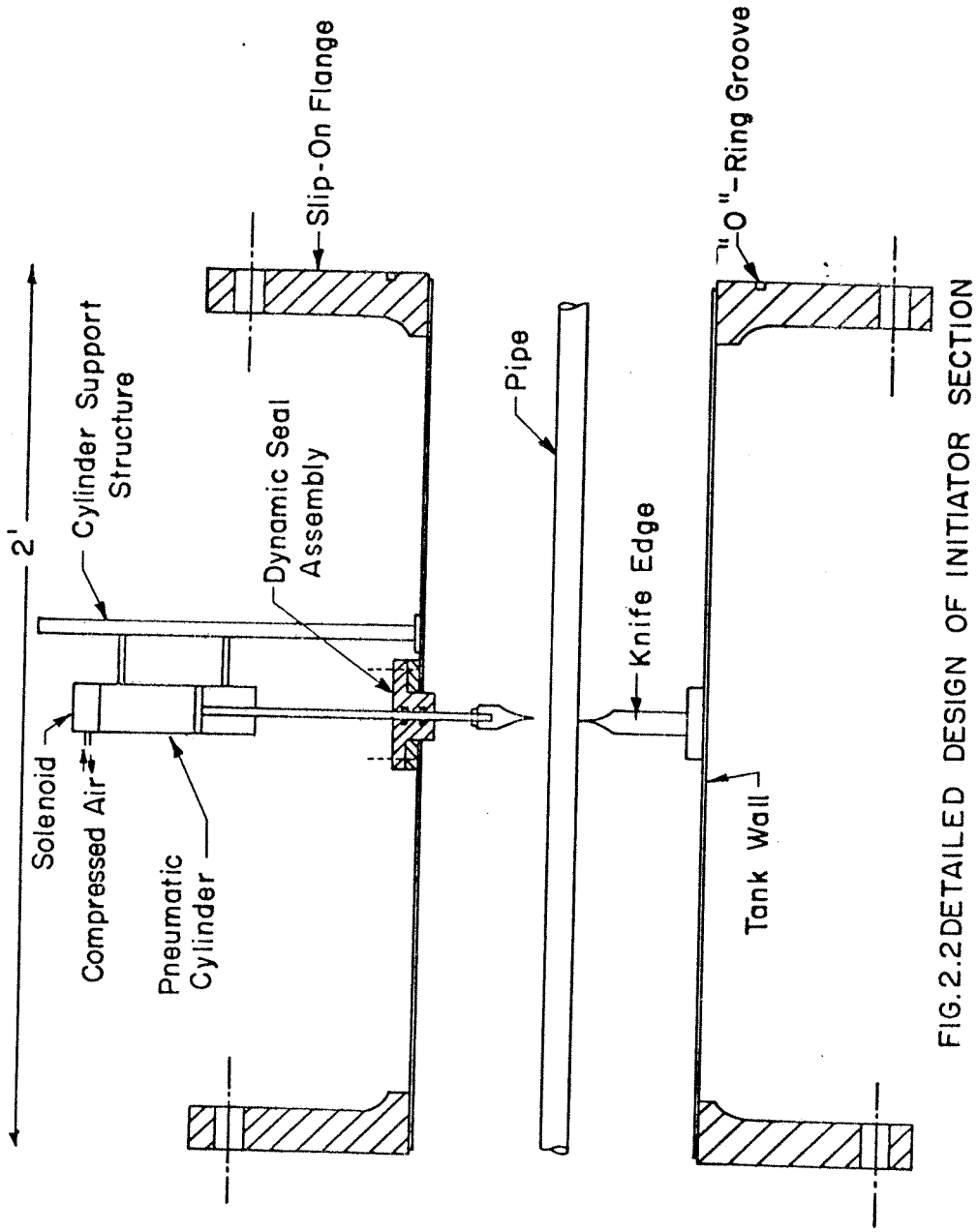

FIG. 2.2 DETAILED DESIGN OF INITIATOR SECTION

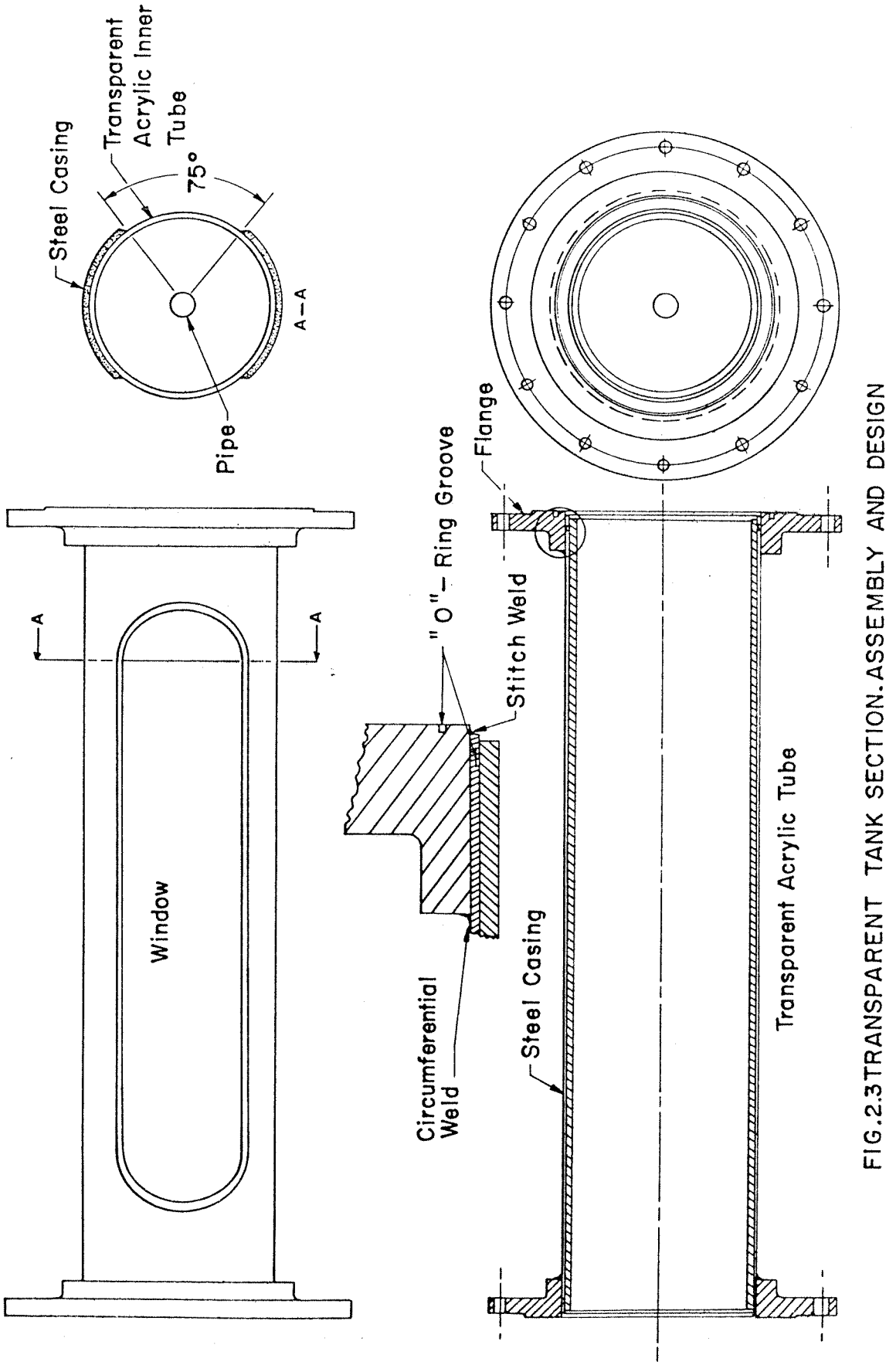

FIG.2.3TRANSPARENT TANK SECTION.ASSEMBLY AND DESIGN

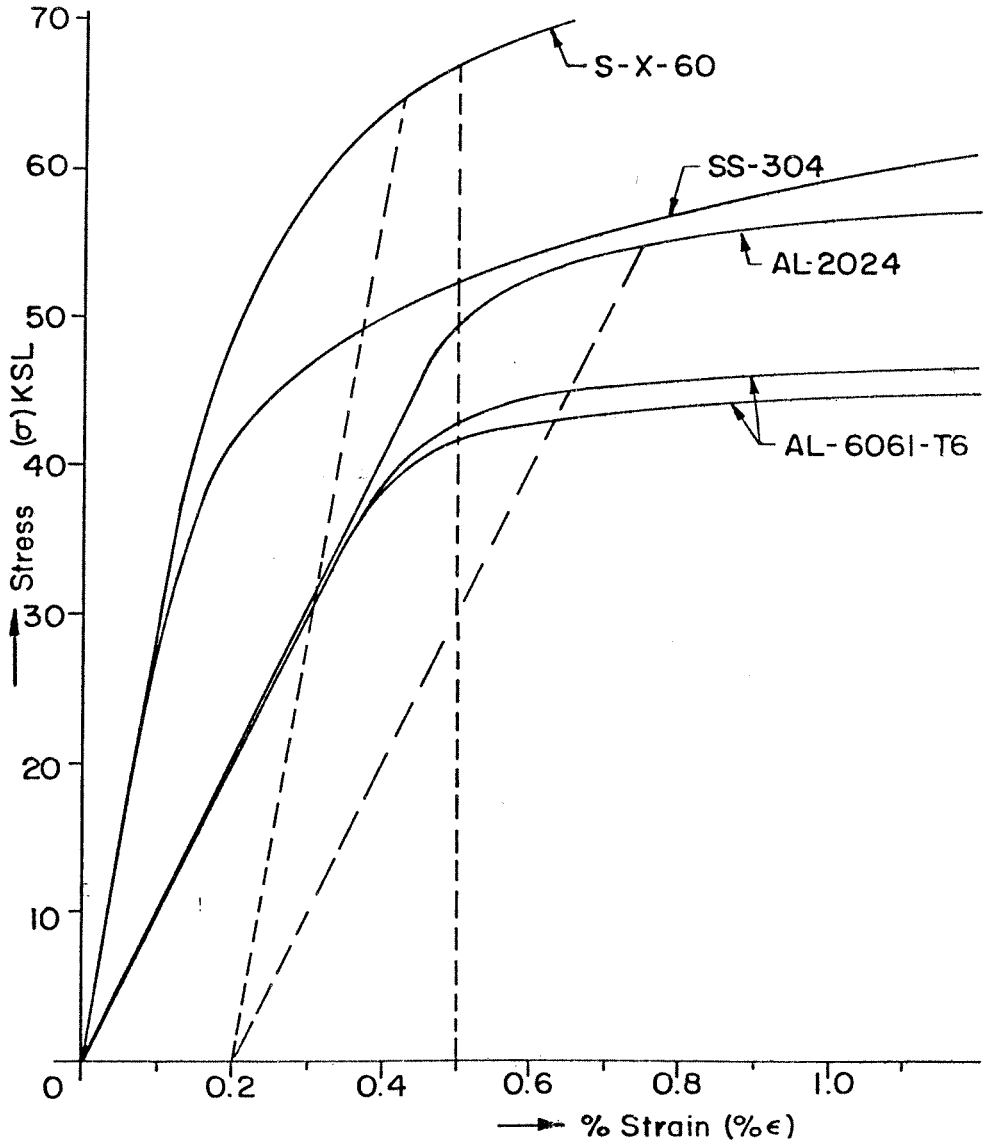

FIG.2.4 TYPICAL STRESS-STRAIN BEHAVIOUR OF ALUMINUM AND STEEL ALLOYS

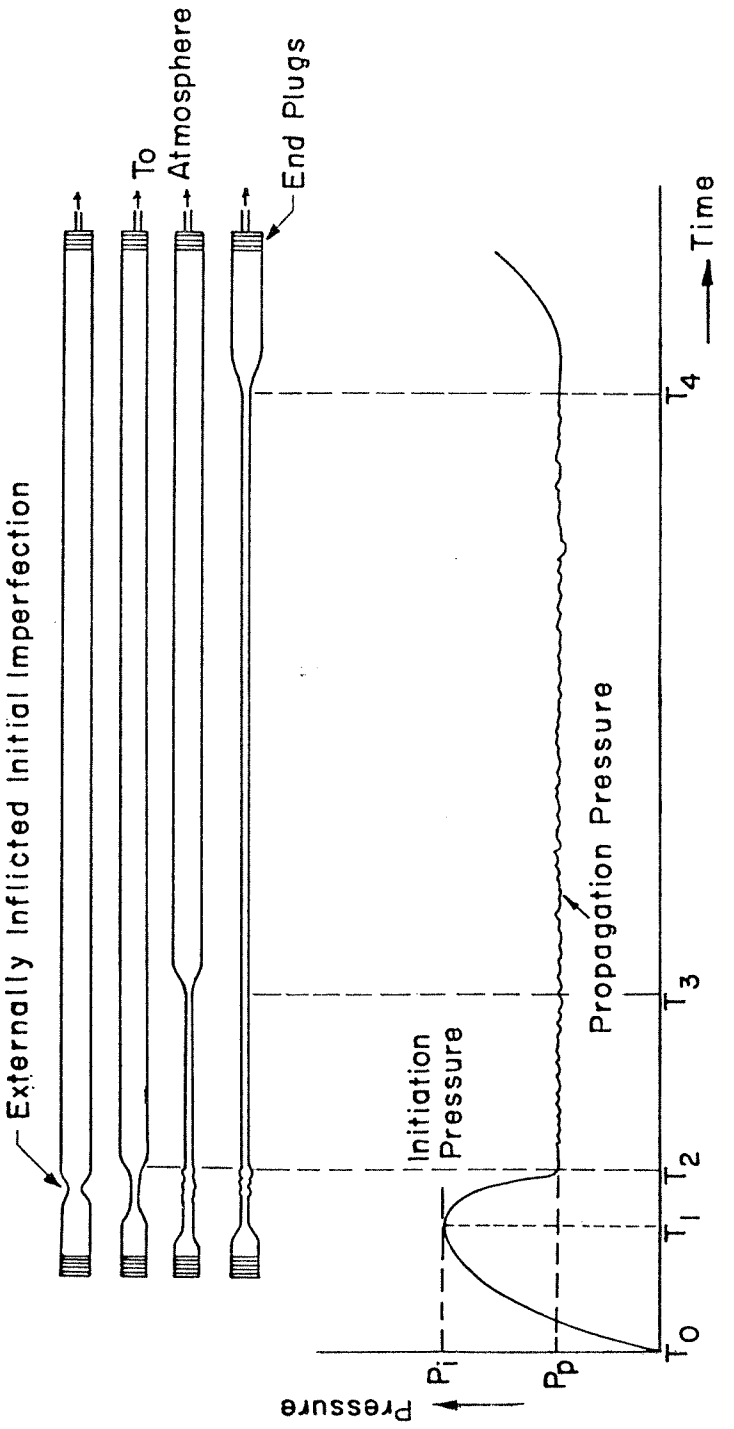

FIG.2.5 SCHEMATIC OF EXPERIMENTAL DETERMINATION OF PROPAGATION PRESSURE

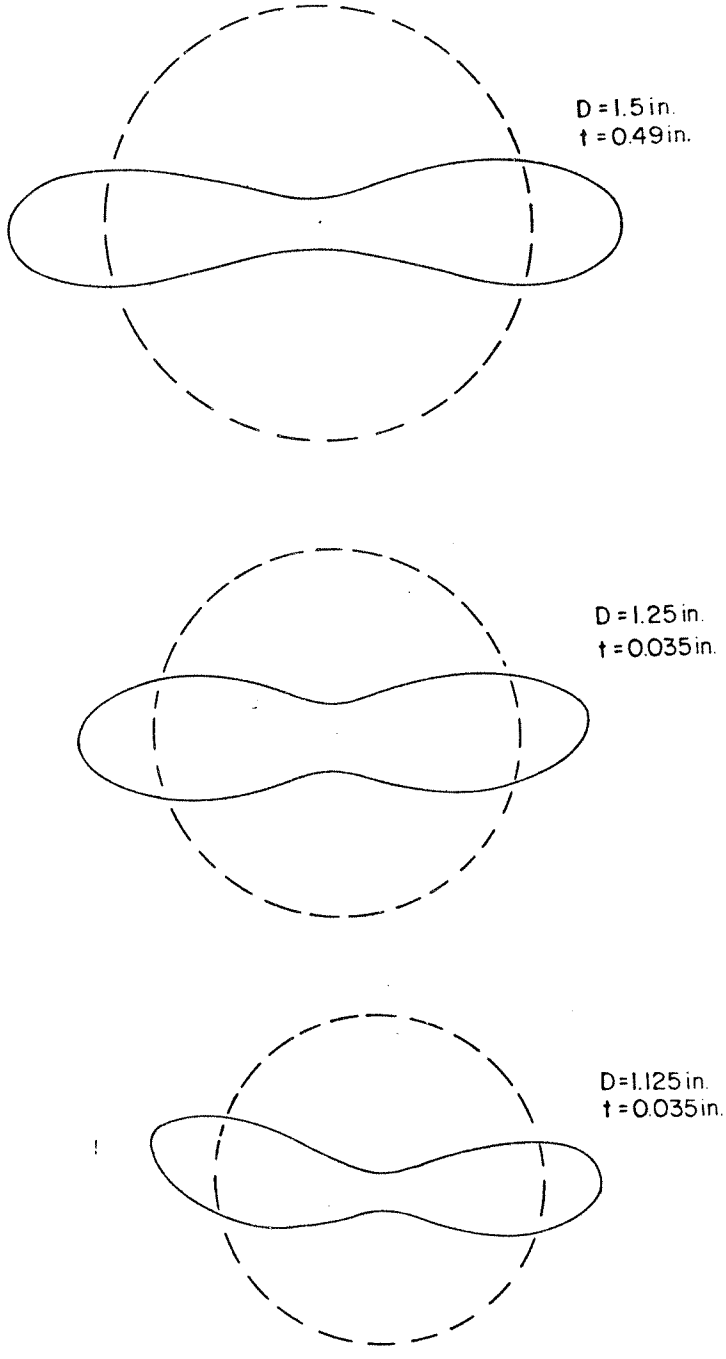

FIG.2.6 CROSSECTIONS OF REPRESENTATIVE COLLAPSED TUBES

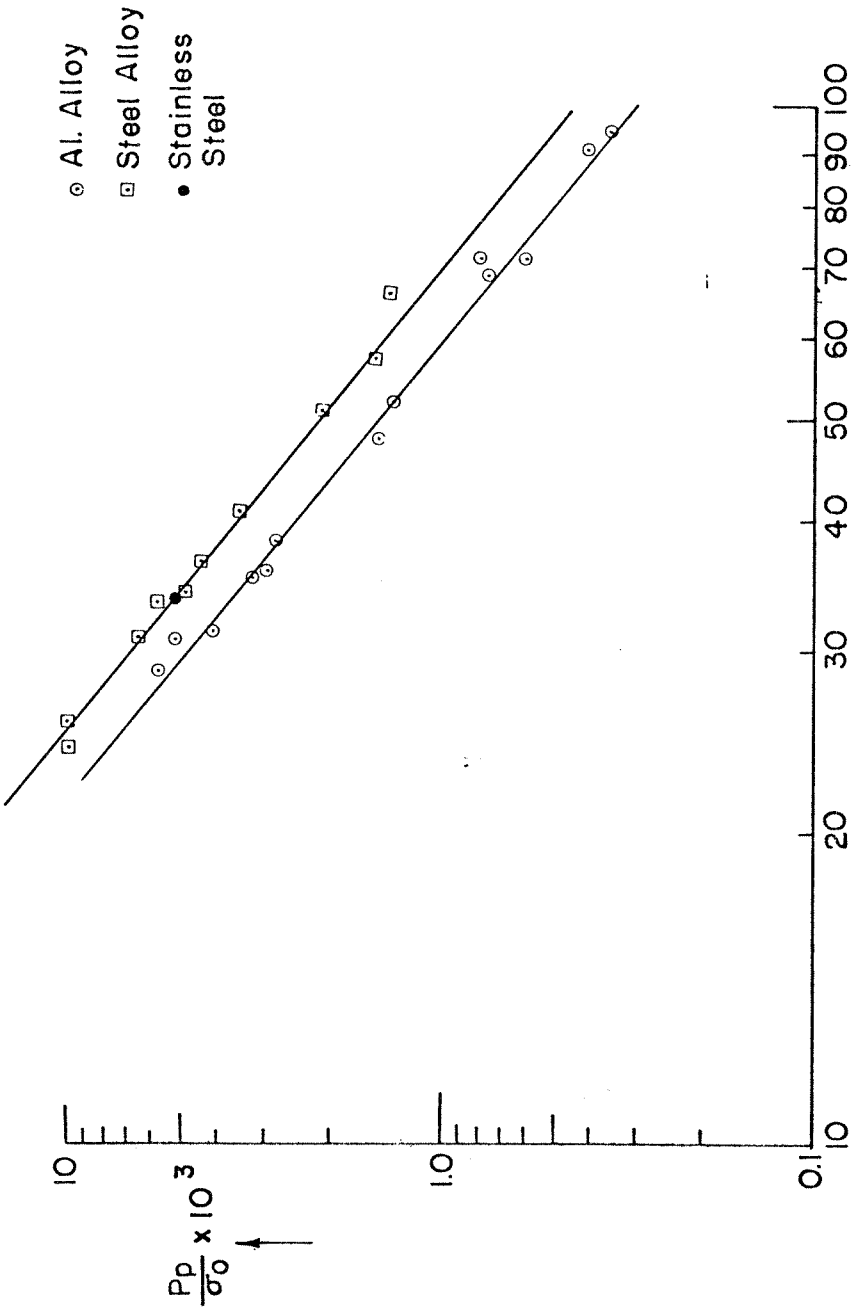

FIG.2.7 NORMALIZED PROPAGATION PRESSURE VS (D/t) ON LOG-LOG SCALE FITTED WITH A STRAIGHT LINE

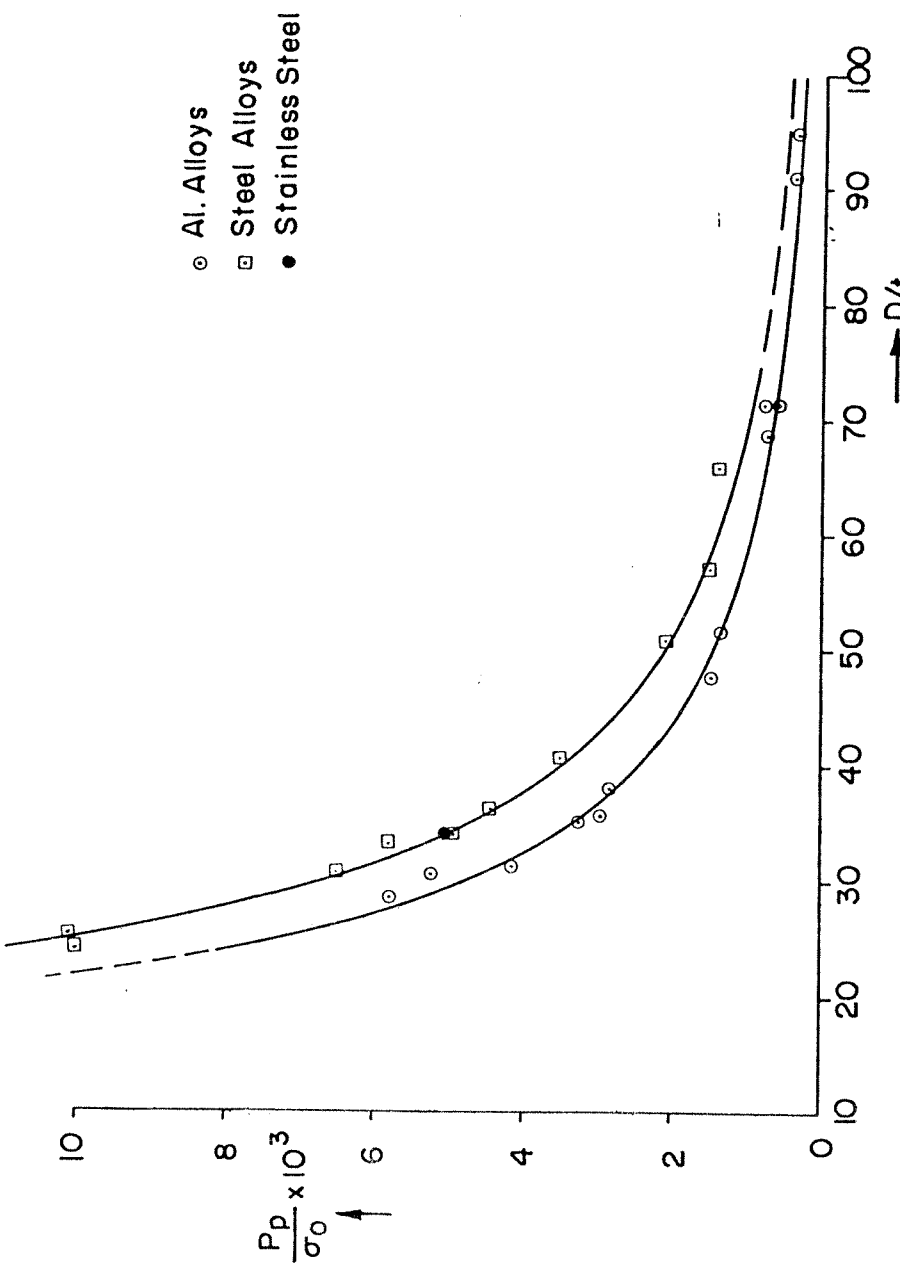

FIG. 2.8 NORMALIZED PROPAGATION PRESSURE VS D/t FITTED WITH POWER LAW CURVES

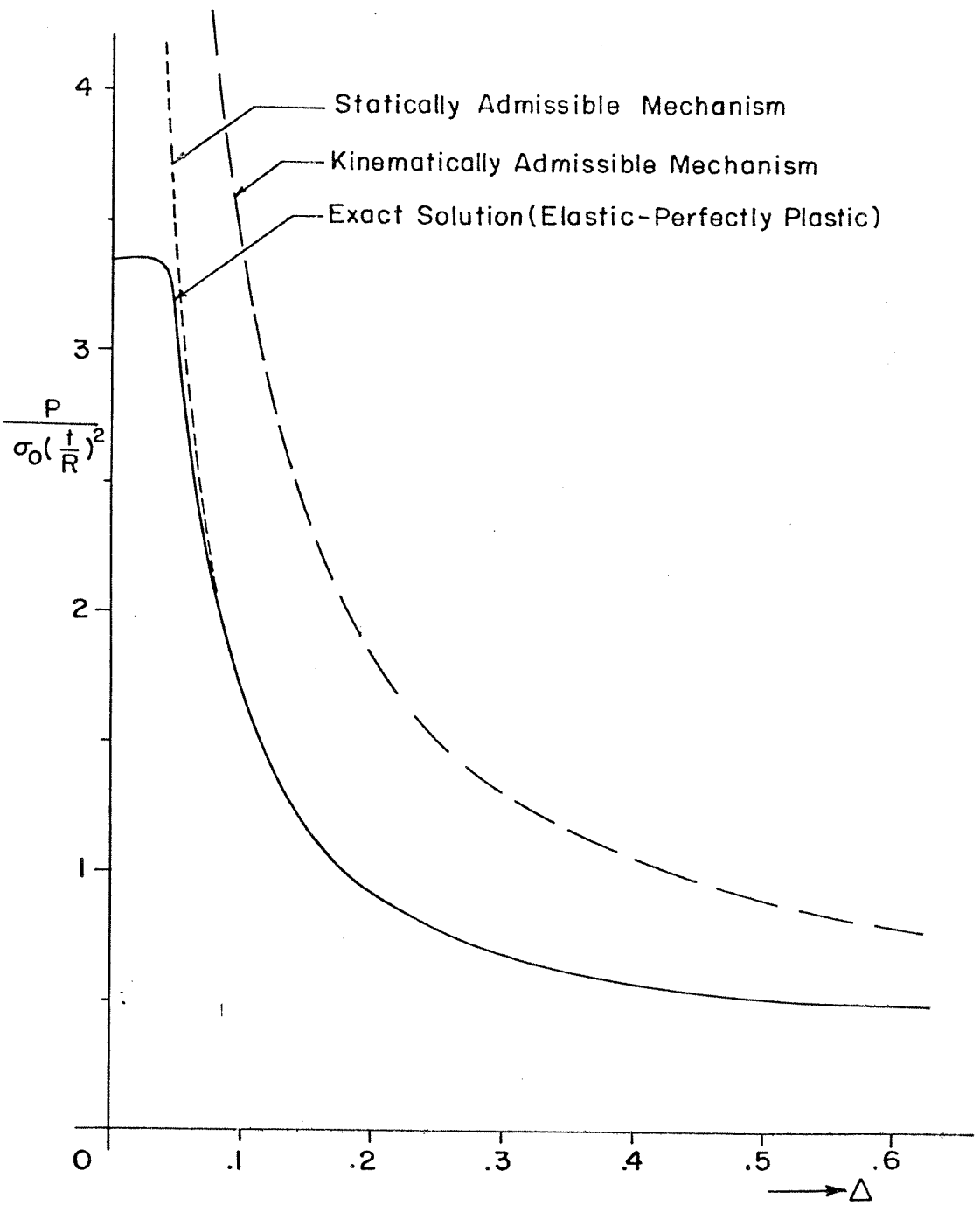

FIG.2.11 UPPER AND LOWER BOUND PATHS FOR THE COLLAPSE PATH COMPARED TO THE EXACT SOLUTION

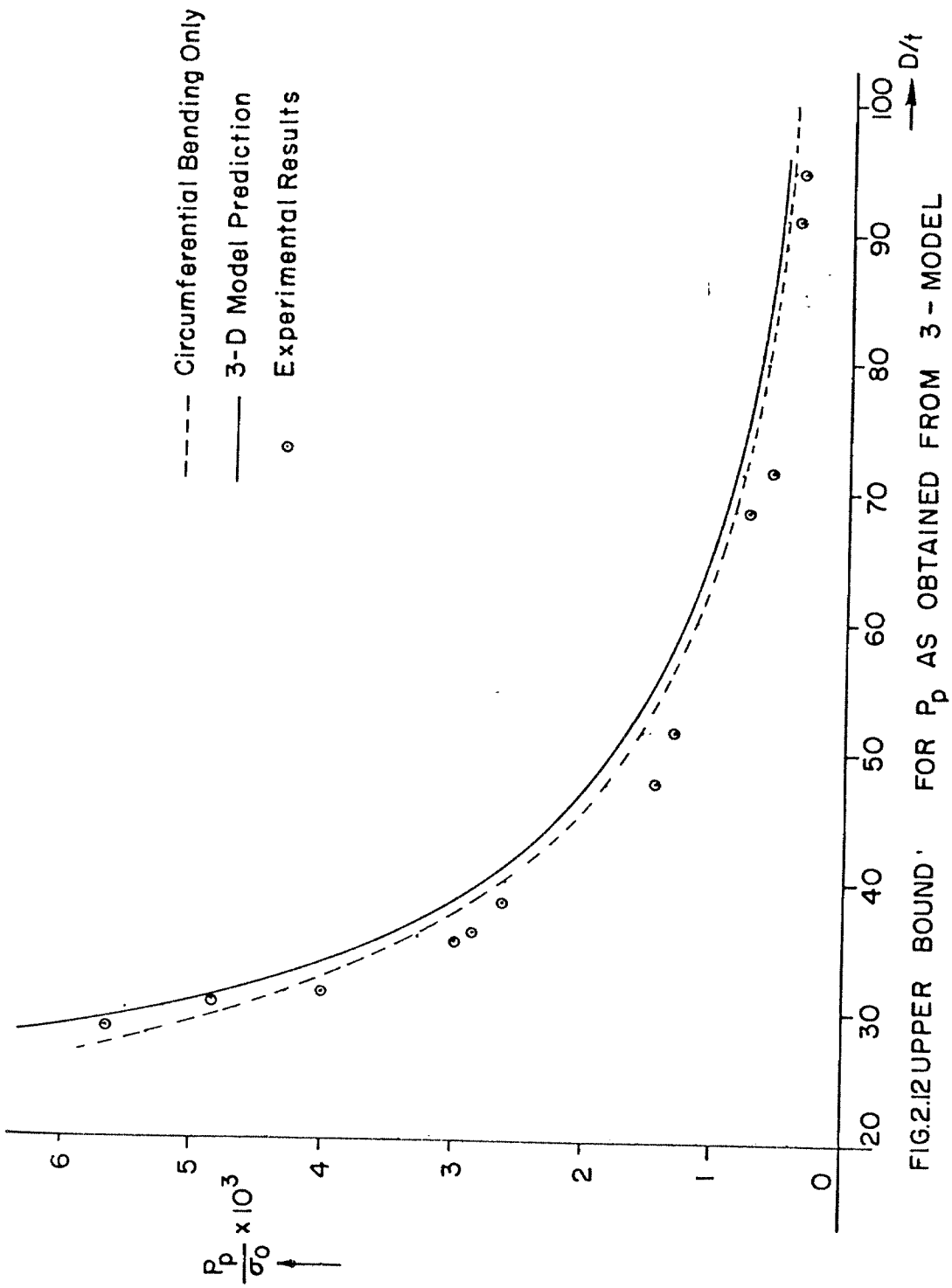

FIG.2.12 UPPER BOUND FOR P_p AS OBTAINED FROM 3-MODEL

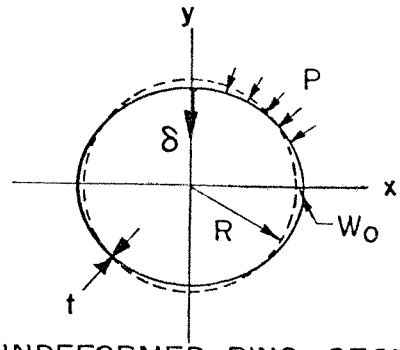

FIG. 2.13 UNDEFORMED RING GEOMETRY

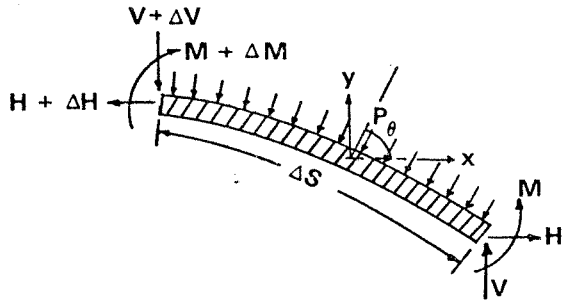

FIG. 2.14 EQUILIBRIUM OF ELEMENTAL RING SECTION

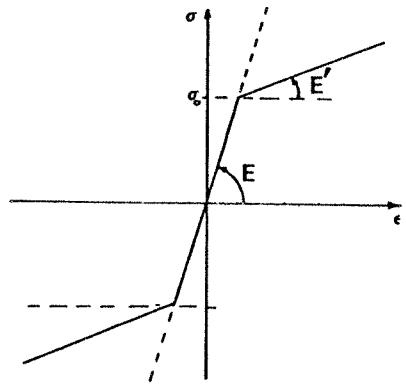

$$\alpha = \frac{E}{E'}$$

FIG. 2.15 ELASTIC-LINEAR STRAIN HARDENING MATERIAL BEHAVIOUR ASSUMED

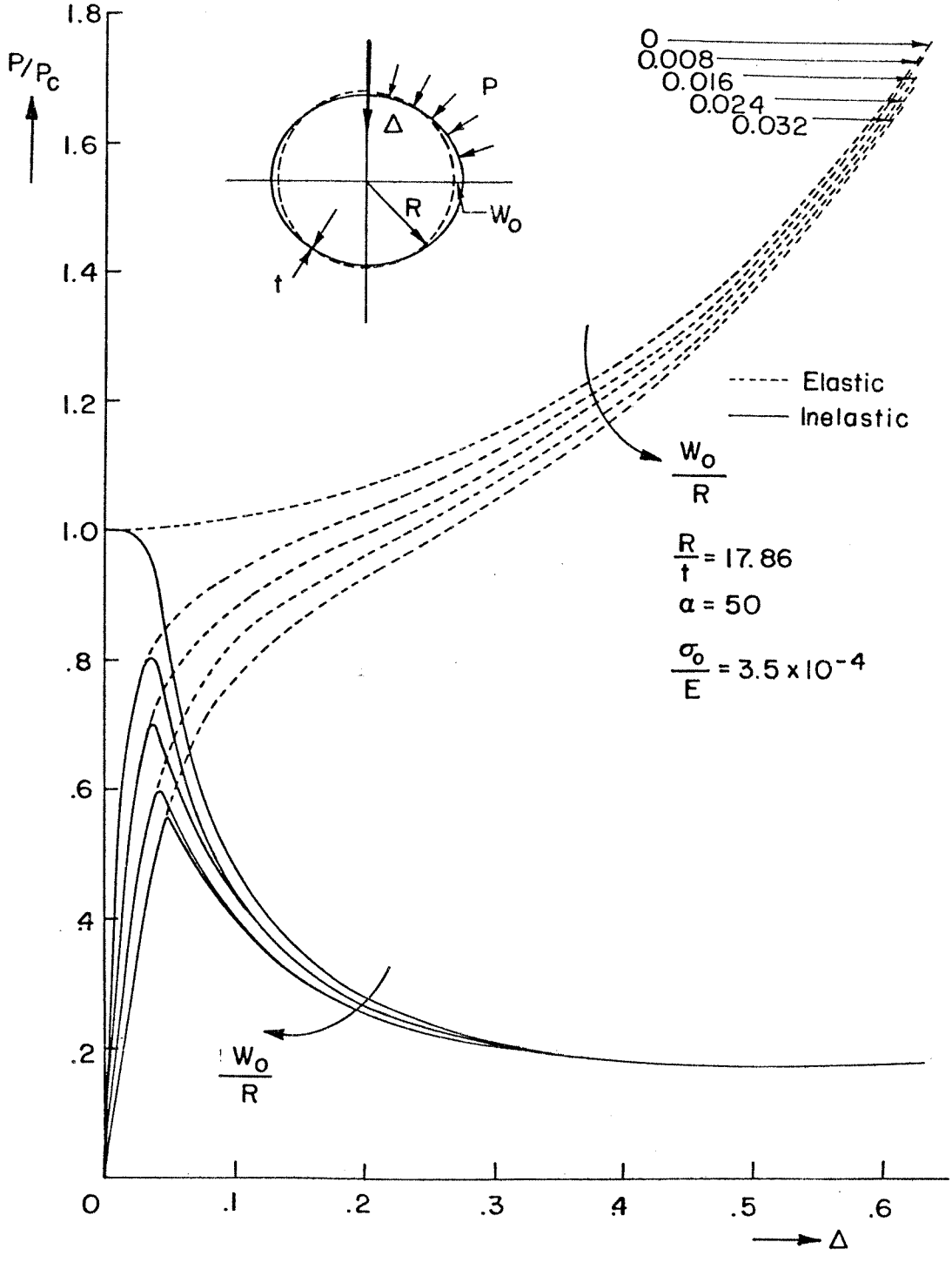

FIG.2.16 COMPLETE POST BUCKLING BEHAVIOUR IN ELASTIC AND INELASTIC CASE

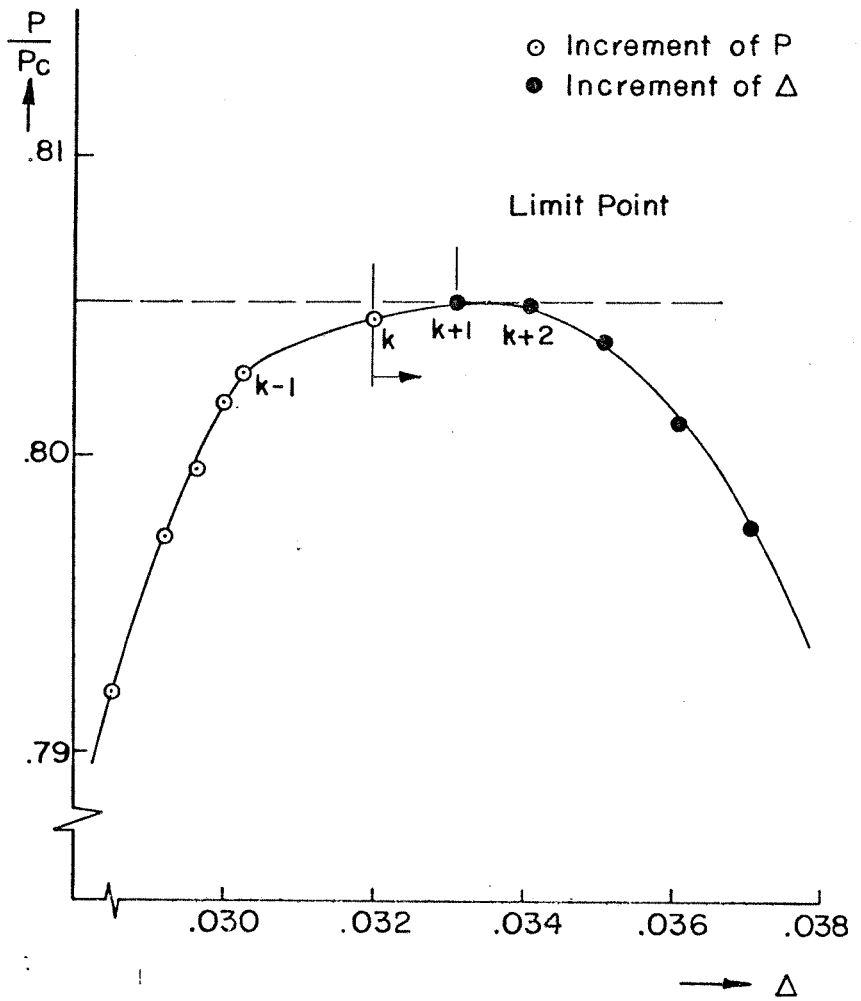

FIG.2.17 DETAILED DRAWING OF LIMIT POINT

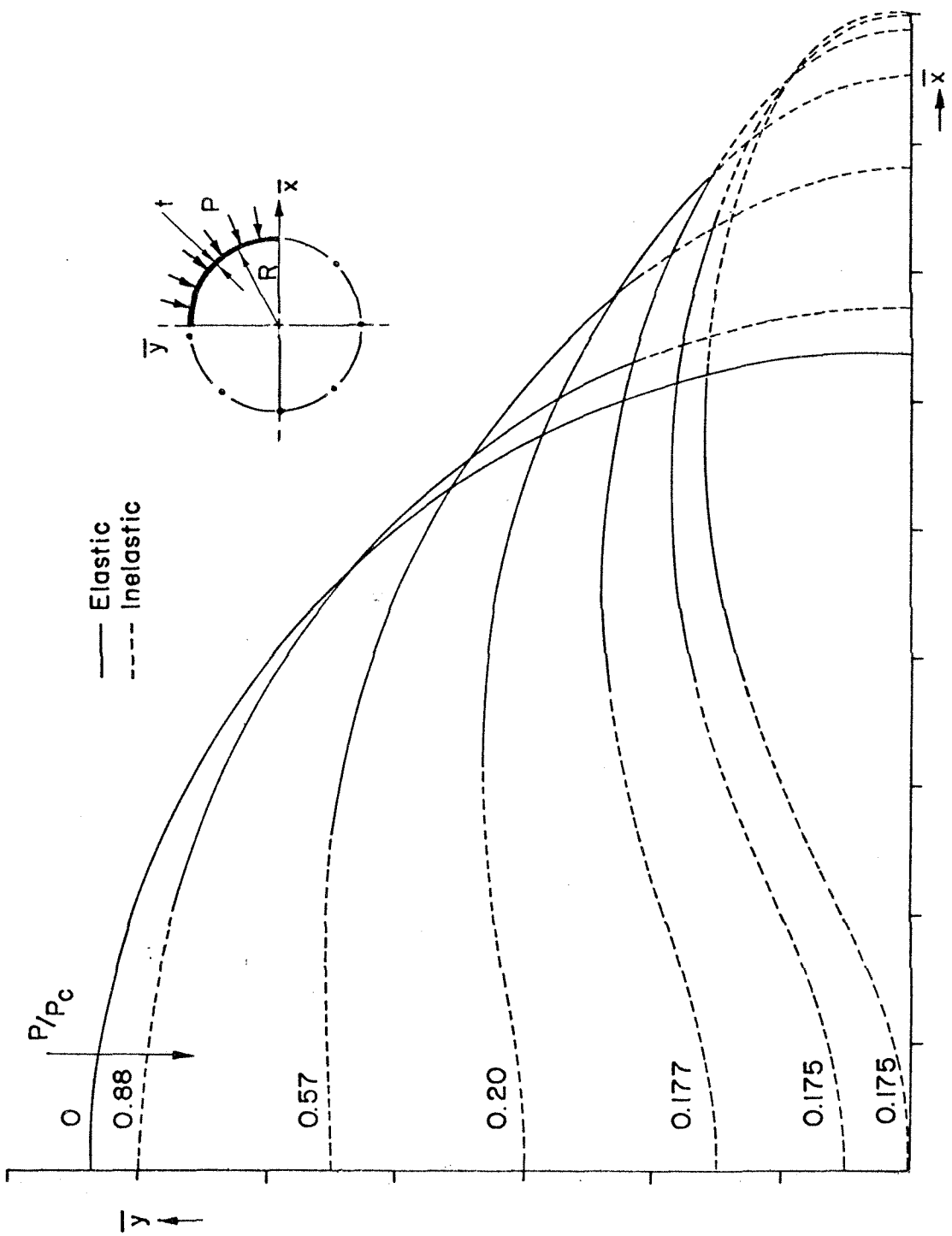

FIG.2.18 INELASTIC DISTRIBUTION ON QUATRAND OF COLLAPSING RING

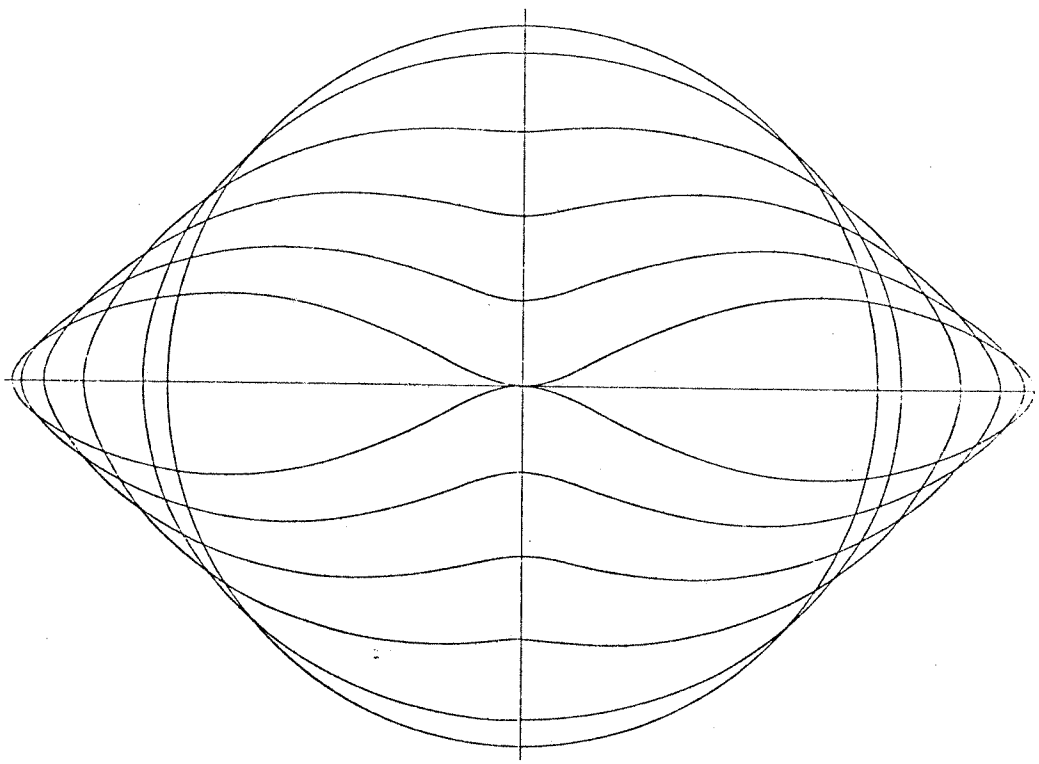

FIG. 2.19 COLLAPSE SEQUENCE OF A CIRCULAR RING

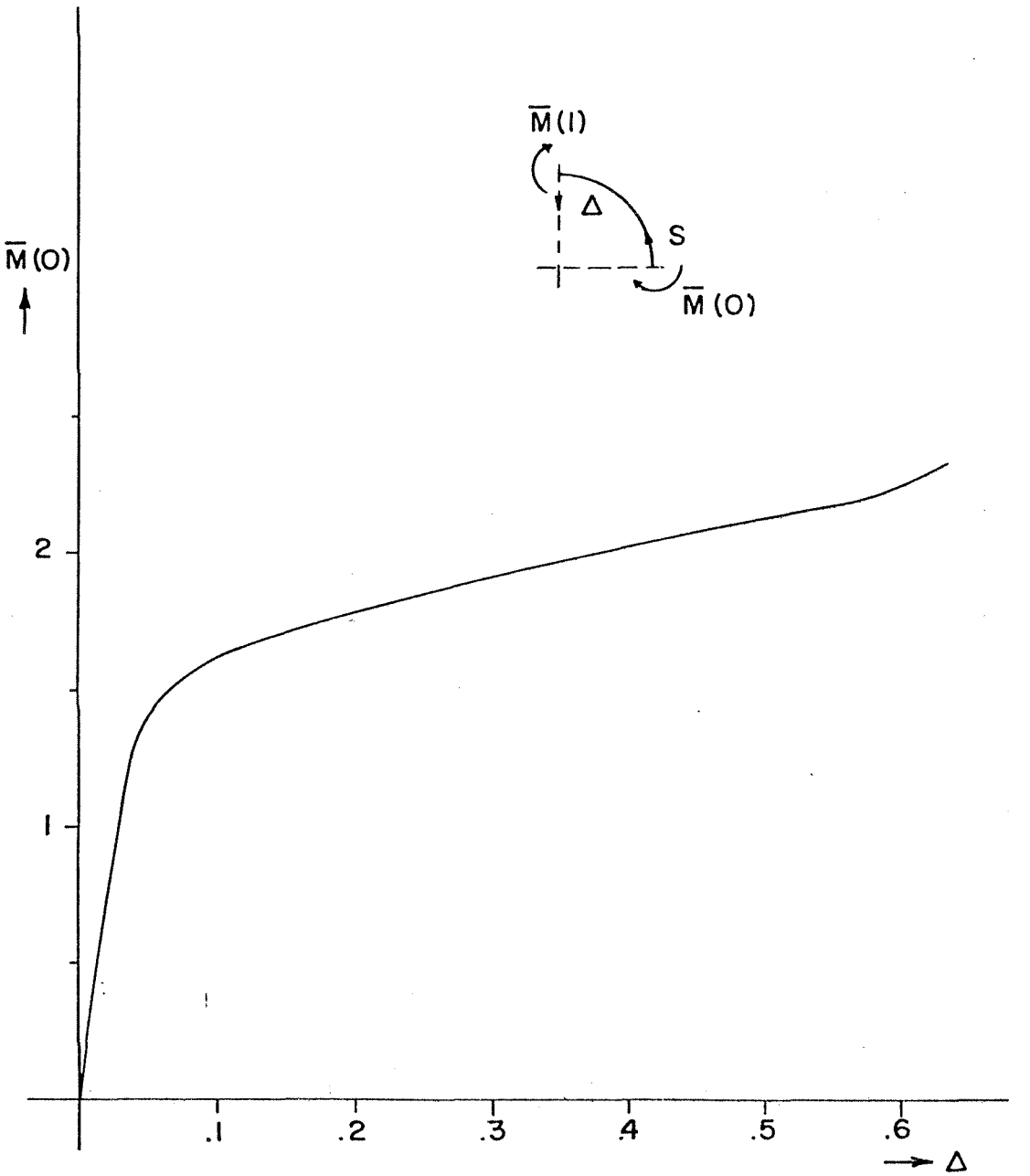

FIG.2.20VARIATION OF MOMENT AT S = 0 WITH DISPLACEMENT AT S = 1

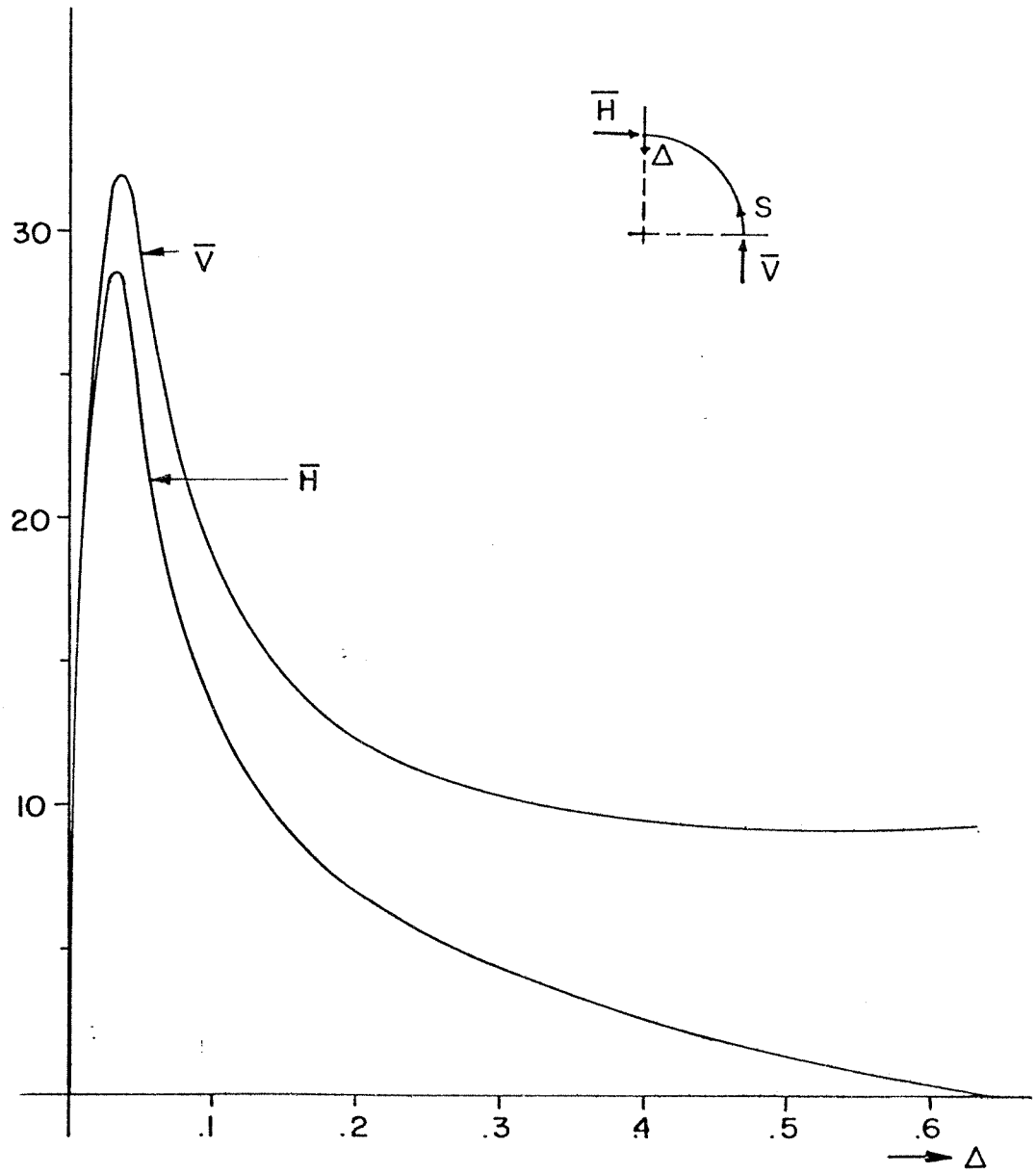

FIG.2.21 VARIATION OF END FORCES WITH DISPLACEMENT

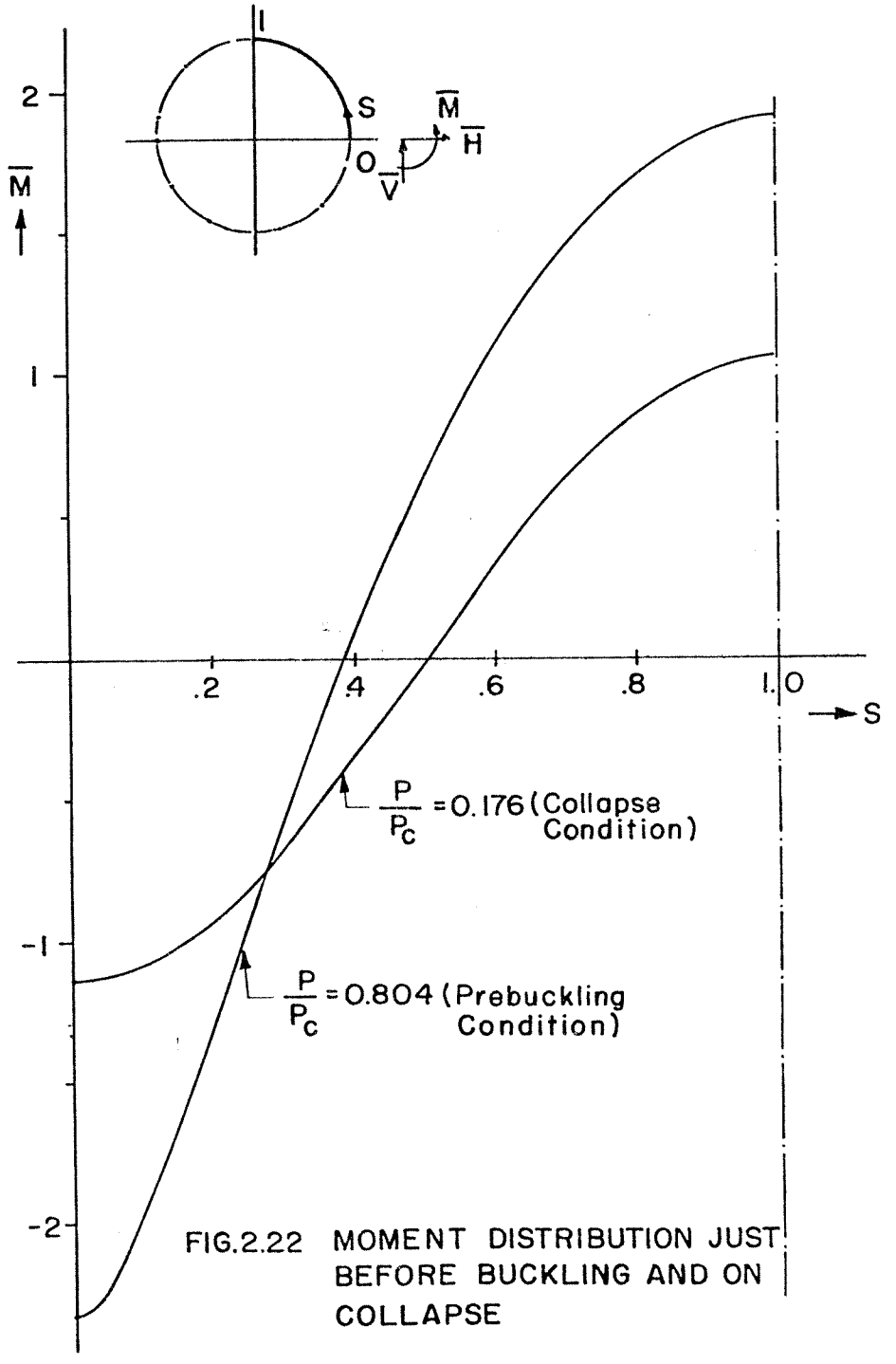

FIG.2.22 MOMENT DISTRIBUTION JUST BEFORE BUCKLING AND ON COLLAPSE

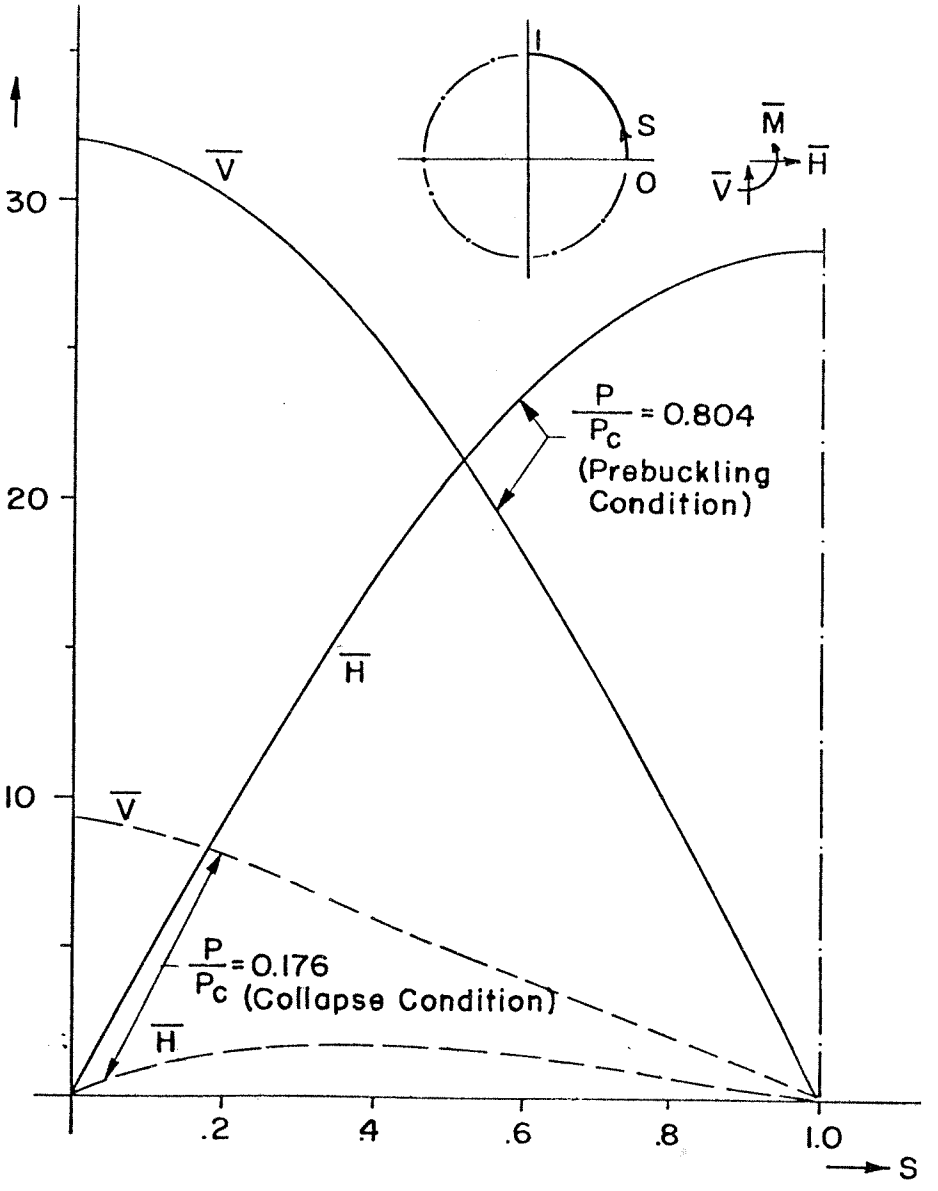

FIG.2.23 FORCE DISTRIBUTION JUST BEFORE BUCKLING AND ON COLLAPSE

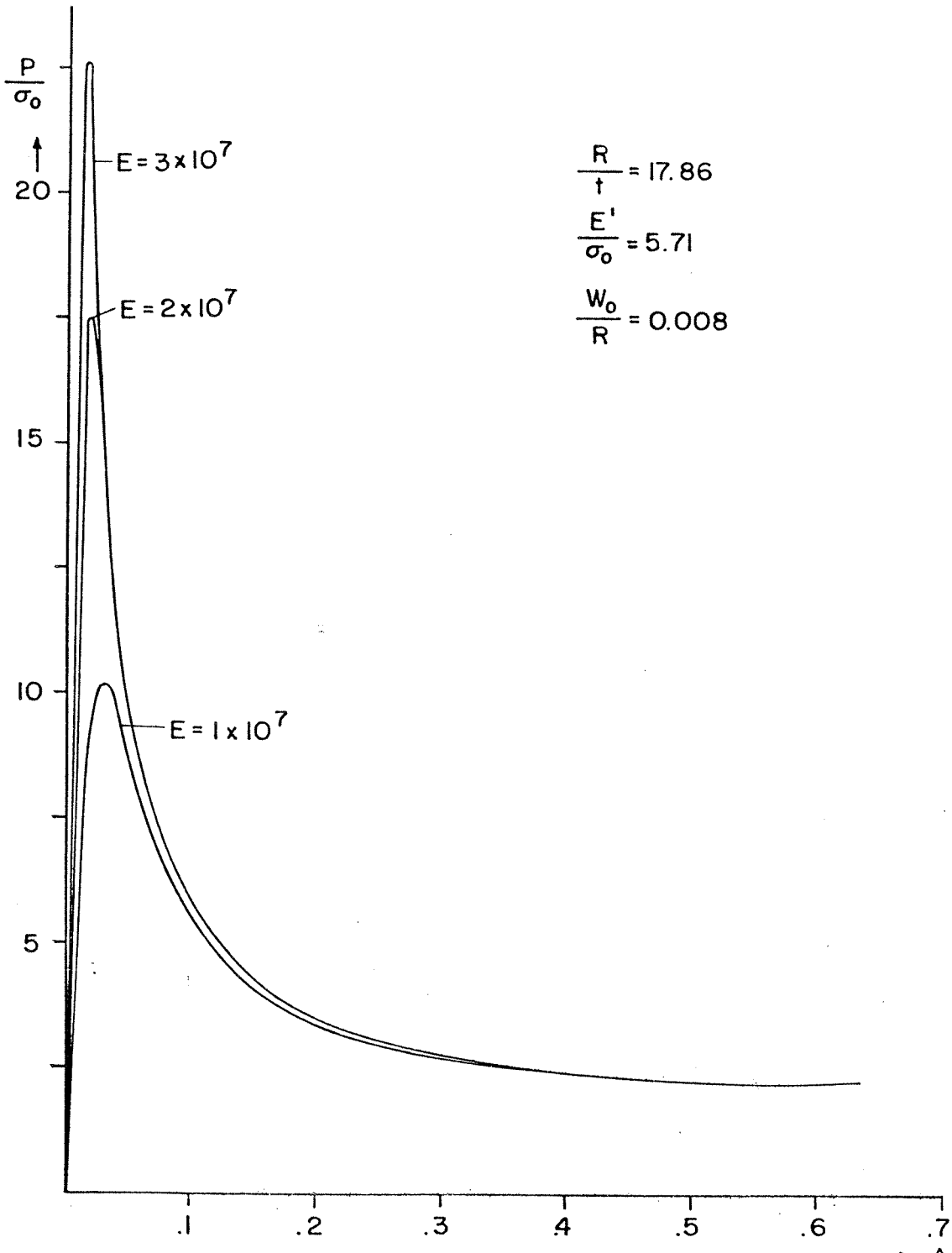

FIG.2.24 POST BUCKLING BEHAVIOUR FOR DIFFERENT VALUES OF E

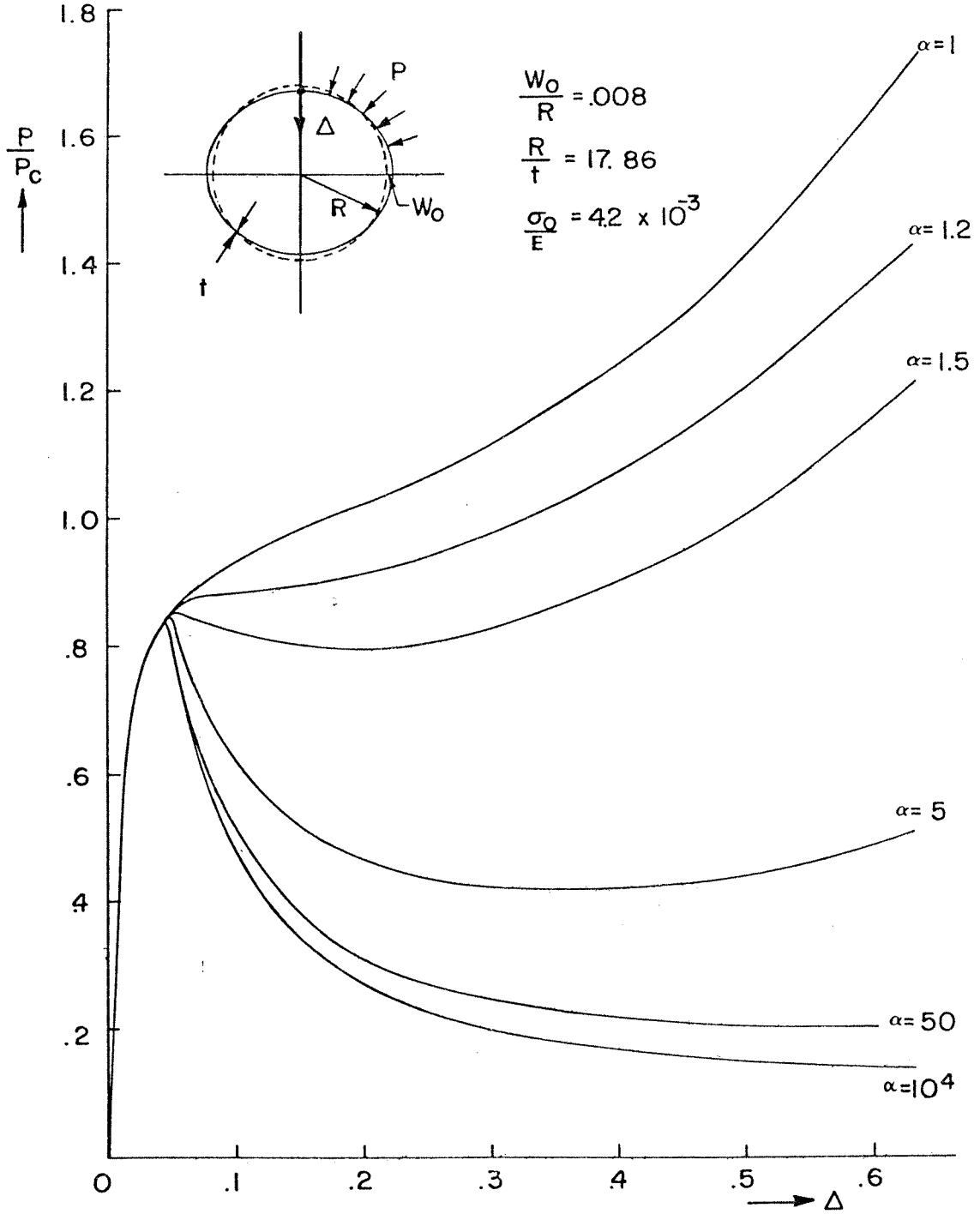

FIG. 2.25 VARIATION OF POST BUCKLING BEHAVIOUR WITH STRAIN HARDENING PARAMETER α

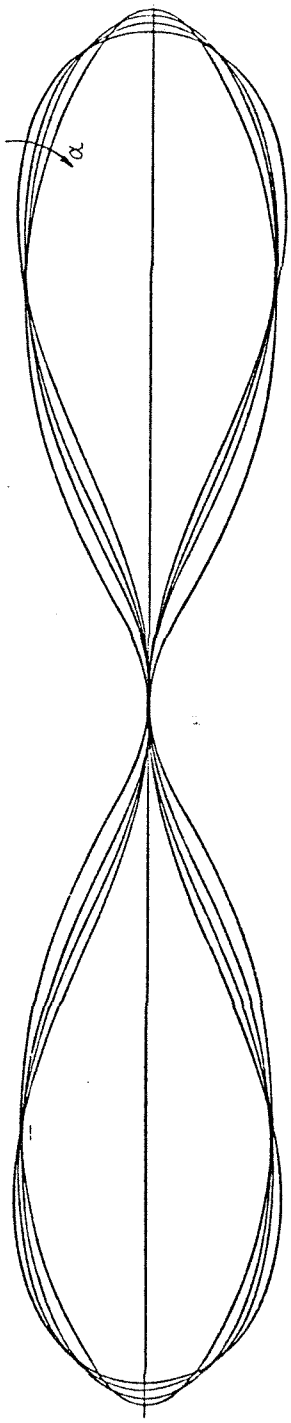

FIG.2.26VARIATION OF COLLAPSE SHAPE WITH STRAIN HARDENING PARAMETER α

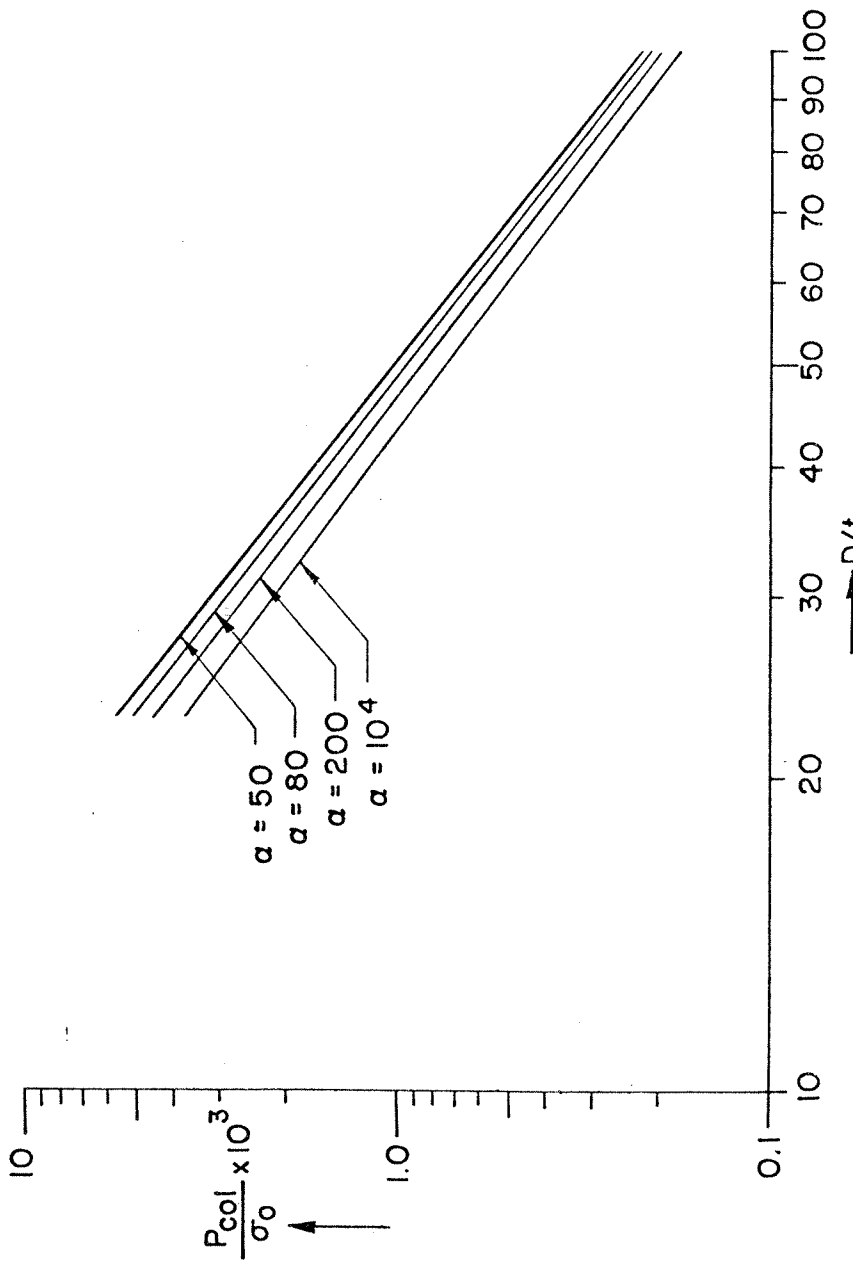

FIG. 2.27 RING COLLAPSE PRESSURE AS A FUNCTION OF (D/t) FOR DIFFERENT VALUES OF α

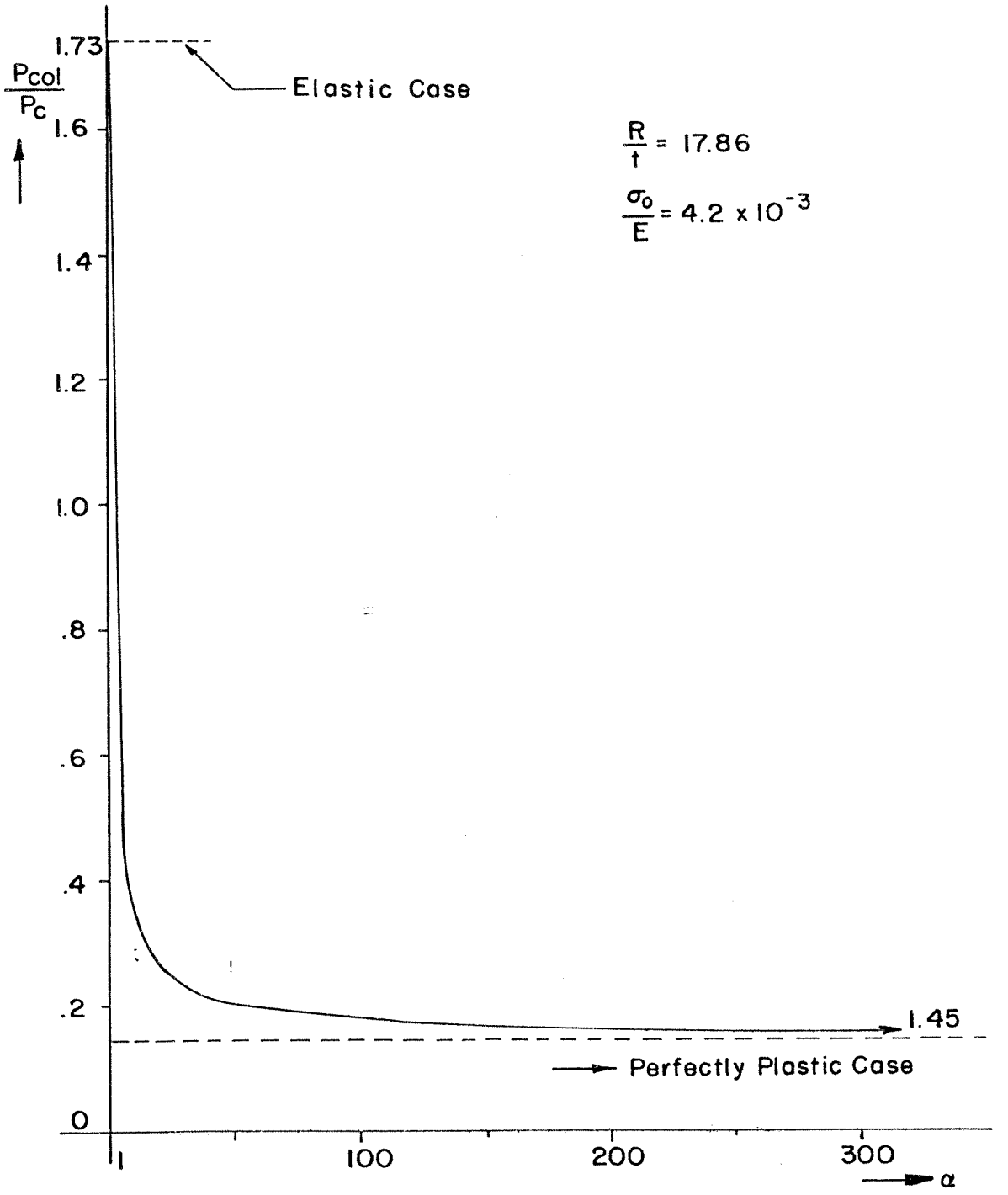

FIG.2.28 VARIATION OF COLLAPSE PRESSURE WITH α

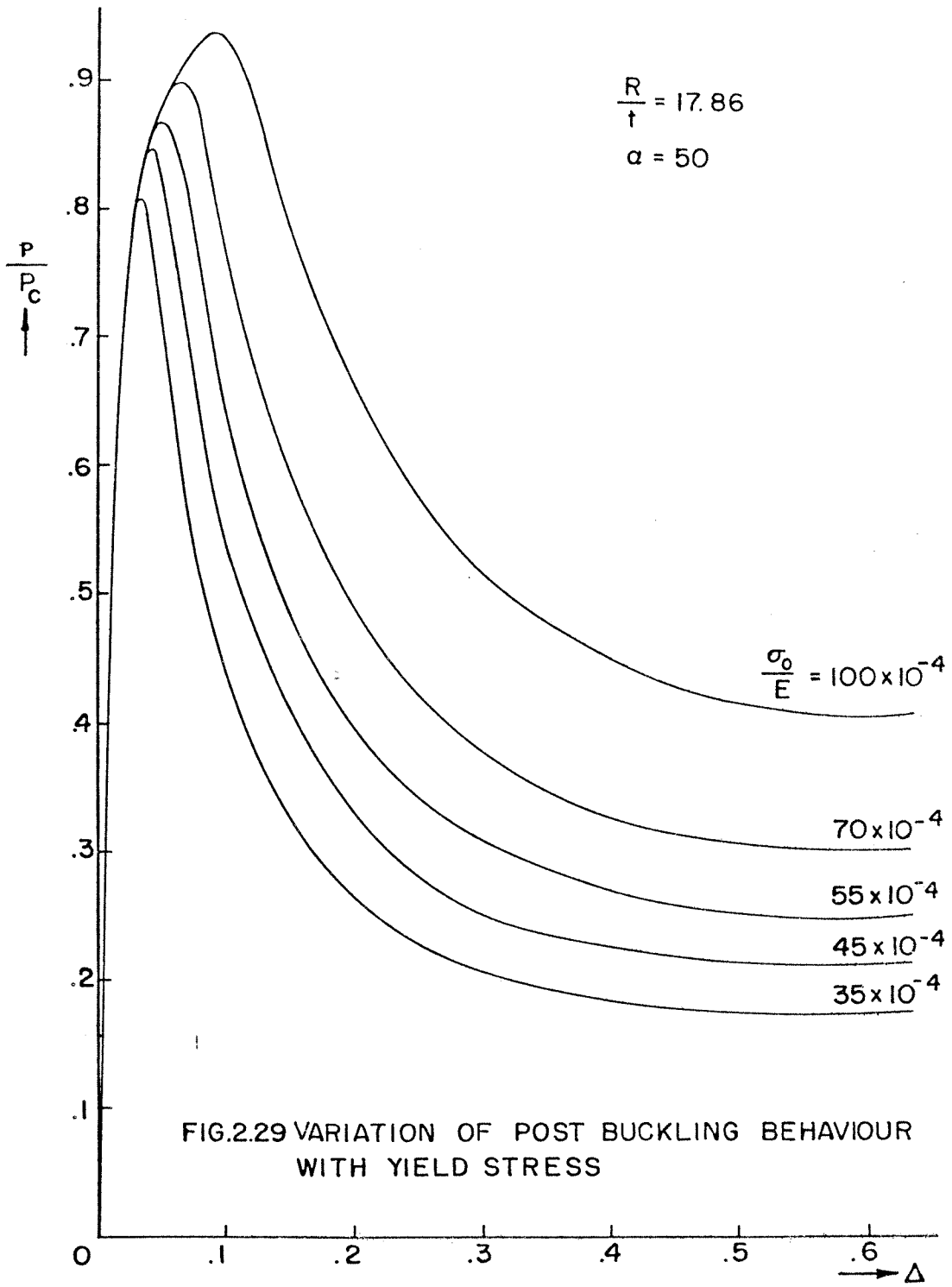

FIG.2.29 VARIATION OF POST BUCKLING BEHAVIOUR WITH YIELD STRESS

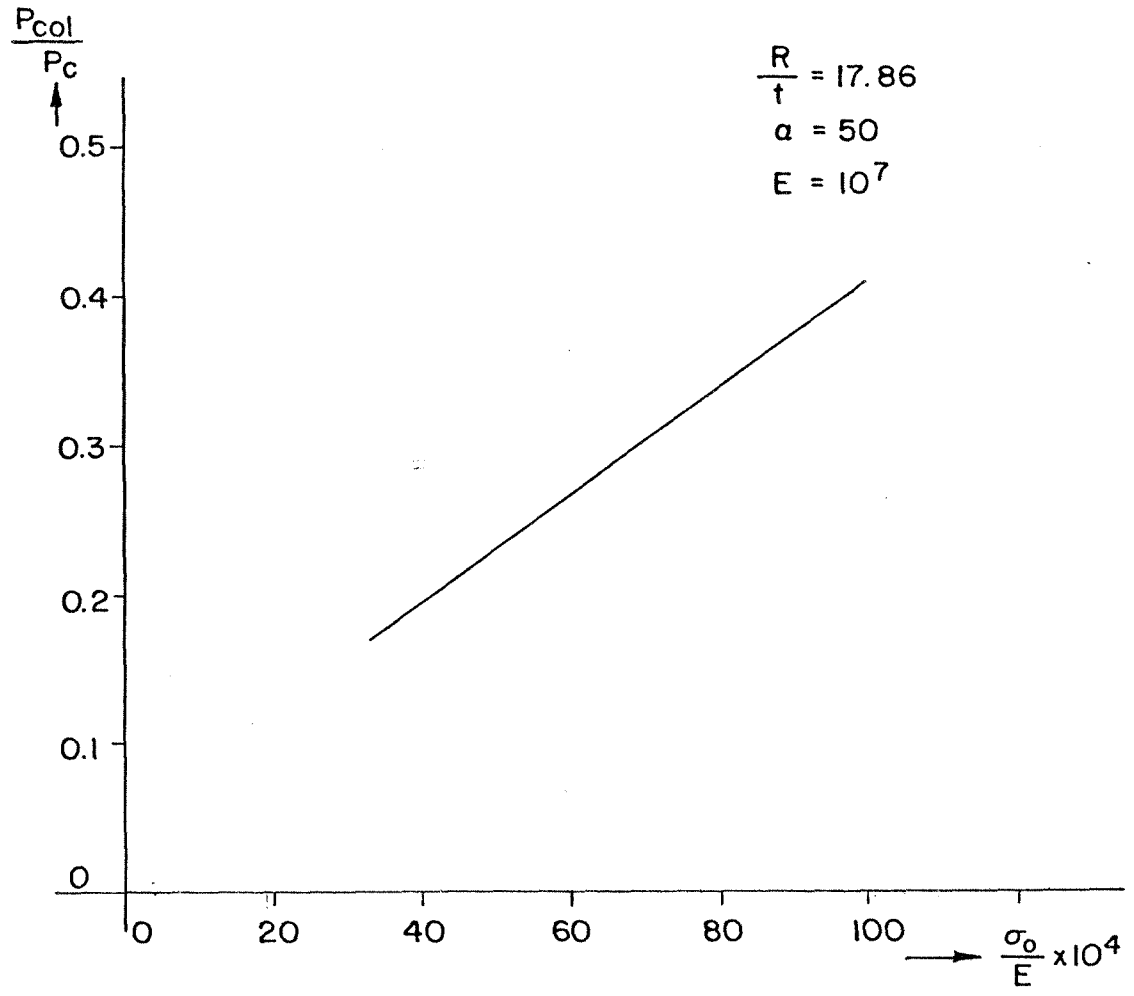

FIG. 2.30 VARIATION OF COLLAPSE LOAD WITH YIELD STRESS

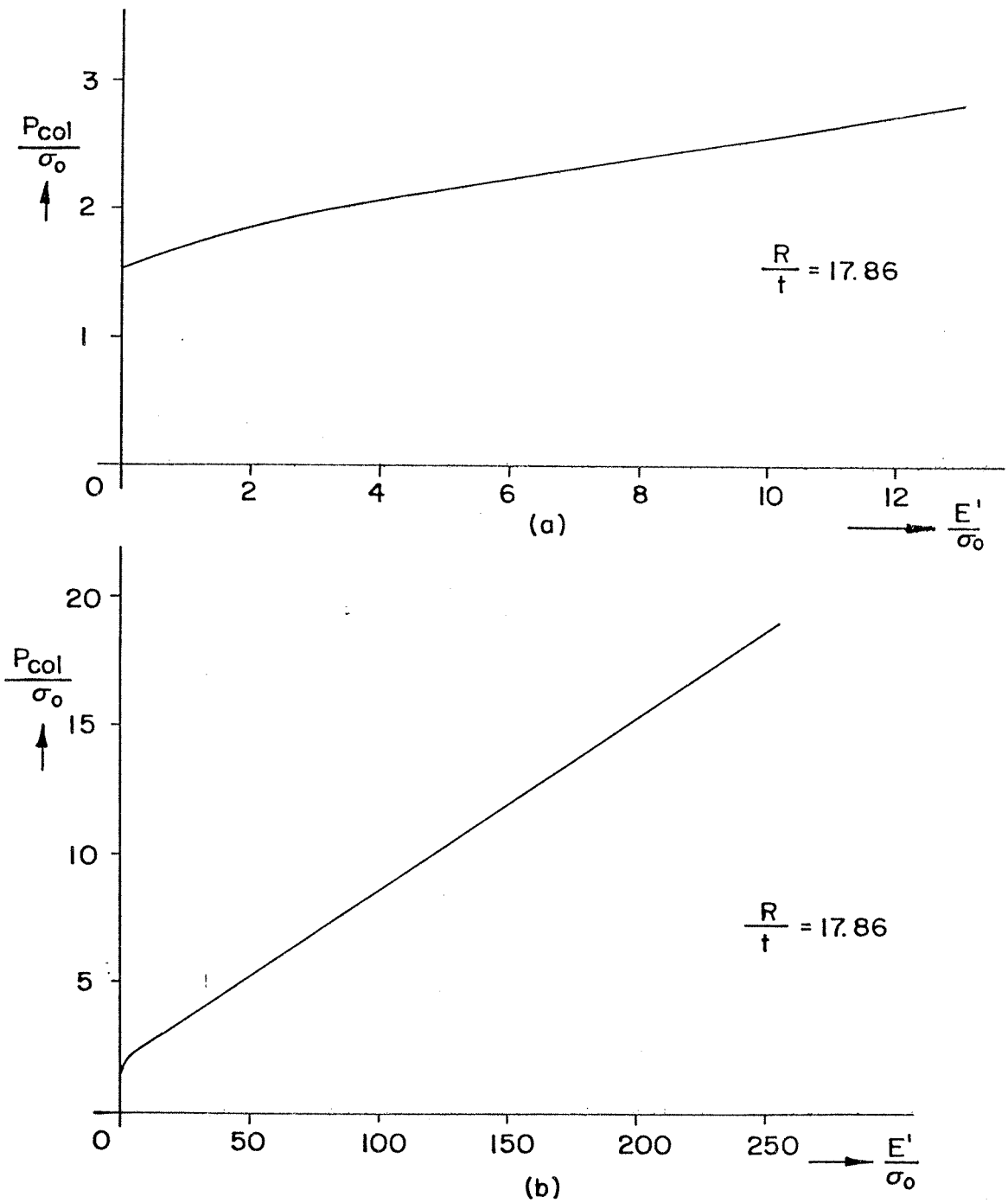

FIG.2.31 VARIATION OF COLLAPSE PRESSURE WITH $\frac{E'}{\sigma_0}$

	D in (mm)	t in (mm)	D/t	P_p psi (bar$^+$)	$\sigma_o^{++} \times 10^{-3}$ psi (bar$^+$)	$P_p/\sigma_o \times 10^3$
1	1.001 (25.43)	.035 (.889)	28.6	243 (16.75)	42 (2.895)	5.783
2	1.503 (38.18)	.049 (1.245)	30.67	225 (15.51)	43 (2.965)	5.233
3	1.126 (28.6)	.036 (.9144)	31.25	178.5 (12.31)	43 (2.965)	4.156
4	1.254 * (31.85)	.0365 (.9271)	34.36	262 (18.00)	52 (3.585)	5.038
5	1.251 ** (31.78)	.0355 (.9017)	35.24	163.4 (11.27)	50 (3.447)	3.268
6	1.253 (31.85)	.035 (.889)	35.8	157.4 (10.85)	53 (3.654)	2.970
7	1.376 (34.95)	.036 (91.44)	38.22	128 (8.825)	45 (3.103)	2.844
8	1.003 (25.48)	.021 (.5334)	47.76	74.6 (5.143)	50 (3.447)	1.492
9	1.500 (38.1)	.029 (.7366)	51.72	57.3 (3.951)	42 (2.895)	1.364
10	1.375 (34.93)	.020 .508	68.75	32.9 (2.268)	43 (2.965)	.765
11	2.500 (63.5)	.035 (.889)	71.43	29.6 (2.041)	49 (3.378)	.604
12	2.003 (50.88)	.022 (.5588)	91.05	17.5 (1.207)	42.5 (2.93)	.412
13	2.750 (69.85)	.029 (.7366)	94.83	15 (1.034)	41.5 (2.861)	.361

TABLE 2.1 CHARACTERISTICS OF PIPES TESTED AND PROPAGATION PRESSURE RESULTS

\+ 1 bar = 10^5 N/m^2 ≃ 14.5 psi
++ $\sigma_0 \Longrightarrow \sigma_{0.005}$
* SS-304
** Aℓ-2024-T3
All others Aℓ-6061-T6

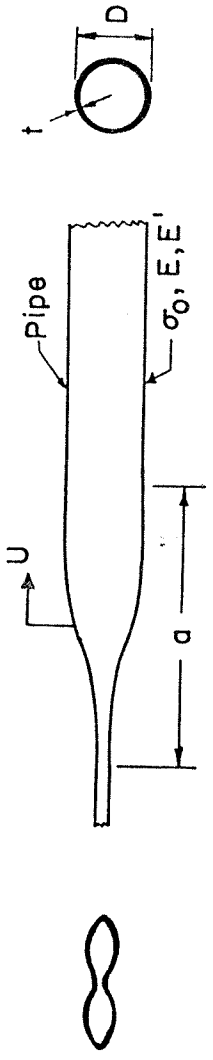

FIG. 3.1 DYNAMIC PROPAGATION-PROBLEM PARAMETERS

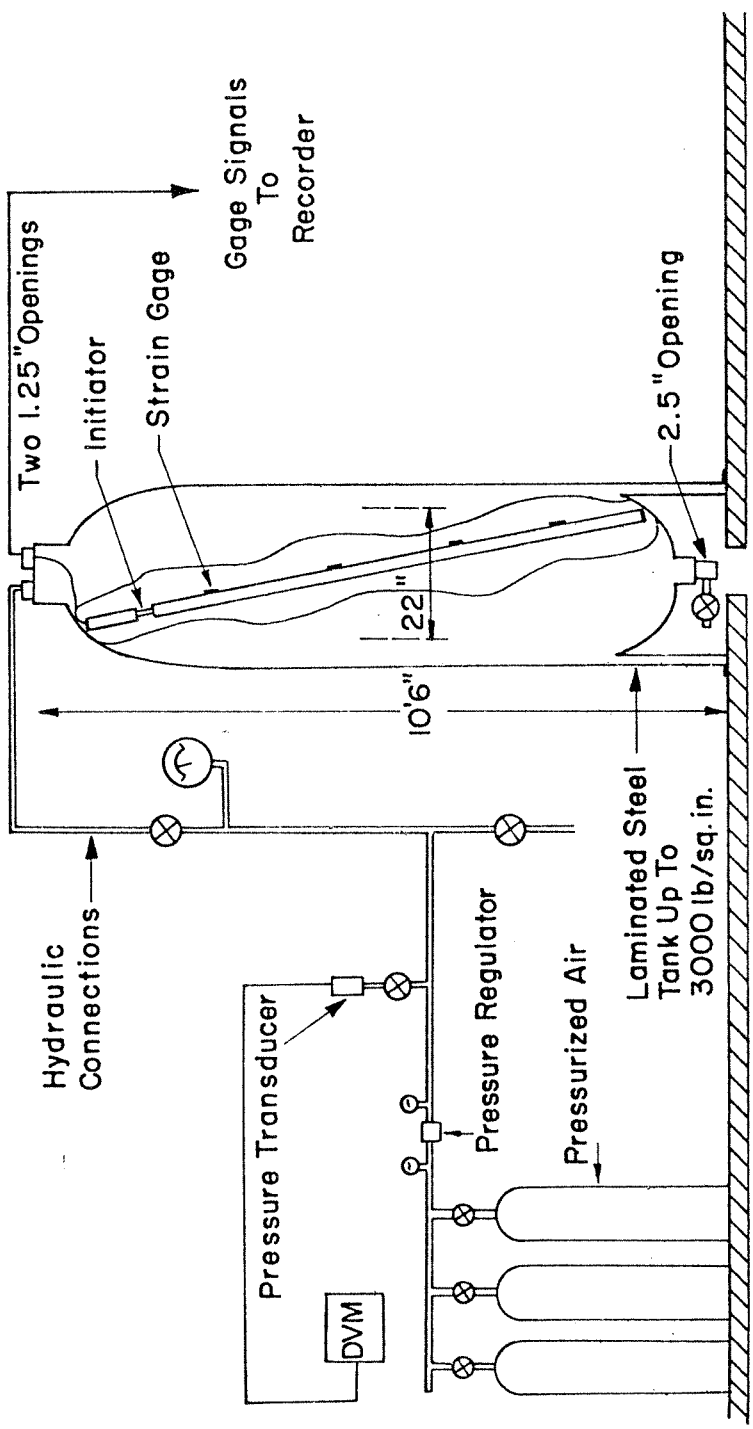

FIG. 3.2 HIGH PRESSURE TEST FACILITY

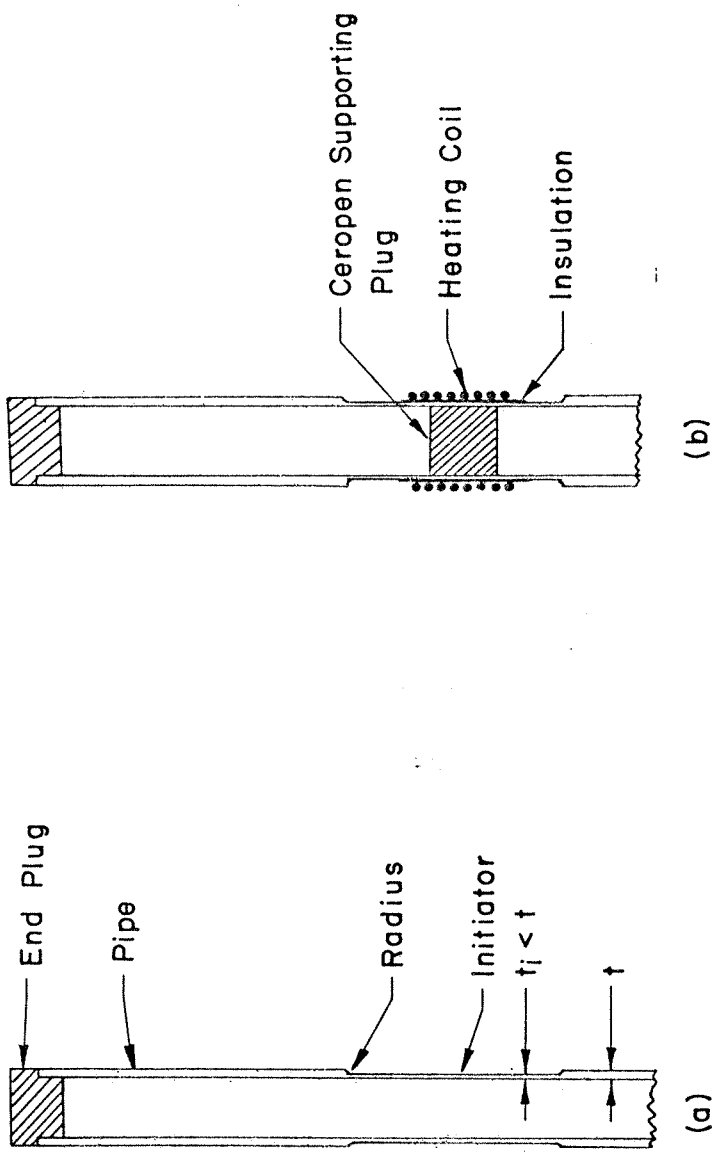

FIG. 3.3 DESIGN OF INITIATOR SECTION

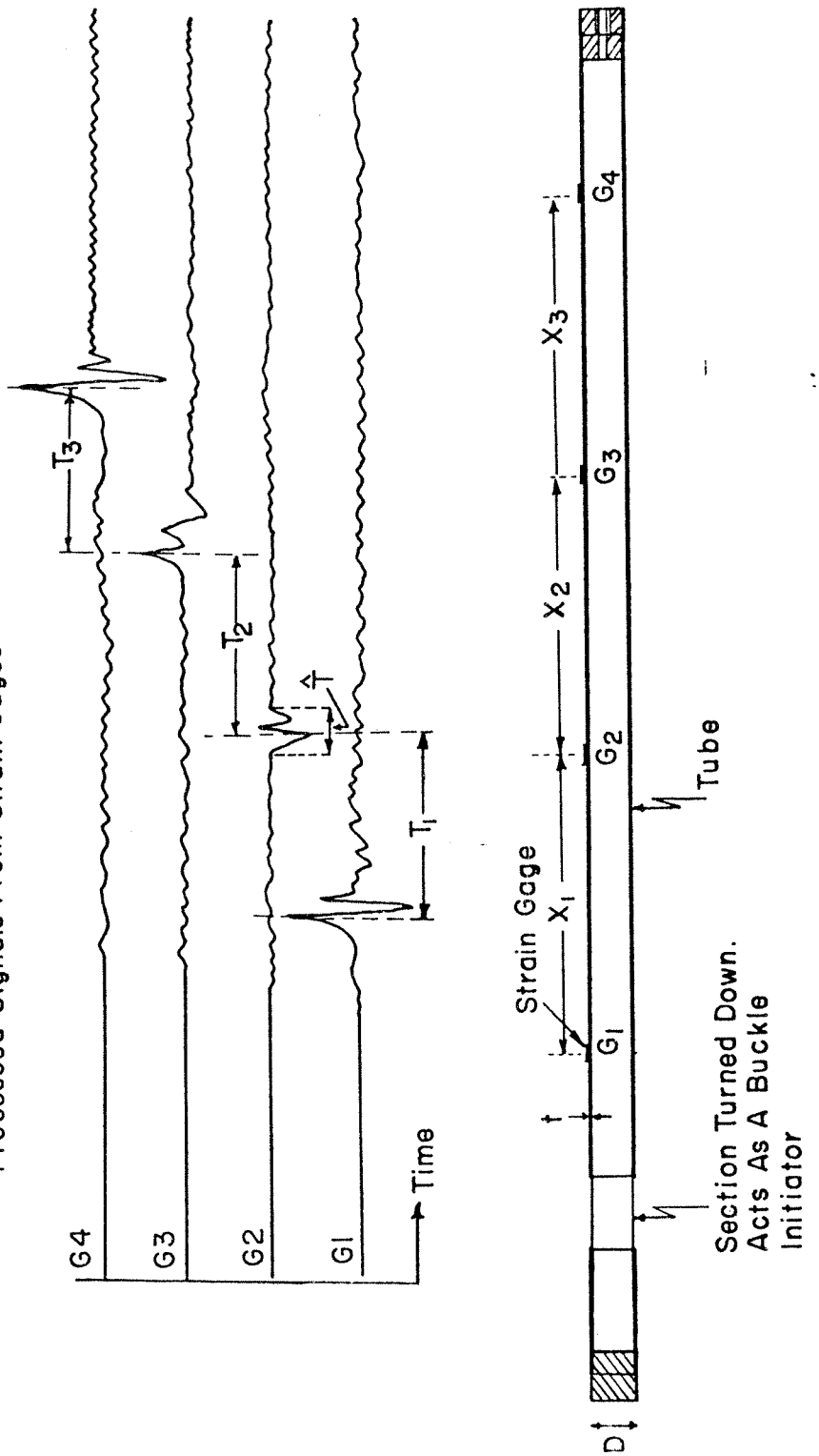

FIG.3.4 VELOCITY MEASUREMENT SCHEME

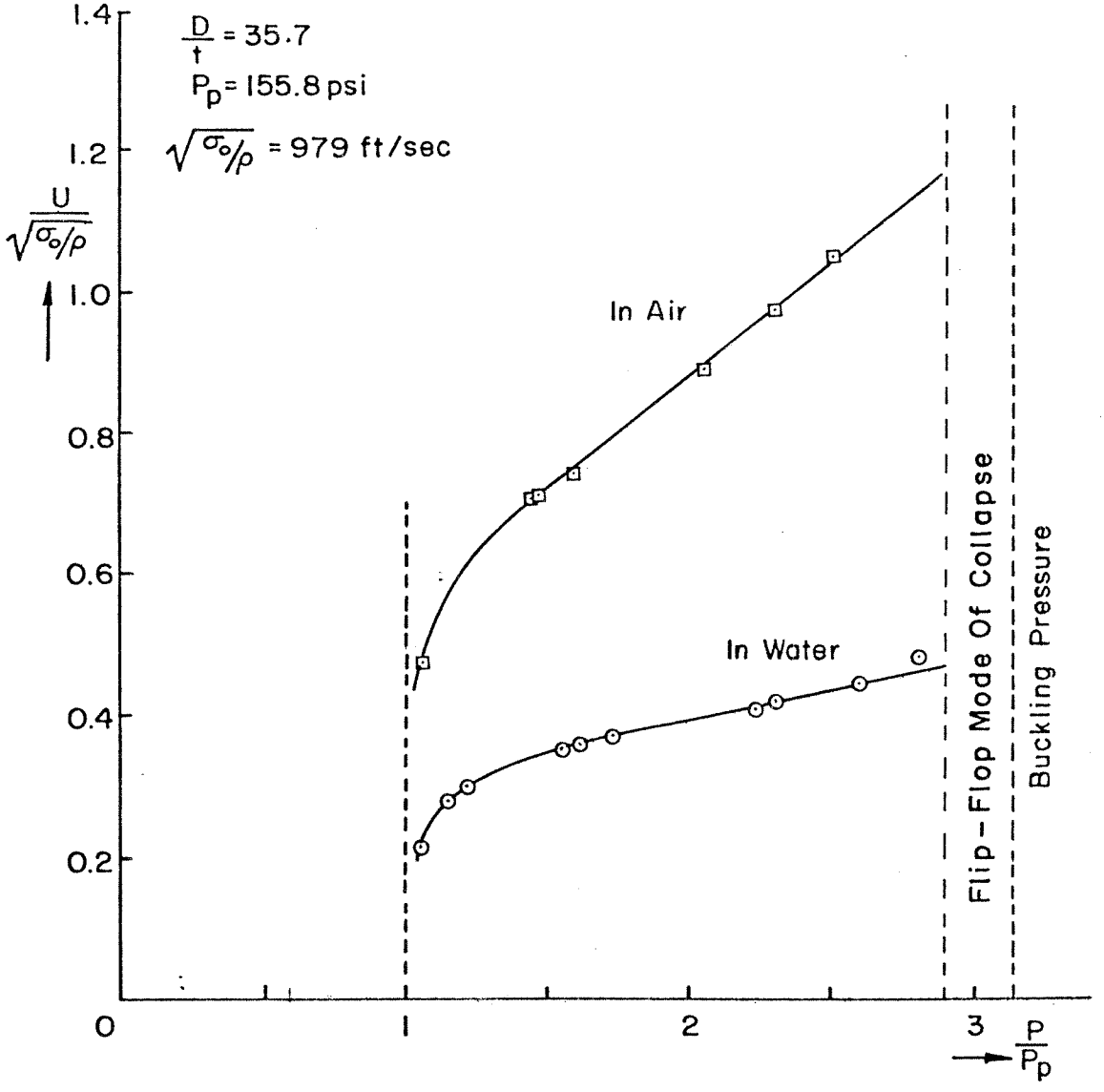

FIG.3.5PROPAGATING BUCKLE VELOCITY VS PRESSURE

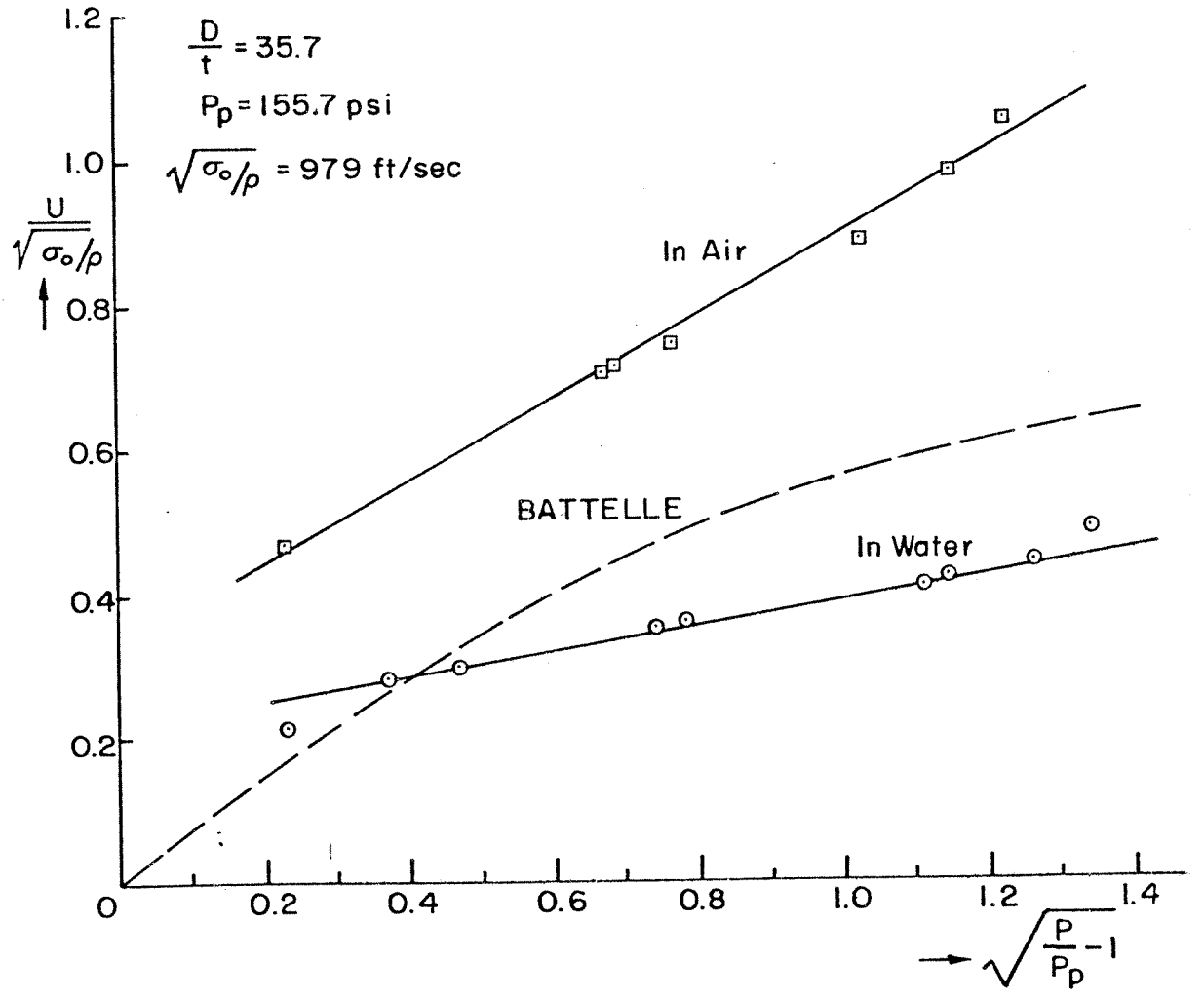

FIG.3.6 PROPAGATION VELOCITY VS PRESSURE PARAMETER

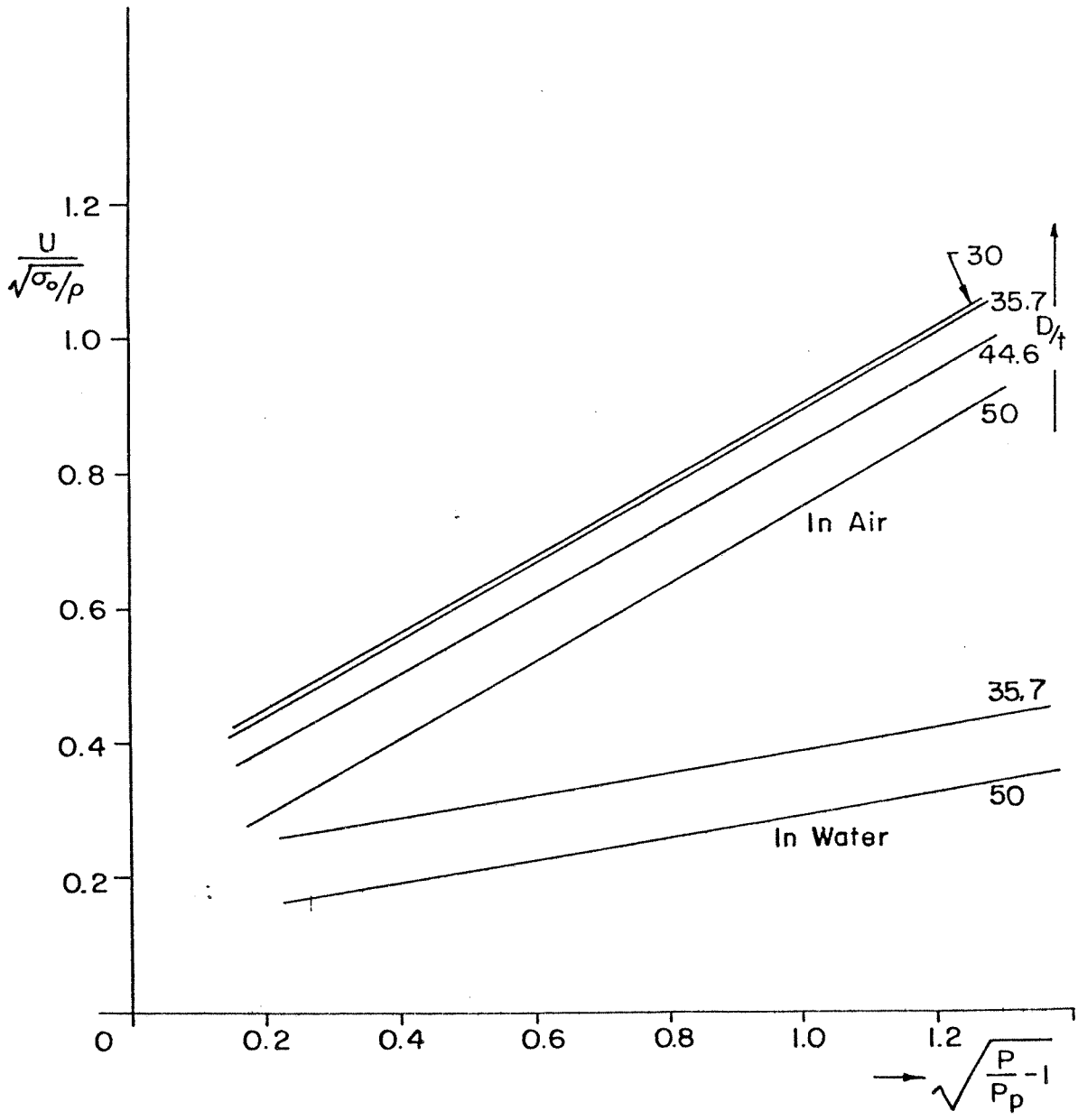

FIG.3.7 PROPAGATION VELOCITY FOR DIFFERENT D/t

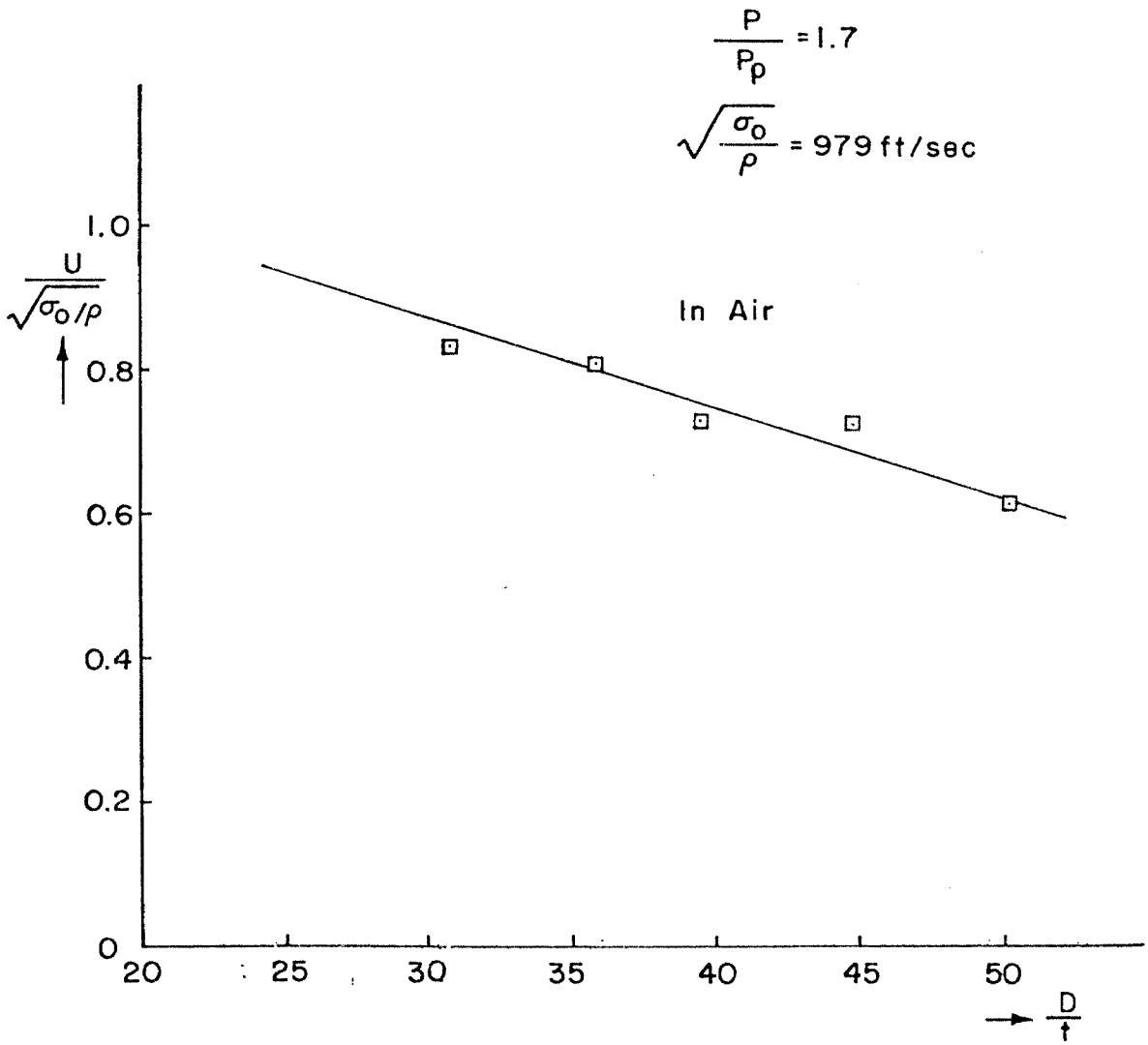

FIG. 3.8 PROPAGATION VELOCITY AS A FUNCTION OF PIPE GEOMETRIC PARAMETERS

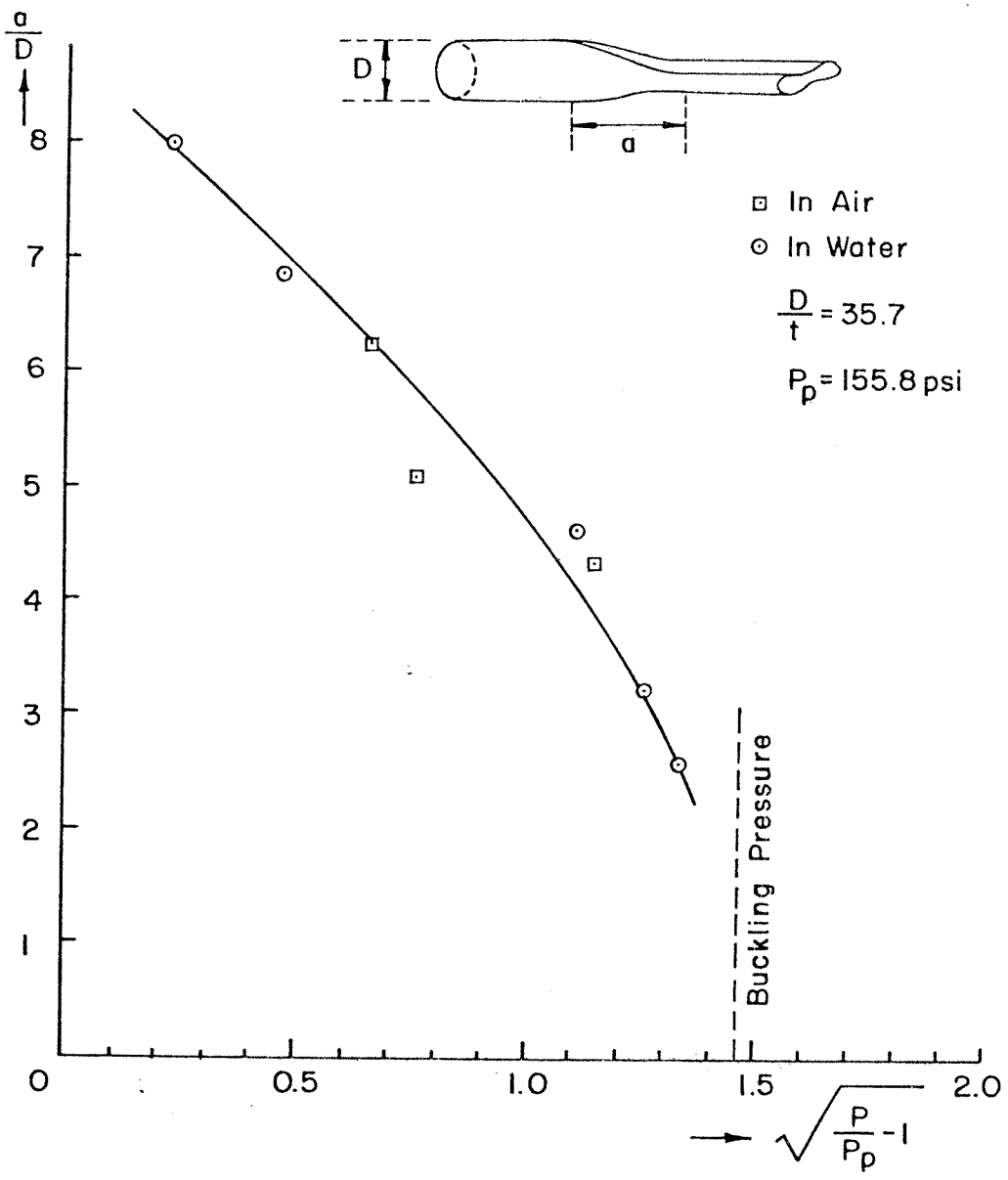

FIG.3.9 BUCKLE PROFILE LENGTH VS PRESSURE

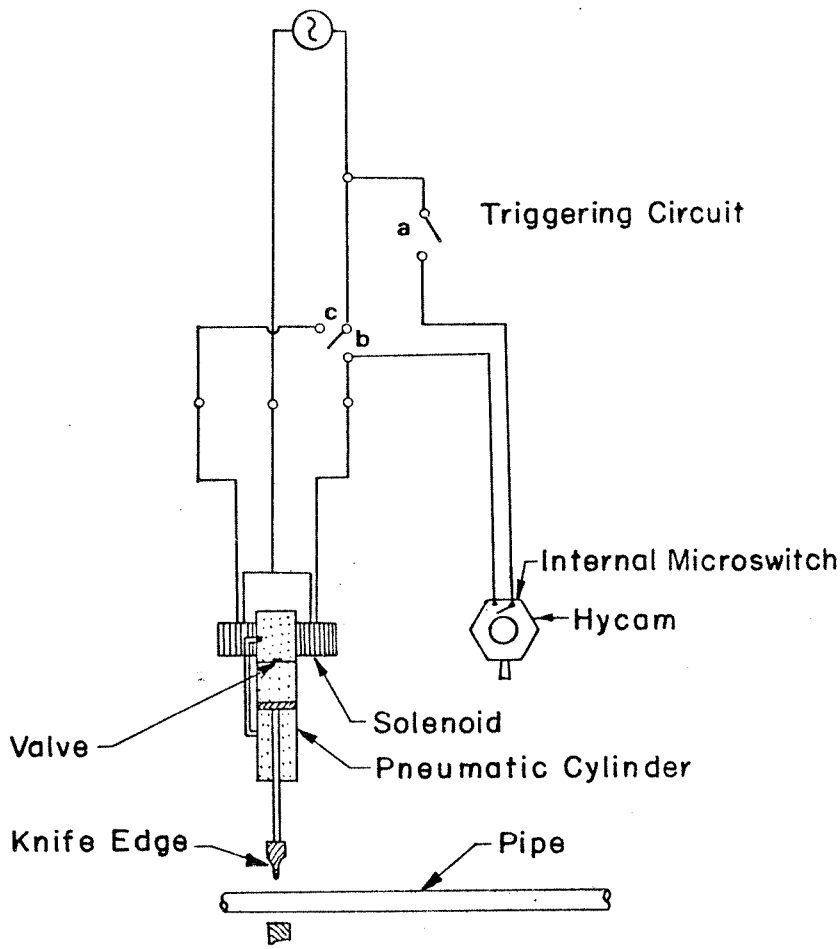

FIG.3.10TRIGGERING CIRCUIT AND SOLENOID OPERATED PNEUMATIC CYLINDER USED FOR INITIATING BUCKLE

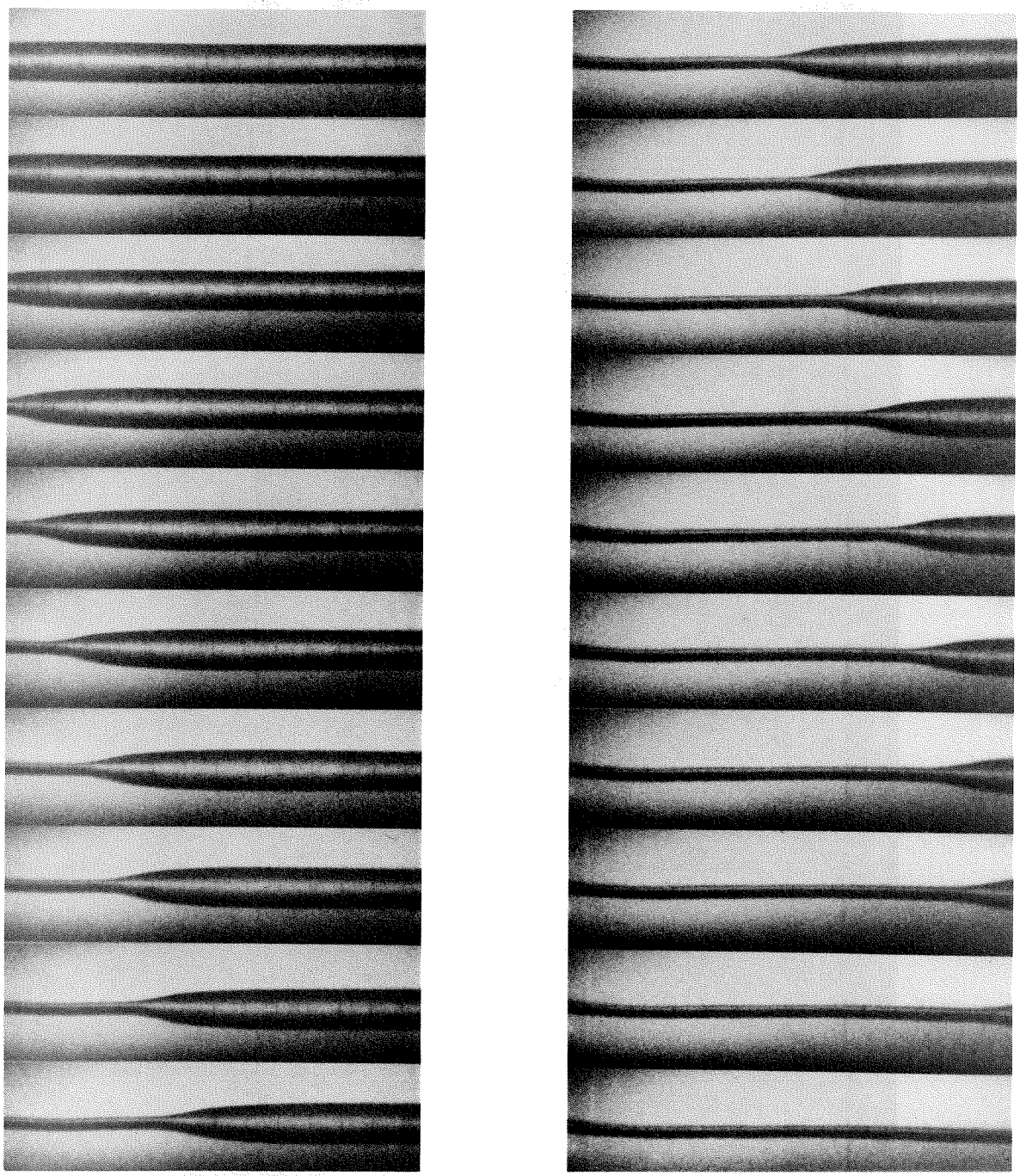

FIG. 3.11
DYNAMIC BUCKLE PROPAGATION--FRONT VIEW
(4500 fr/sec, P/P_c = .902, U = 372 ft/sec, Water)

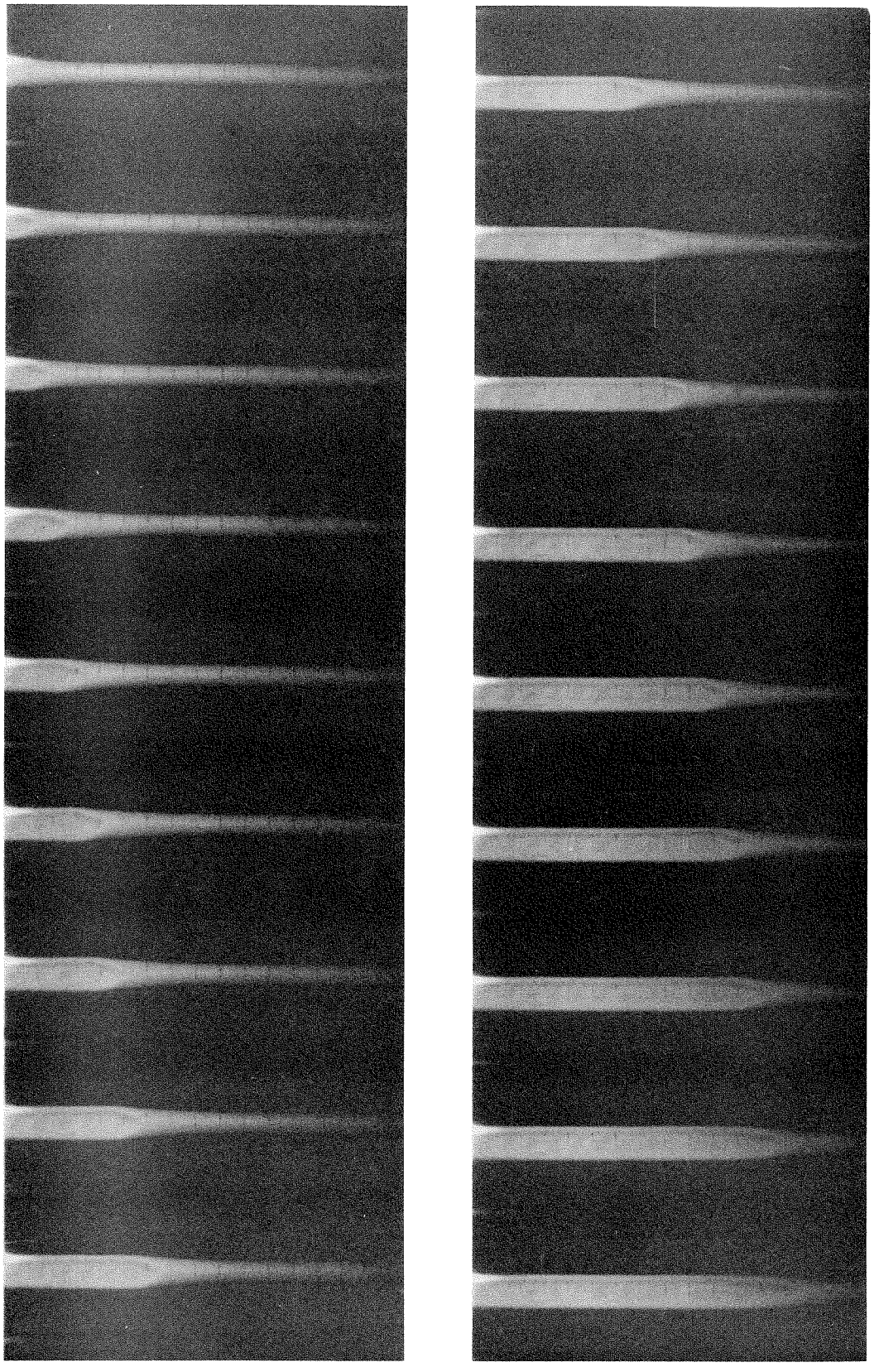

FIG. 3.12
DYNAMIC BUCKLE PROPAGATION--PLANE VIEW
(11,500 ft/sec, P/P_c = .890, U = 726 ft/sec, Air)

	D mm (in)	t mm (in)	D/t	P_p* bar (psi)	P_c bar (psi)
1	38.1 (1.50)	1.27 (.050)	30.0	15.5 (225)	62.2 (902)
2	31.8 (1.25)	0.89 (.035)	35.7	10.8 (156)	33.7 (488)
3	31.8 (1.25)	0.74 (.029)	44.6	6.55 (95)	20.4 (296)
4	25.4 (1.00)	0.51 (.020)	50.0	4.97 (72)	12.9 (187)

TABLE 3.1 PROPERTIES OF PIPE USED IN DYNAMIC PROPAGATION EXPERIMENTS

* Experimental Results

$E = 6.90 \times 10^5$ bar $(10 \times 10^6$ PSI) $\nu = 0.3$

$\sigma_0 = 2.41 \times 10^3$ bar $(35 \times 10^3$ PSI)

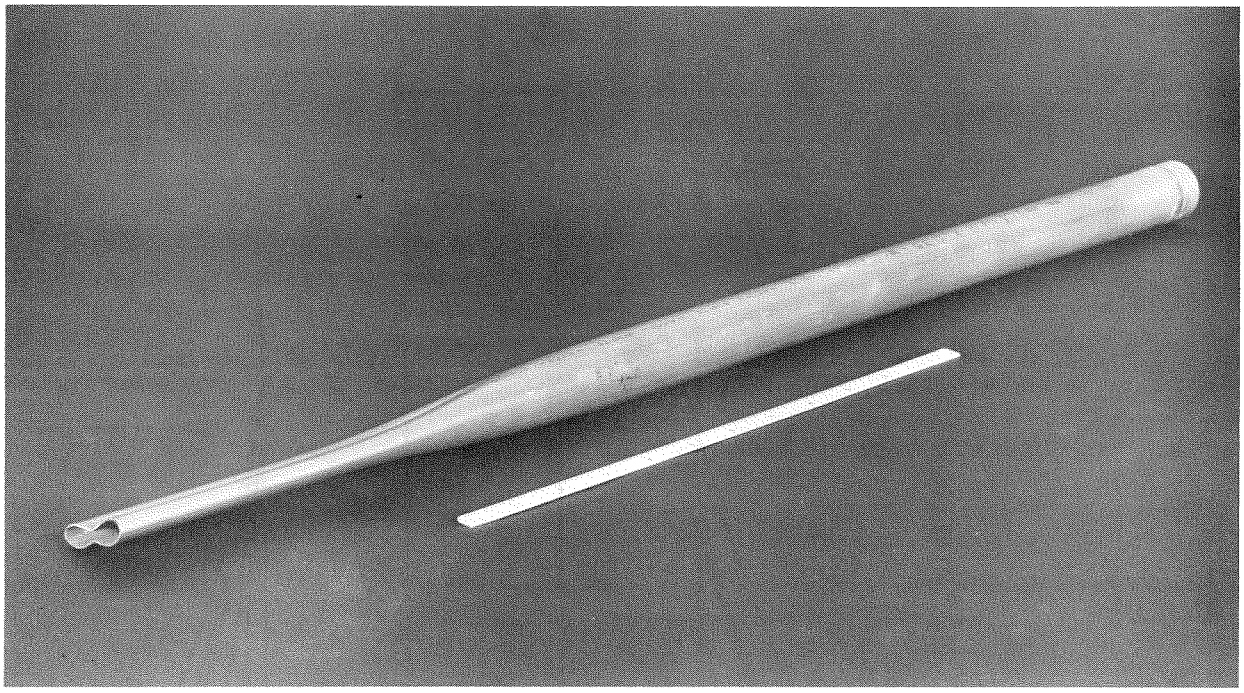

Fig. 4.1a A buckle that propagated and then came to a stop. Note the "dogbone" collapse mode.

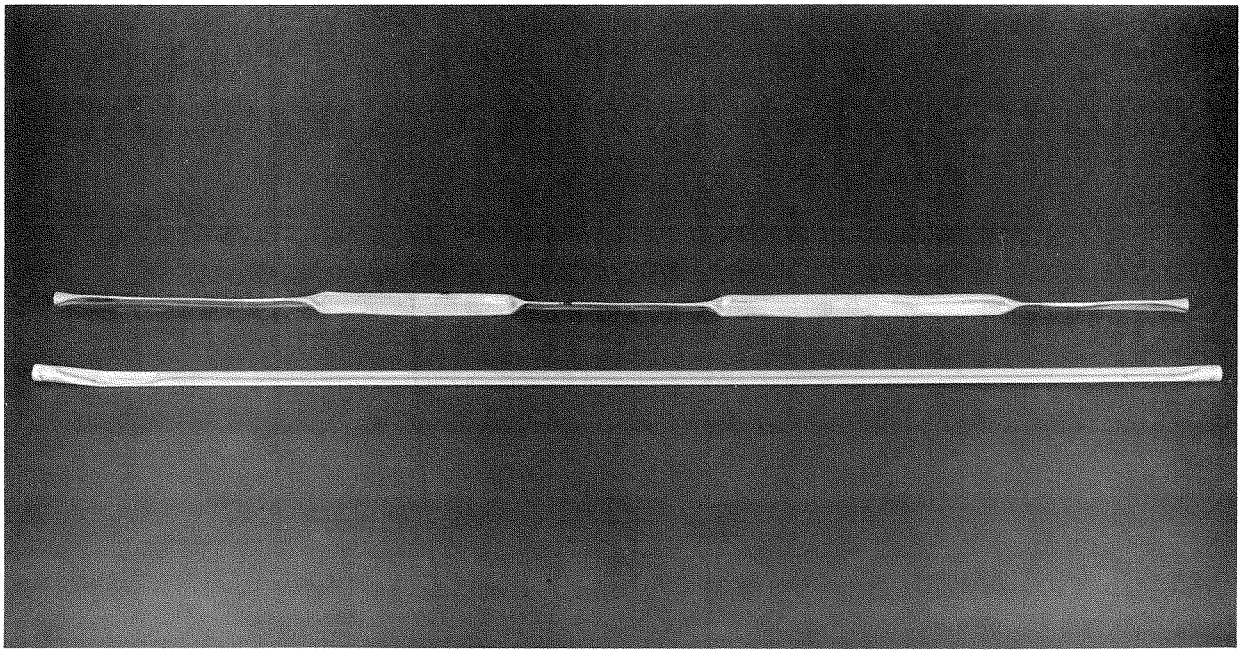

Fig. 4.1b The "flip-flop" compared to the normal collapse mode.

FIG. 4.2 PIPE OVALIZATION DUE TO LOCAL INDENDATION

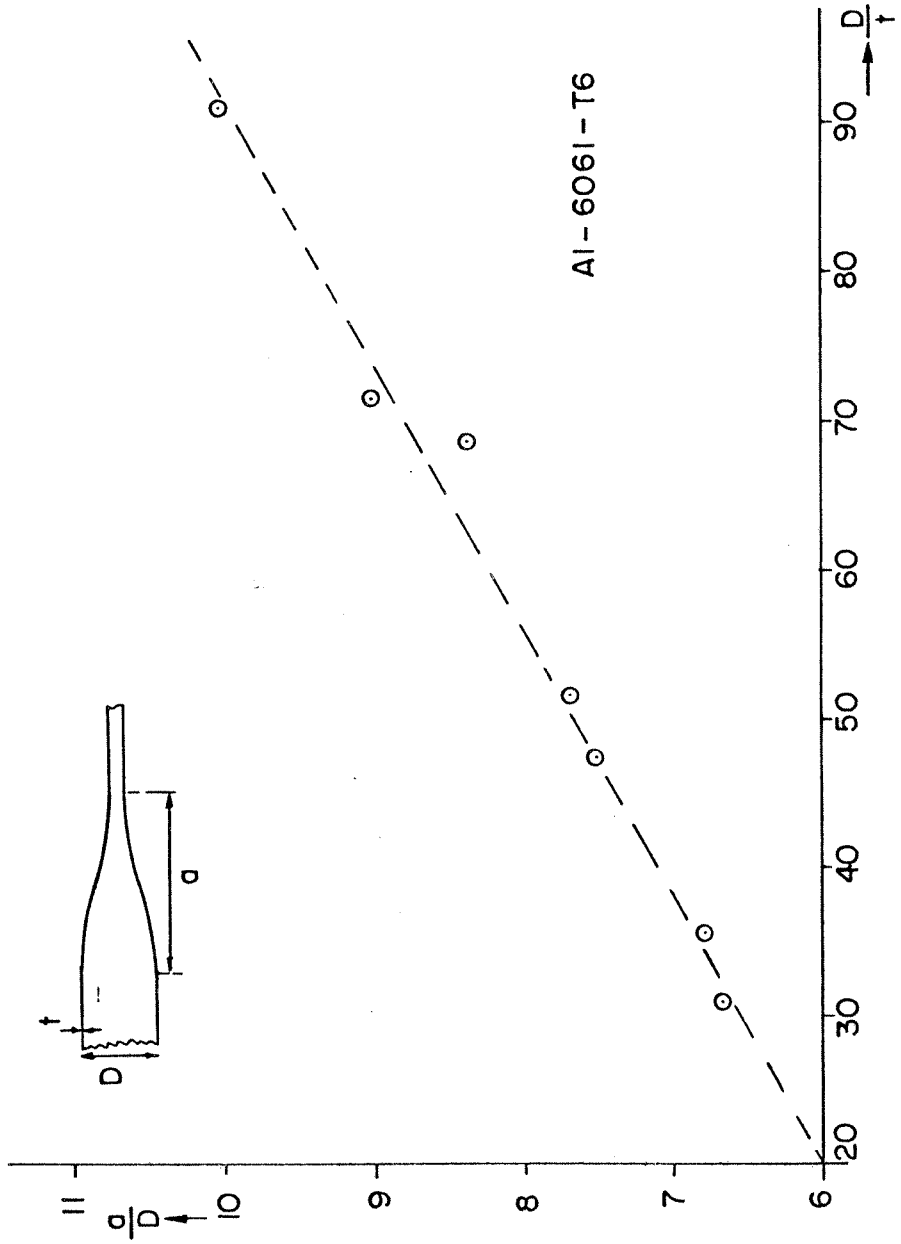

FIG.4.3 VARIATION OF PROFILE LENGTH WITH D/t

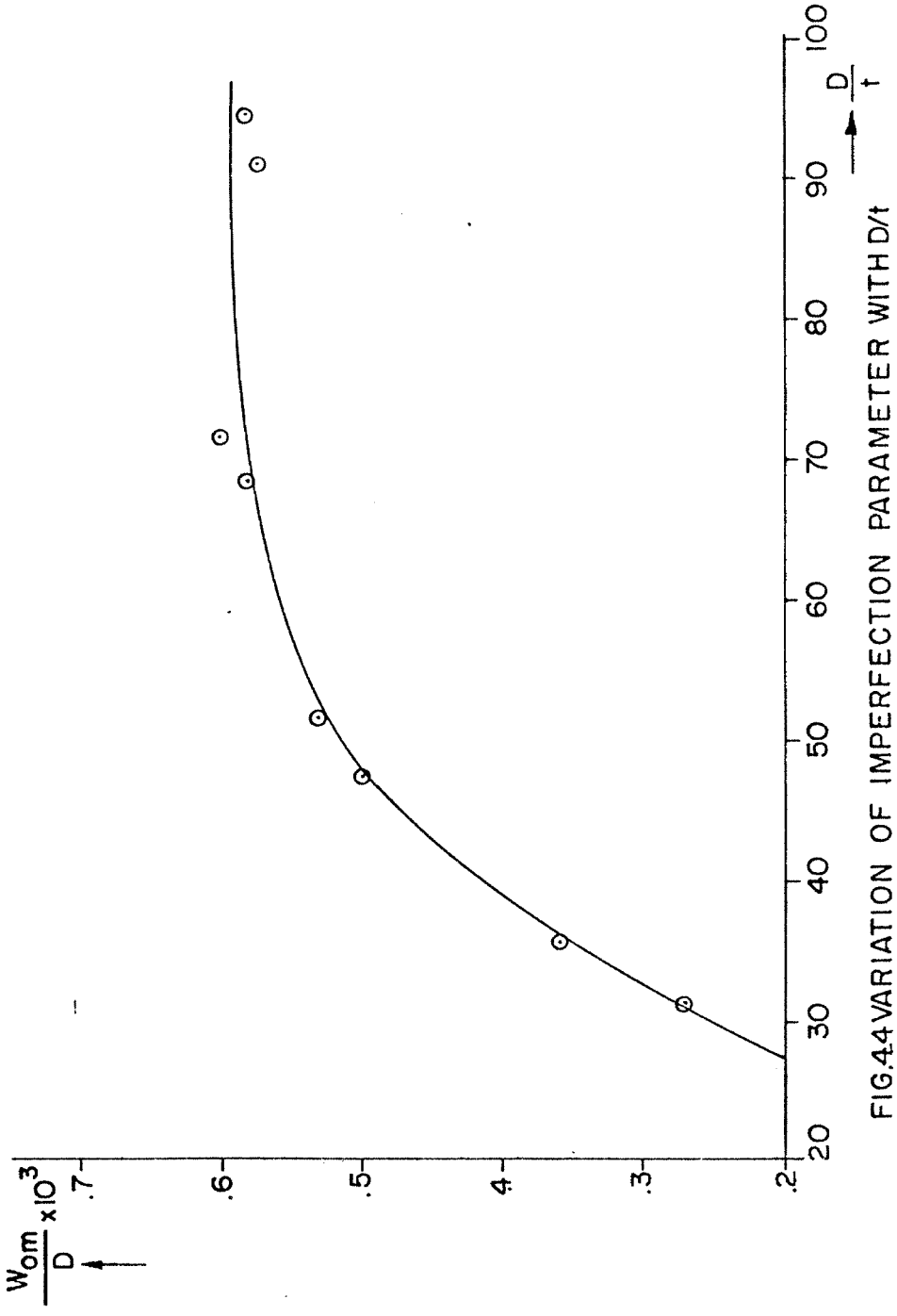

FIG.4.4 VARIATION OF IMPERFECTION PARAMETER WITH D/t

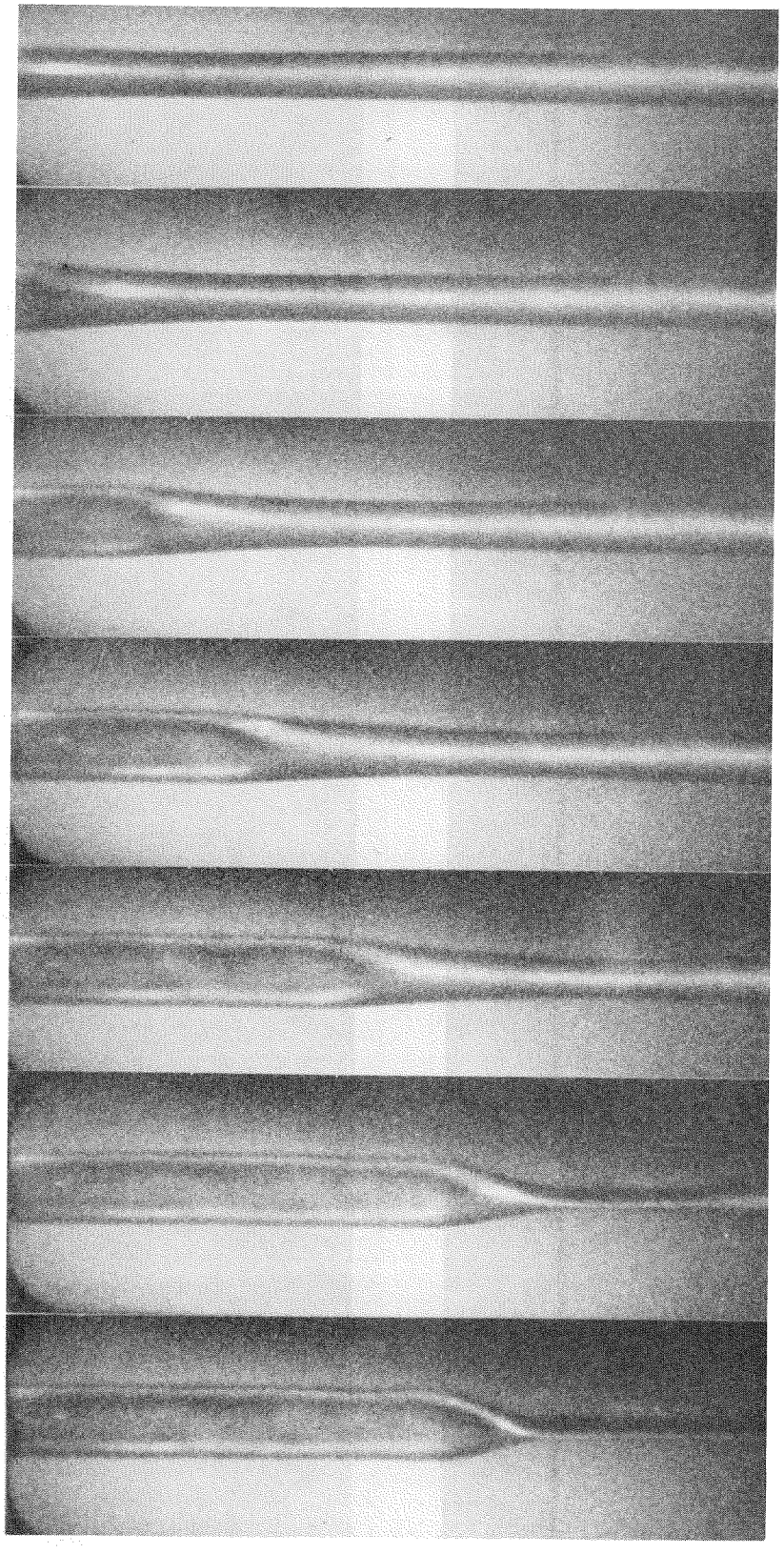

FIG. 4.5 FLIP-FLOP MODE OF COLLAPSE
(4000 fr/sec, P/P_c = .934, U = 790 ft/sec, Air)

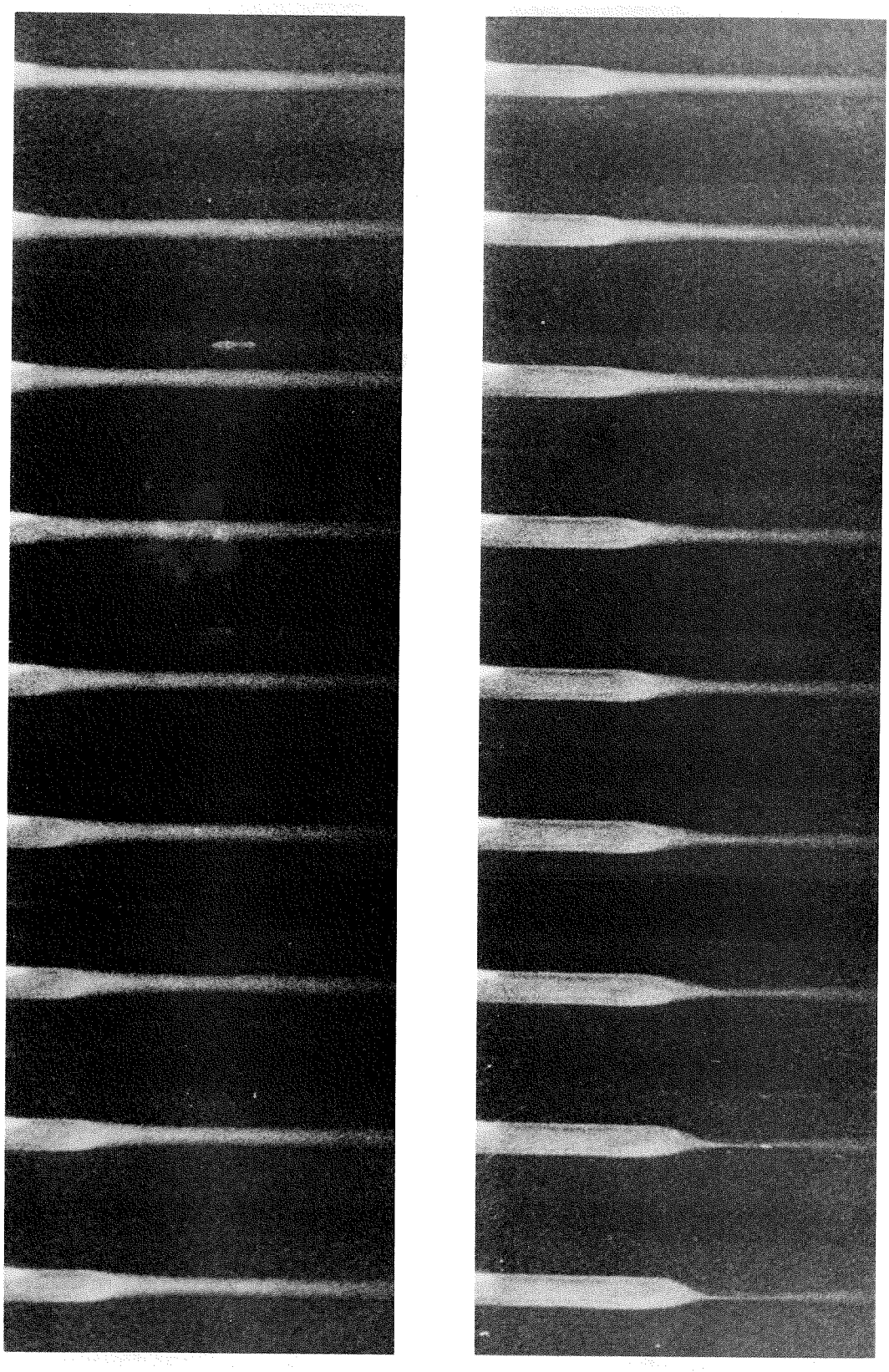

FIG. 4.6
FLIP-FLOP MODE OF COLLAPSE
(15,000 fr/sec, P/P_c = .934, U = 850 ft/sec, Air)

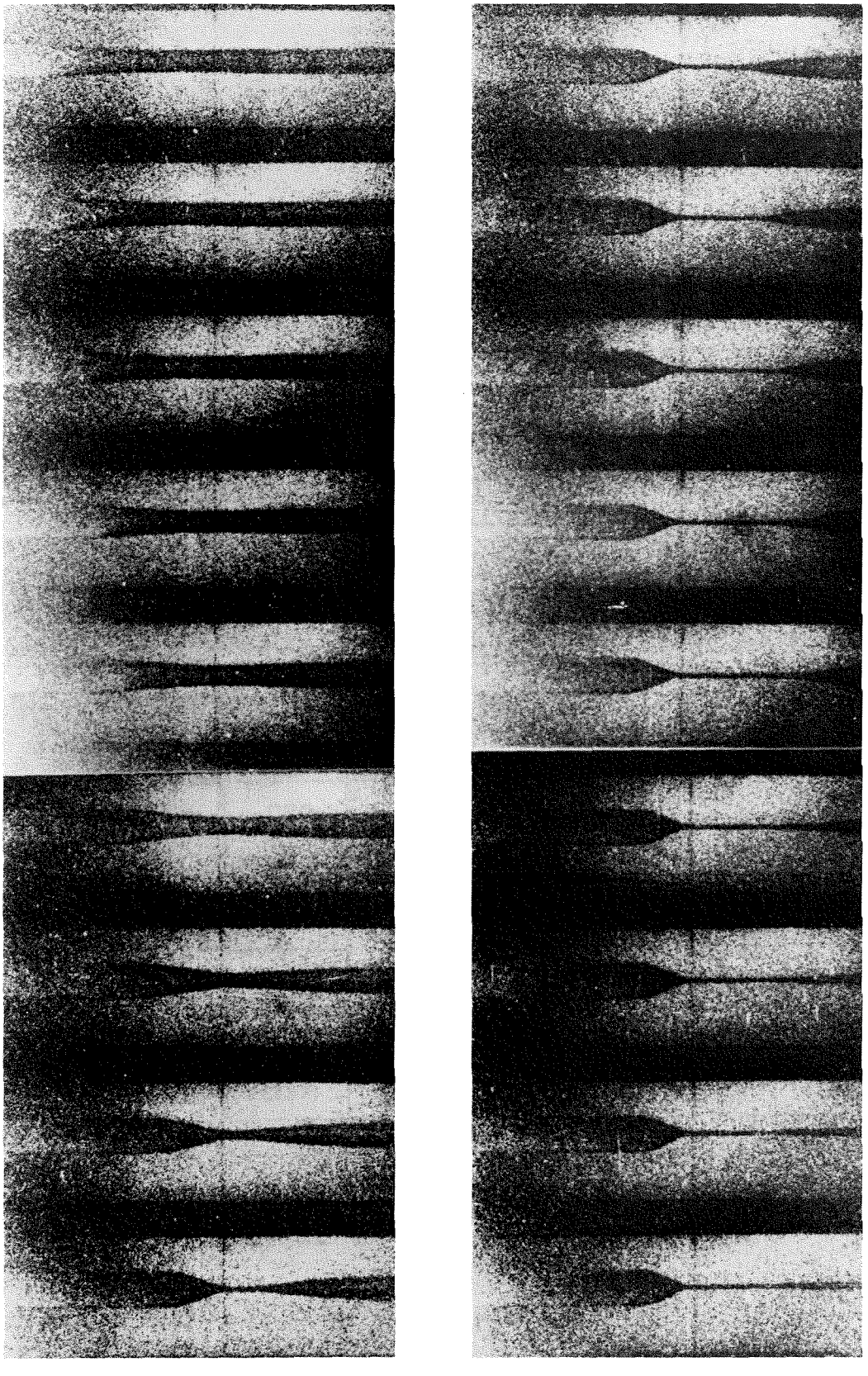

FIG. 4.7
FLIP-FLOP MODE OF COLLAPSE
(13,000 fr/sec, P/P_c = .925, Air)

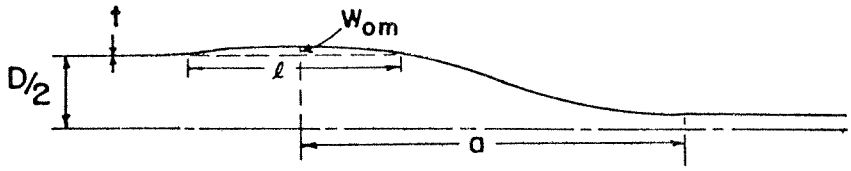

D in (mm)	t in (mm)	D/t	ℓ/D	a/D	W_{om}/D
1.126 (28.6)	.036 (.914)	31.3	4.9	7.6	.0027
1.250 (31.8)	.035 (.885)	35.7	6.0	8.0	.0036
1.001 (25.4)	.022 (.559)	47.7	10.0	9.0	.0050
1.500 (38.1)	.029 (.737)	51.7	6.0	9.3	.0053
1.375 (34.9)	.020 (.508)	68.7	8.0	10.5	.0038
2.500 (63.5)	.035 (.889)	71.4	4.5	11.2	.0060
2.003 (50.9)	.022 (.559)	91.1	7.7	12.7	.0057
1.741 (44.2)	.029 (.737)	94.5	7.3	10.2	.0058

TABLE 4.1 MEASURED DIMENSIONS OF PROFILE OF PROPAGATING BUCKLE

D (in) mm	t (in) mm	D/t	$\frac{P_{ff}}{P_c}$	$\frac{P_{ff}^*}{P_c}$
1.25 (31.8)	.035 (.89)	35.7	.887	.941 .961 .995
1.00 (25.4)	.021 (.51)	47.6	.875	.909 .934 .953

$E = 10^7$ PSI

$\sigma_0 = 42{,}000$ PSI

* Experimental Pressures At Which Flip-Flop Was Observed

TABLE 4.2 FLIP-FLOP EXPERIMENTS

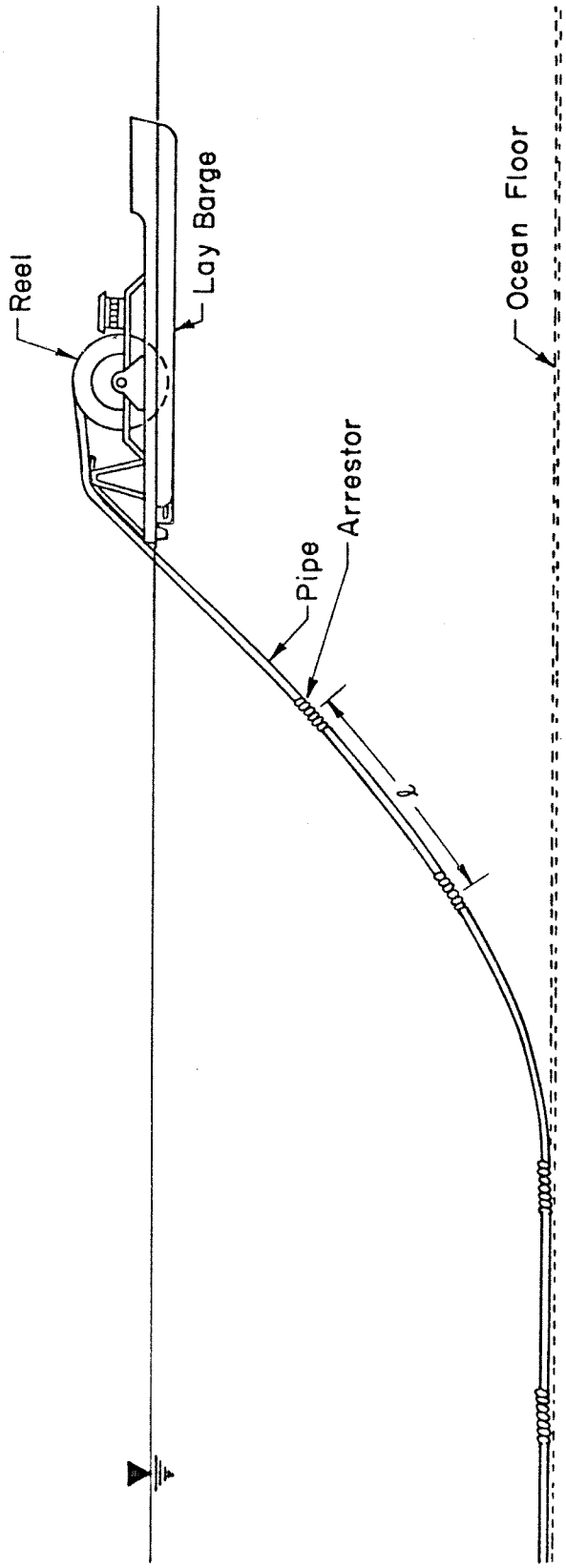

FIG.5.1 PIPE LAYING OPERATION OFF A REEL LAY BARGE

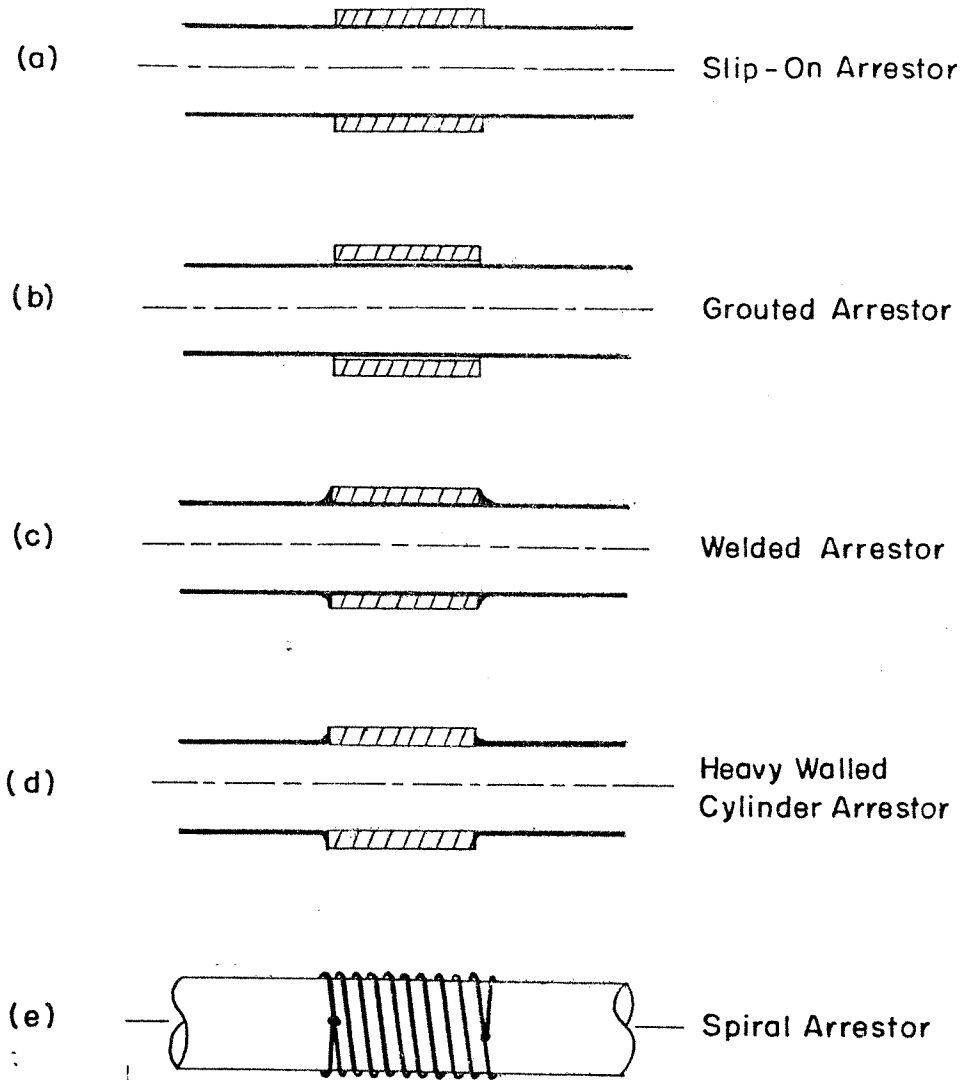

FIG.5.2 DIFFERENT ARRESTOR DESIGNS

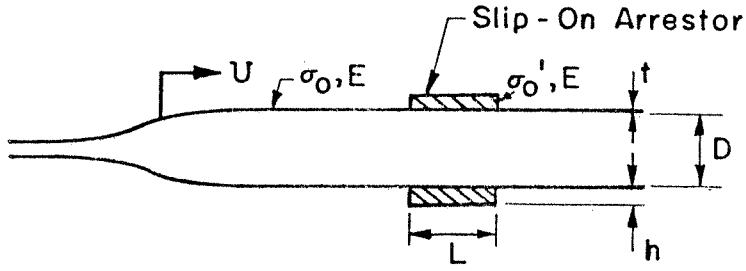

FIG.5.3 PROBLEM PARAMETERS

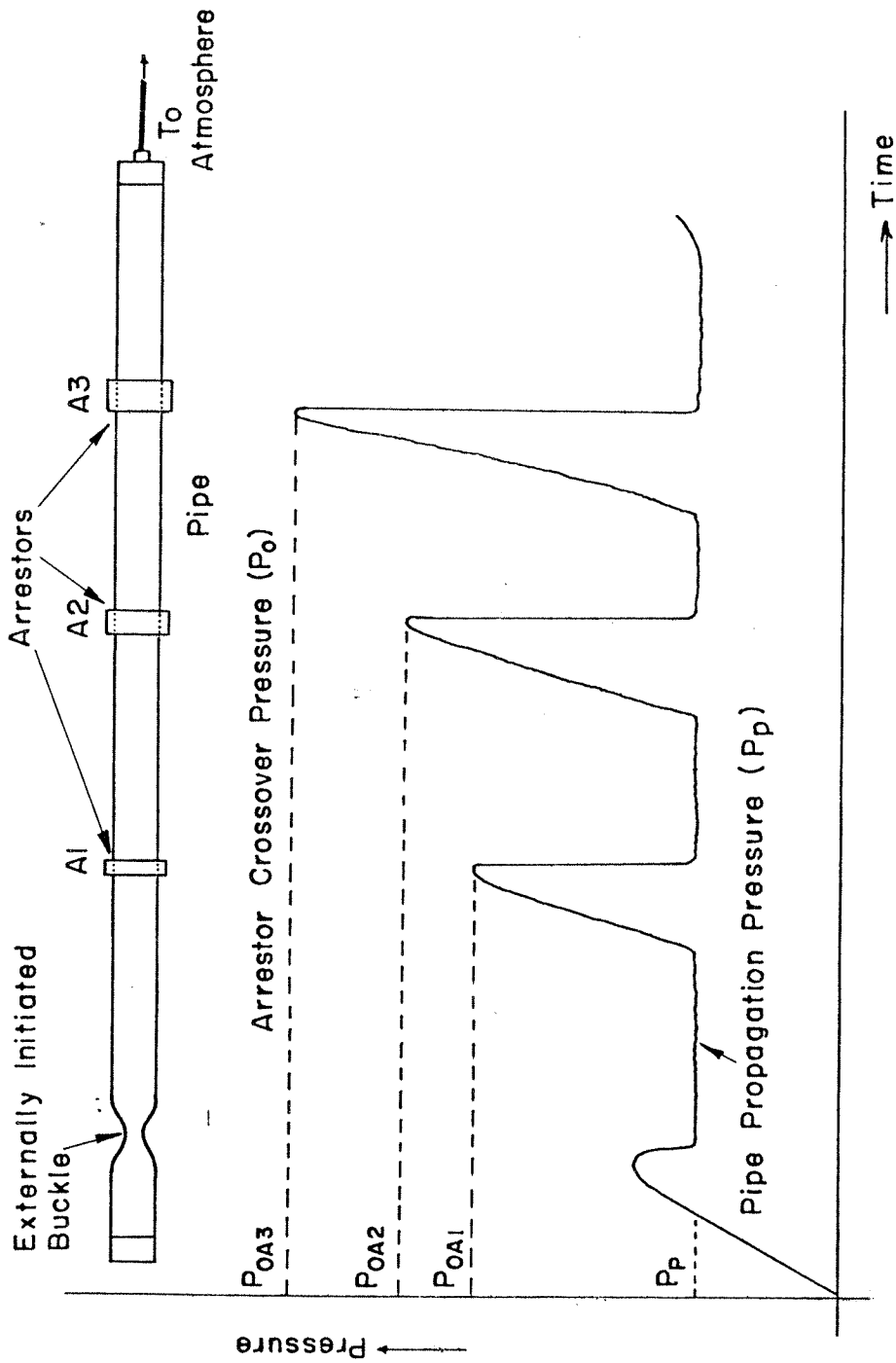

FIG.5.4 SCHEMATIC OF EXPERIMENTAL DETERMINATION OF ARRESTOR CROSSOVER PRESSURE

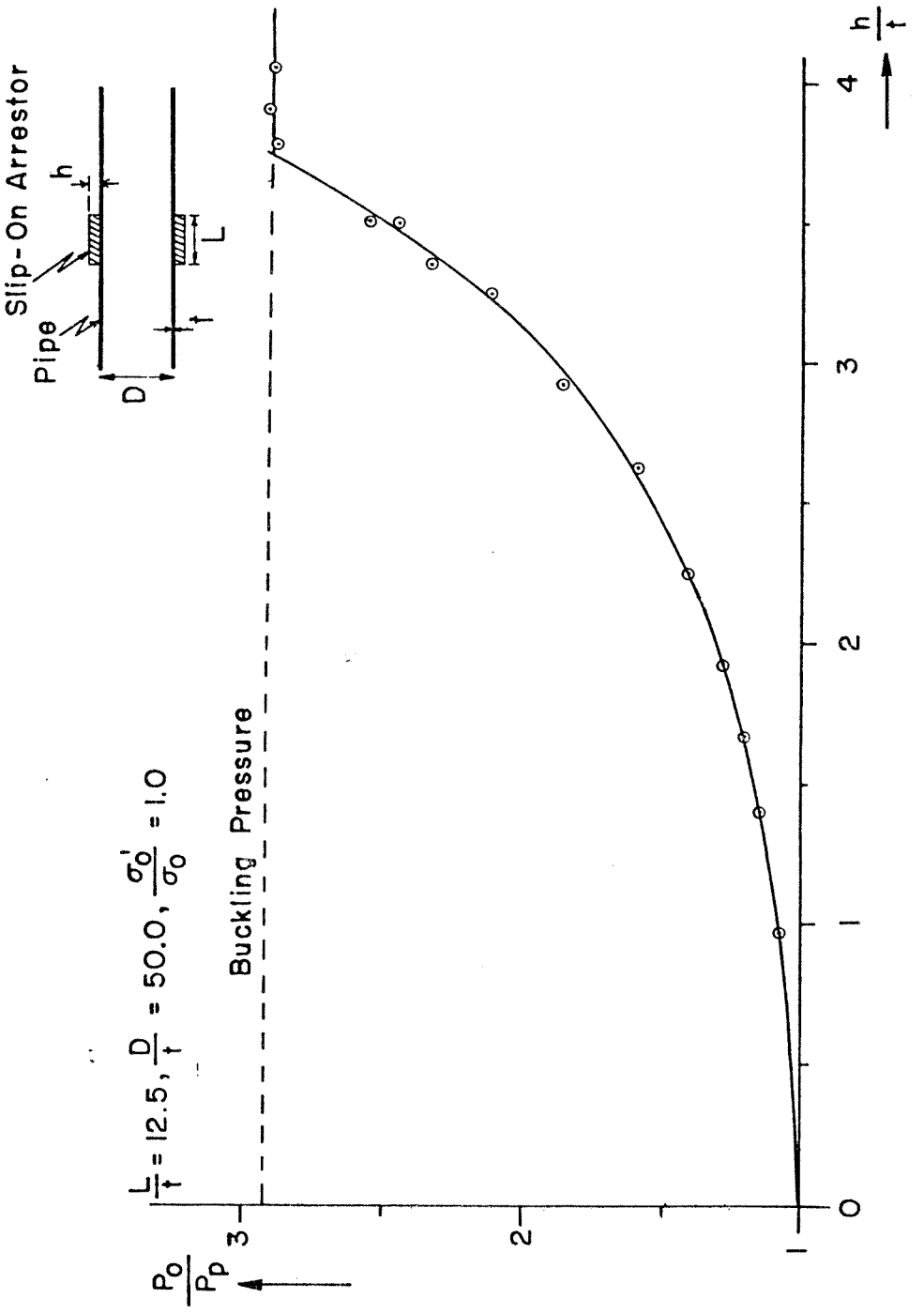

FIG.5.5 VARIATION OF CROSSOVER PRESSURE WITH ARRESTOR THICKNESS

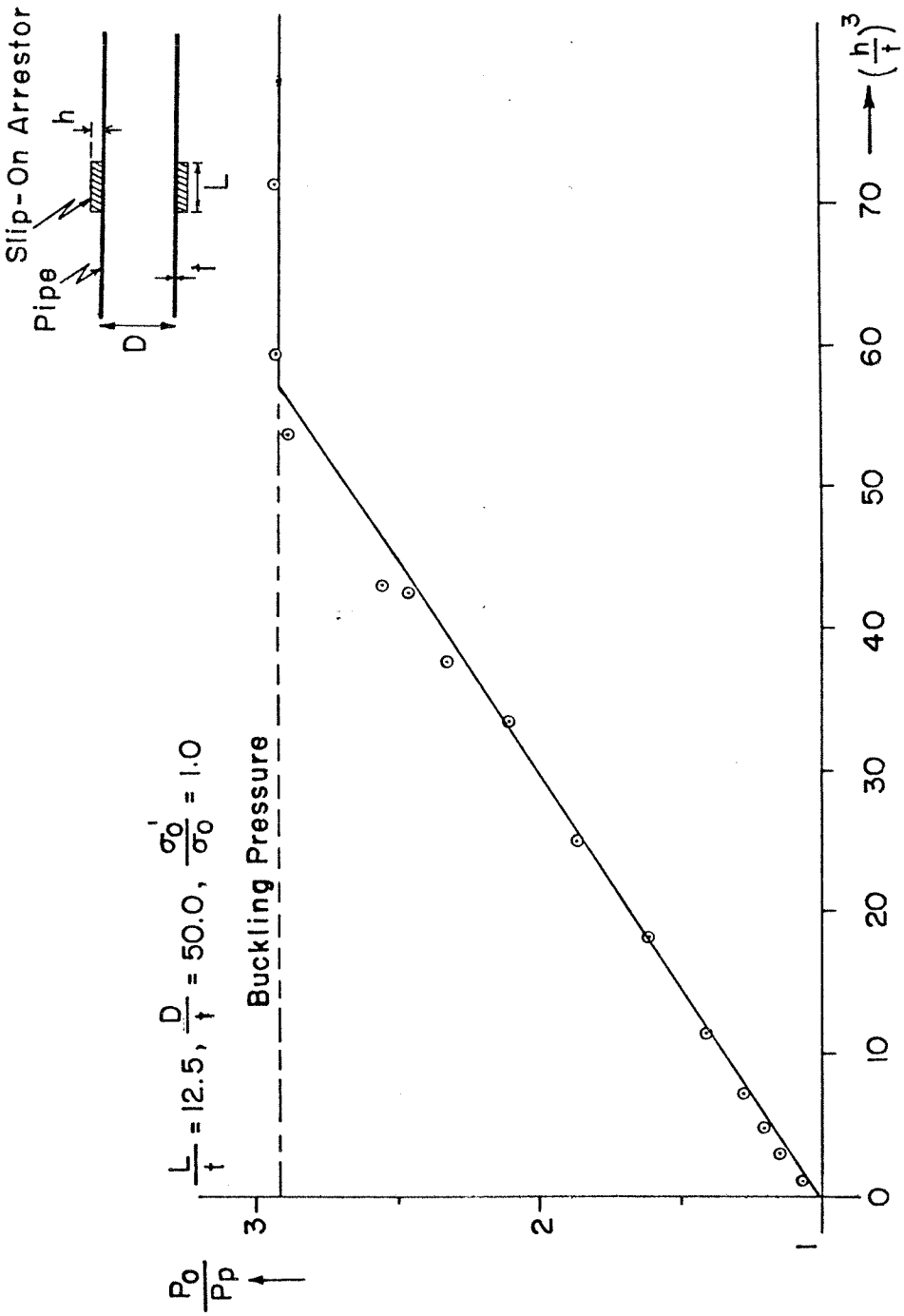

FIG.5.6 VARIATION OF CROSSOVER PRESSURE WITH ARRESTOR THICKNESS PARAMETER

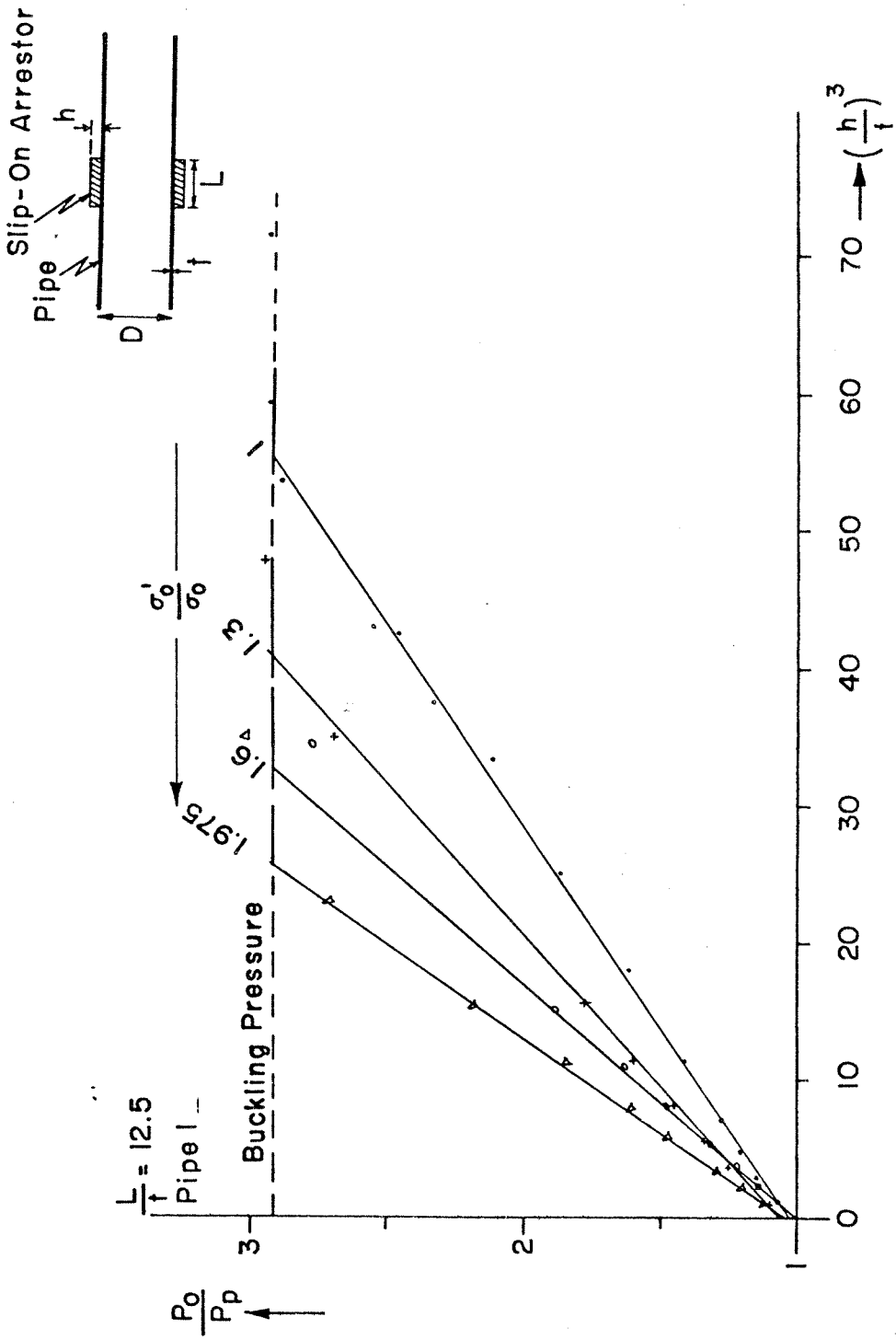

FIG.5.7 CROSSOVER PRESSURE VS THICKNESS PARAMETER FOR DIFFERENT YIELD STRESSES

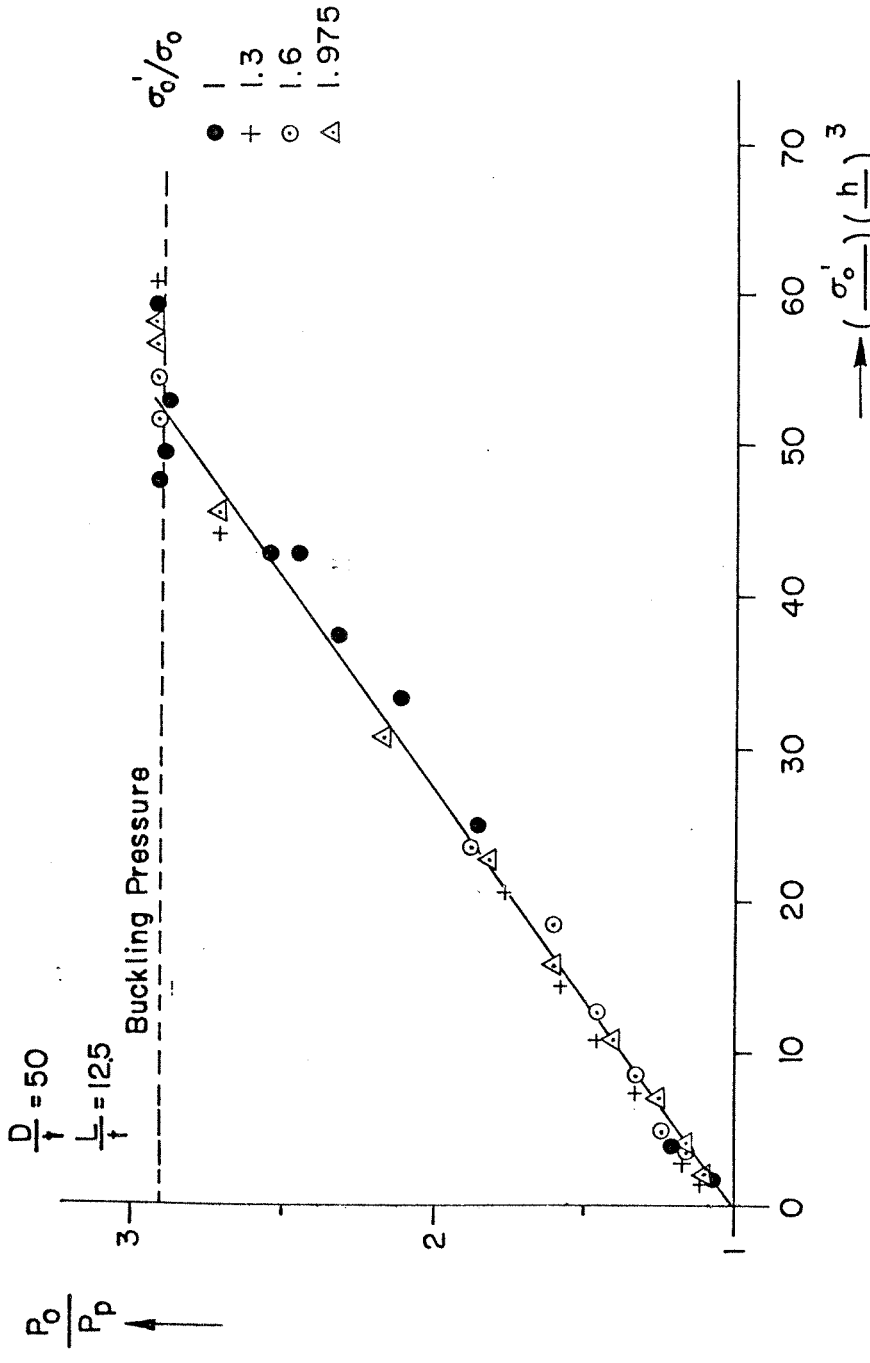

FIG.5.8 VARIATION OF CROSSOVER PRESSURE WITH ARRESTOR THICKNESS AND YIELD STRESS PARAMETERS

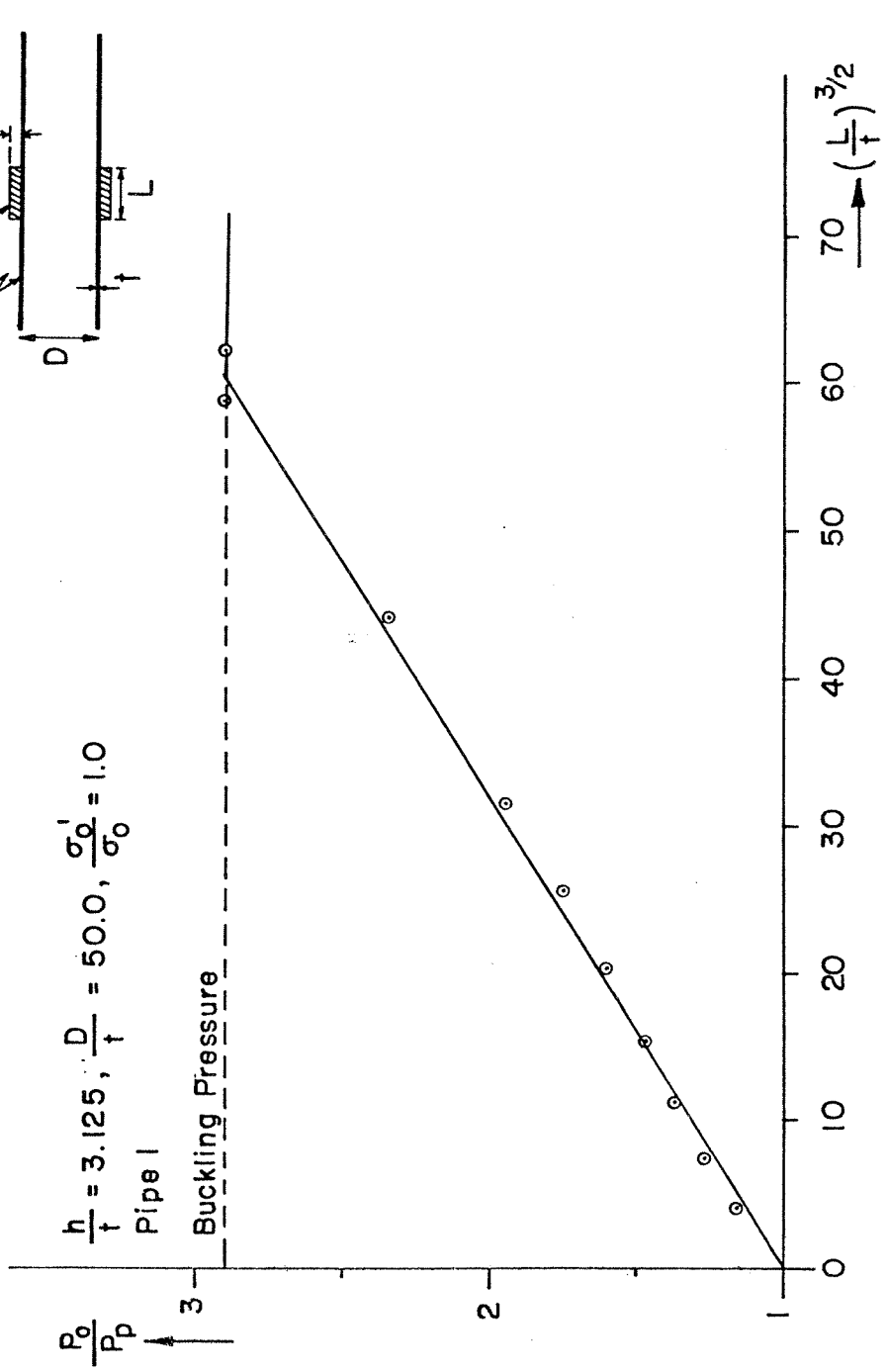

FIG.5.9 VARIATION OF CROSSOVER PRESSURE WITH ARRESTOR LENGTH PARAMETER

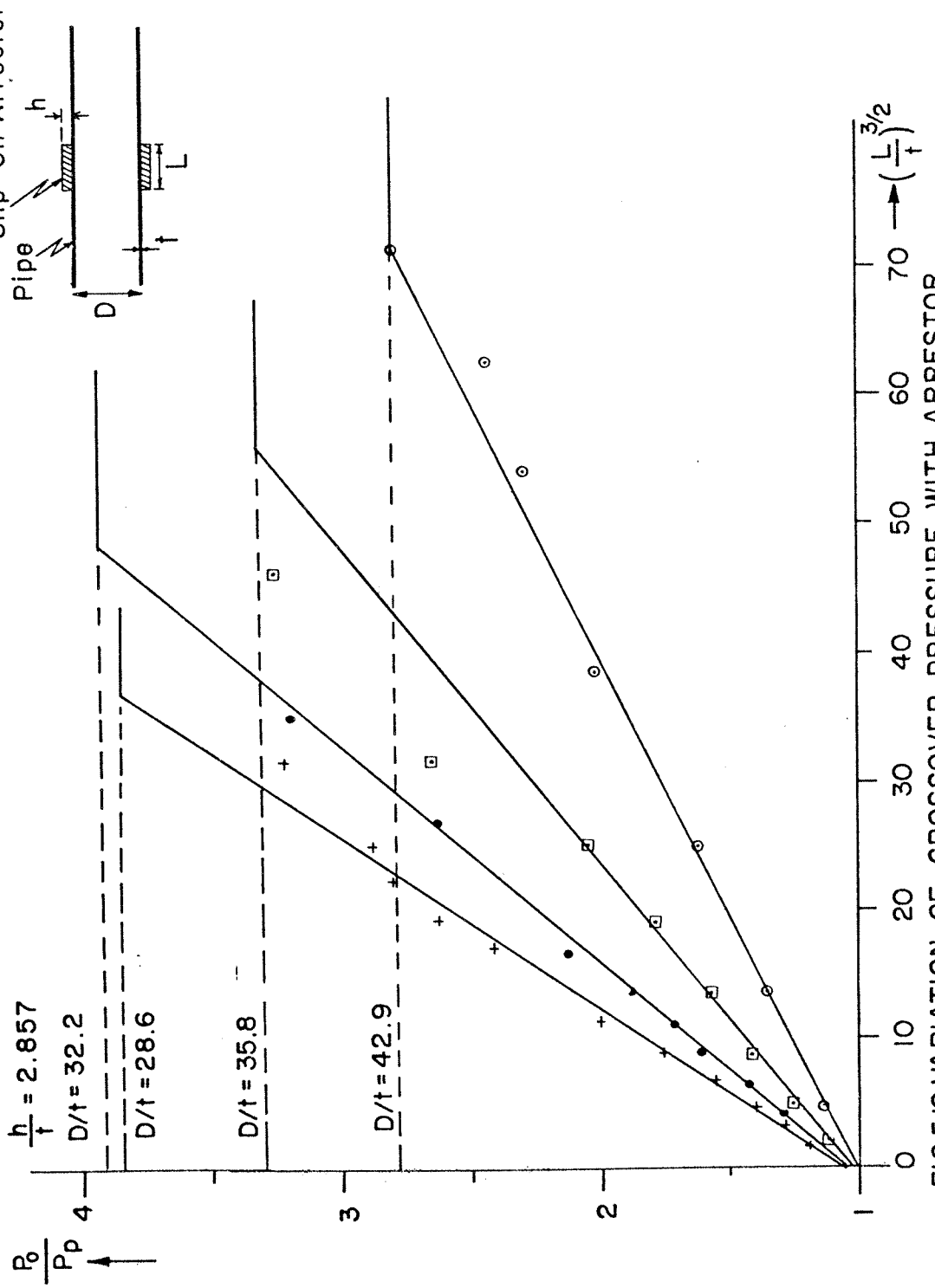

FIG.5.10 VARIATION OF CROSSOVER PRESSURE WITH ARRESTOR LENGTH FOR DIFFERENT PIPE DIMENSIONS

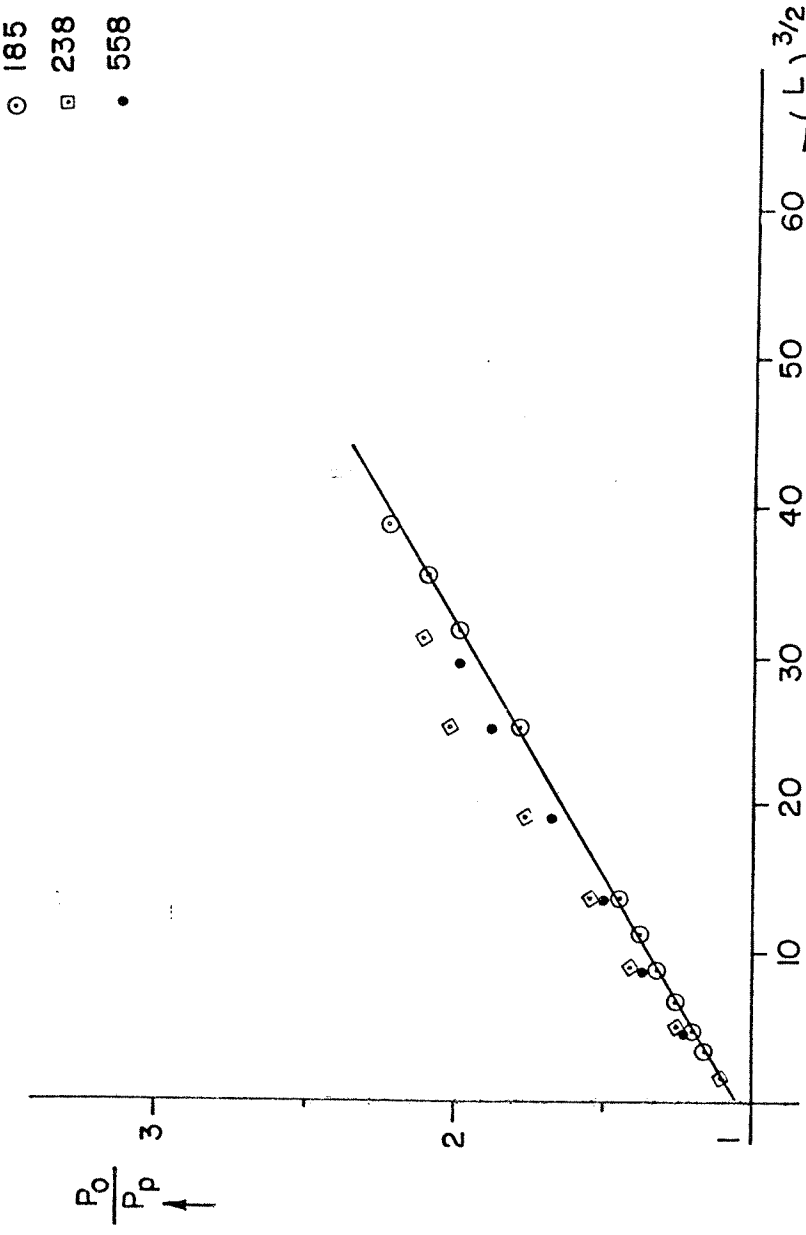

FIG.5.11 CROSSOVER PRESSURE VS ARRESTOR LENGTH PARAMETER FOR DIFFERENT (E/σ_0)

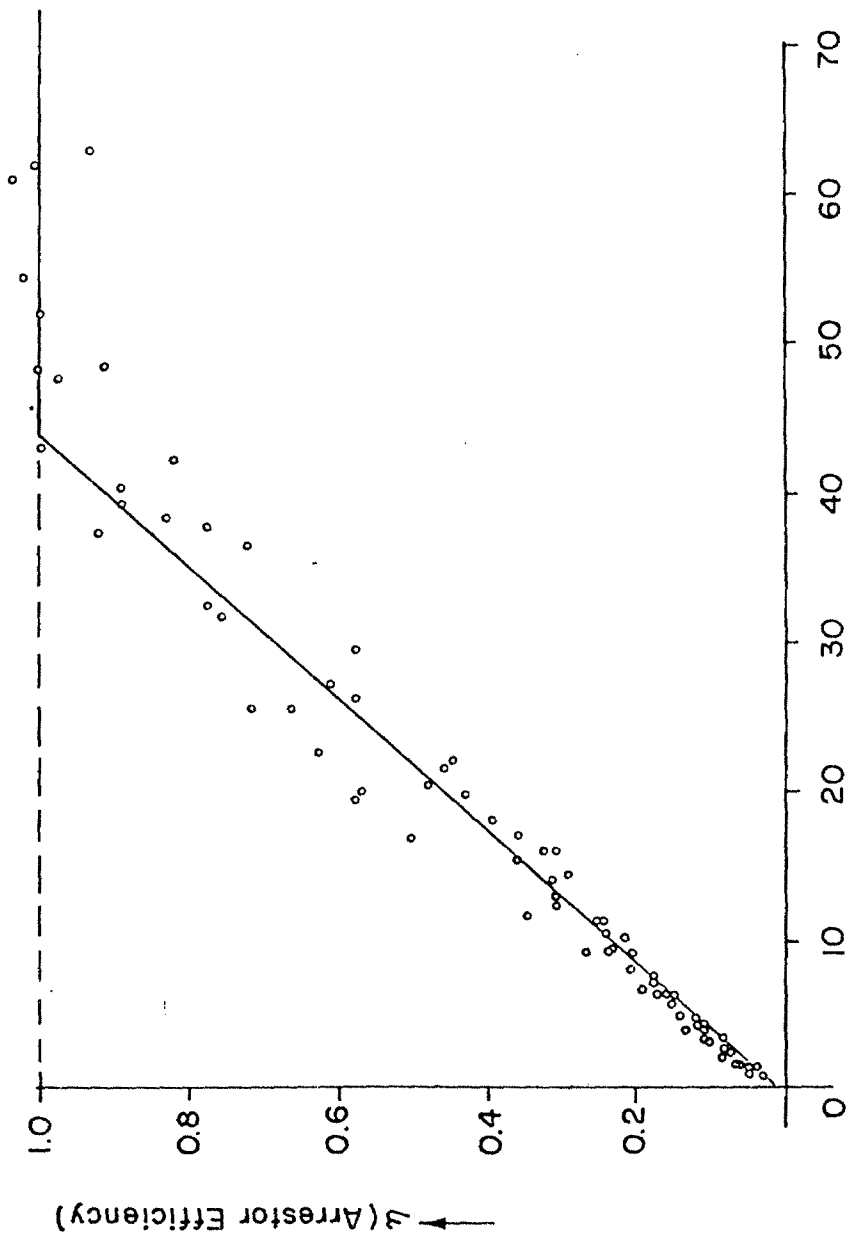

FIG. 5.12 EXPERIMENTAL RESULTS PLOTTED AGAINST ARRESTOR EFFICIENCY EMPIRICAL FORMULA

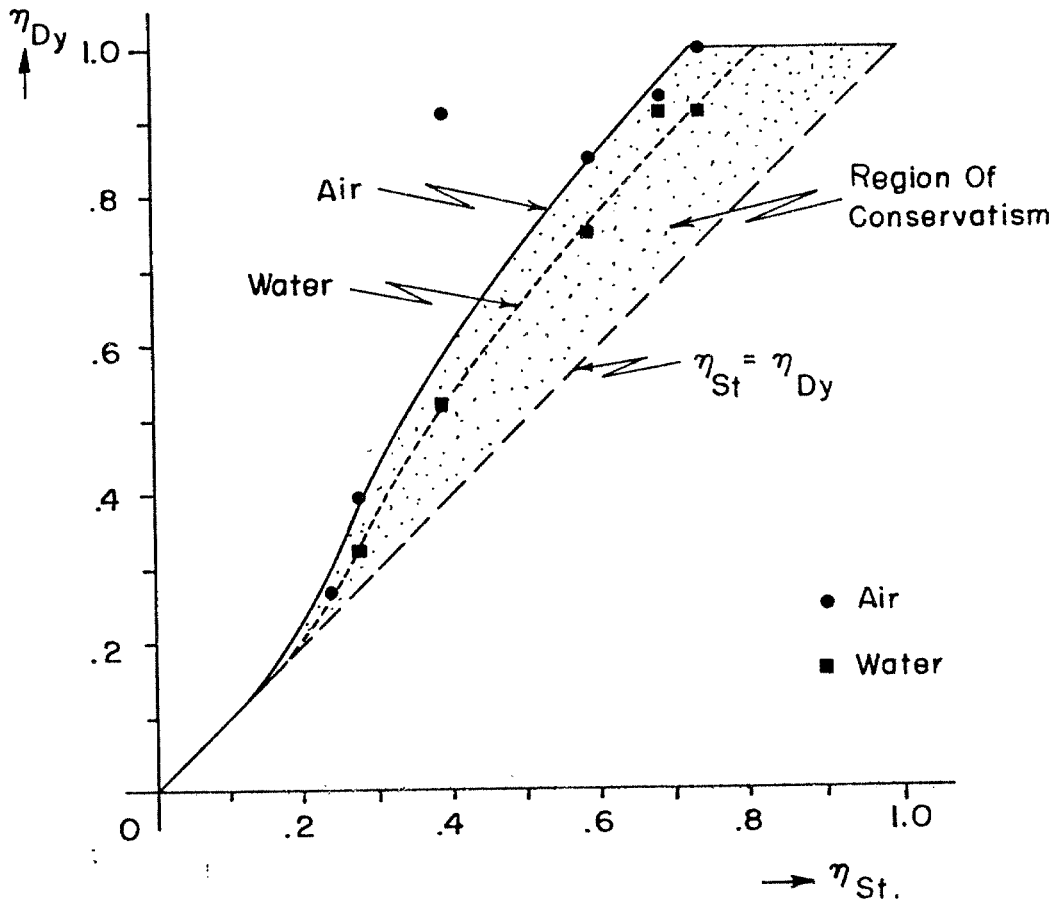

FIG. 5.13 DYNAMIC VS STATIC ARRESTOR EFFICIENCY FOR AIR AND WATER AS PRESSURIZING MEDIA

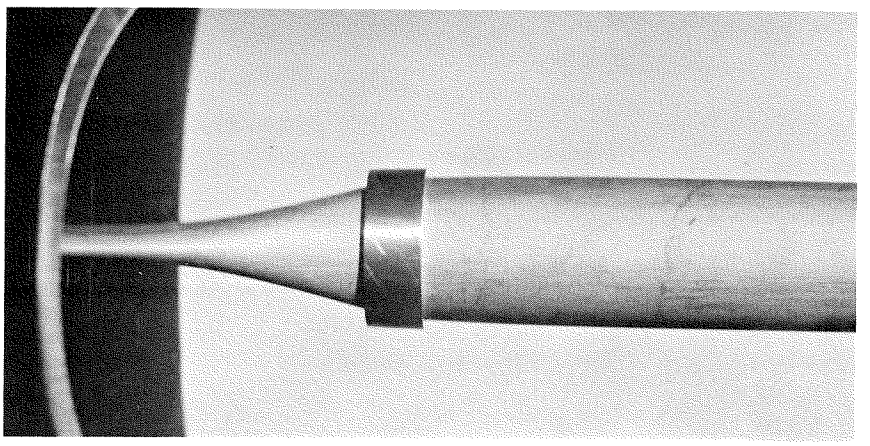

(a)

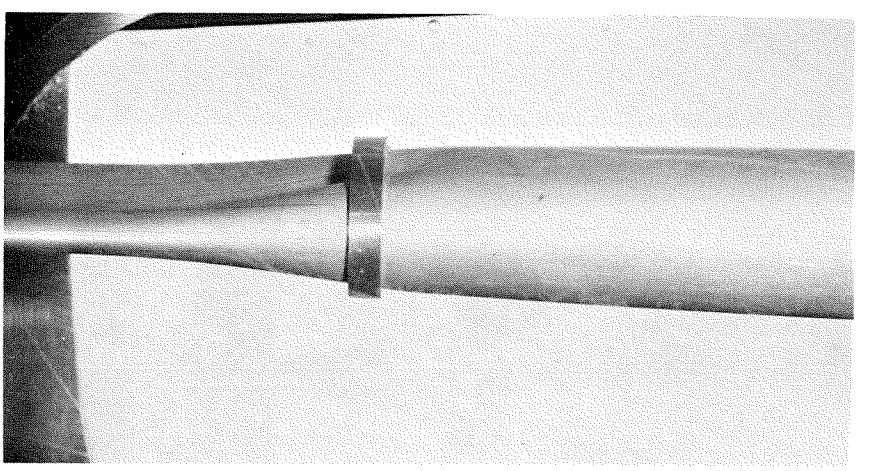

(b)

FIG. 5.14 BUCKLE ARREST

(a) Buckle arrested by slip-on arrestor under quasi-static conditions.

(b) Buckle arrested by slip-on arrestor under dynamic conditions.

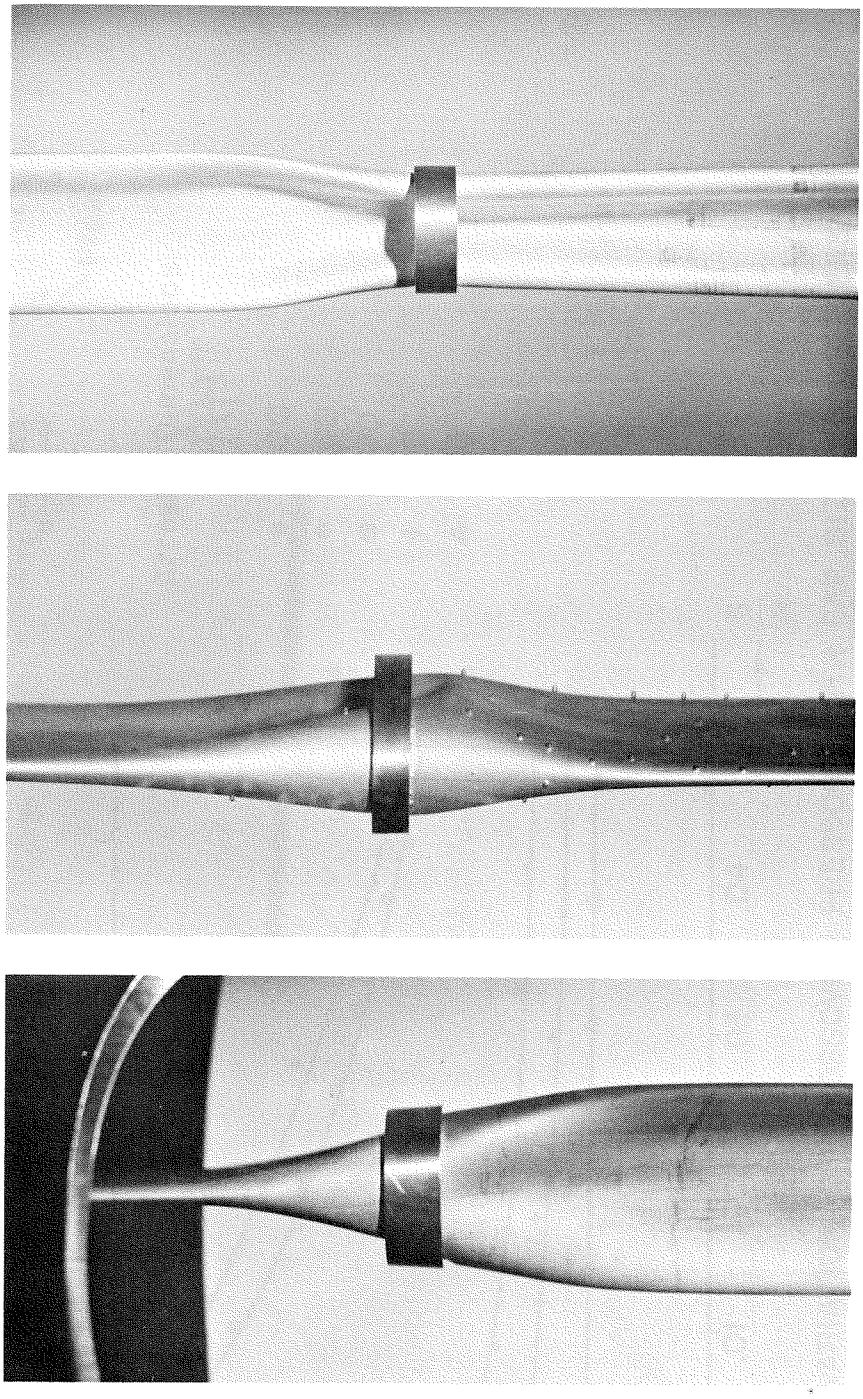

FIG. 5.15 BUCKLE CROSSOVER

(a) Buckle penetrating an arrestor in "U" shaped mode under quasistatic conditions.

(b) Buckle penetrating an arrestor under dynamic conditions.

(c) Flip-flop mode of penetration common to dynamic and quasistatic cases.

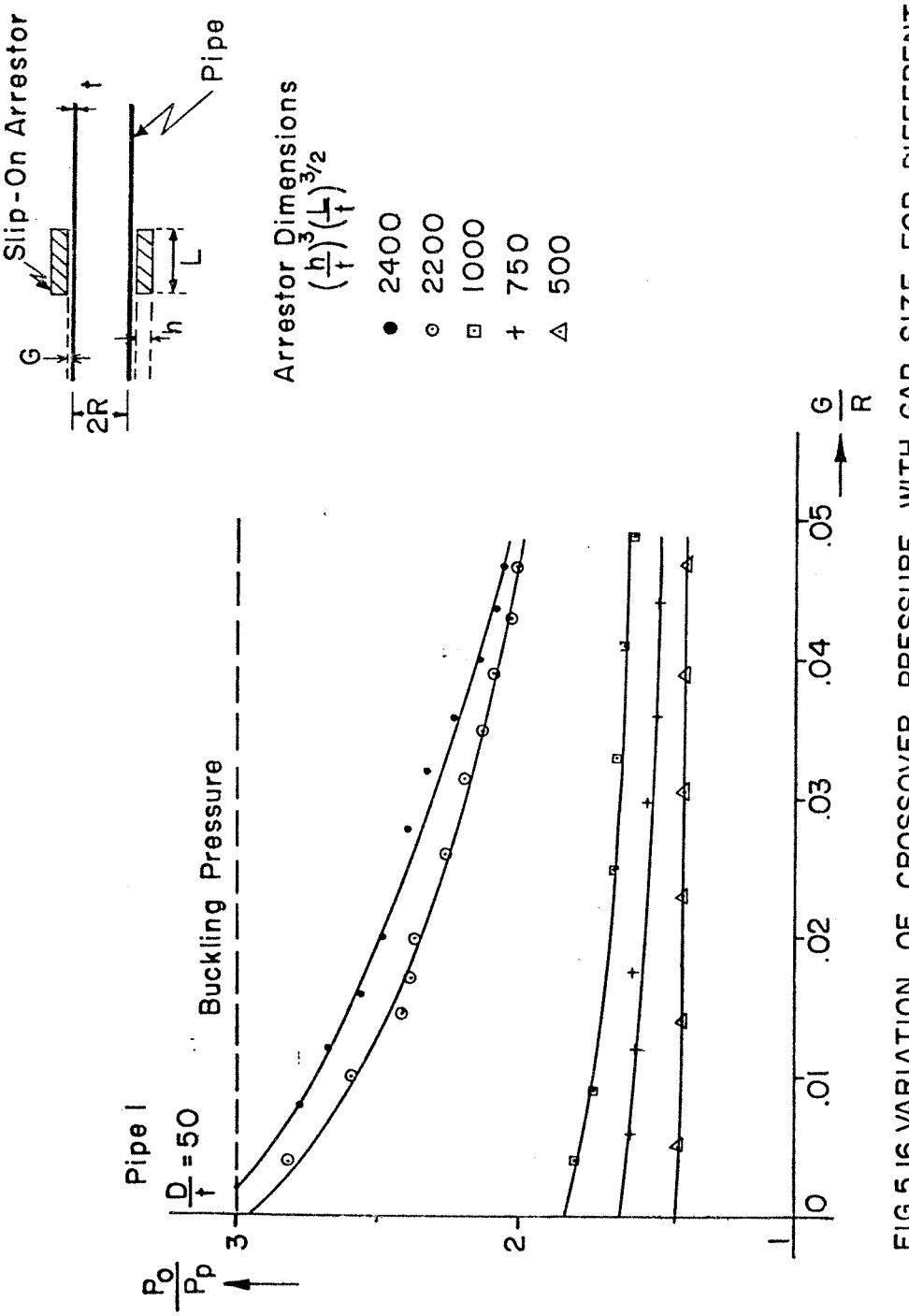

FIG.5.16 VARIATION OF CROSSOVER PRESSURE WITH GAP SIZE FOR DIFFERENT ARRESTOR DIMENSIONS

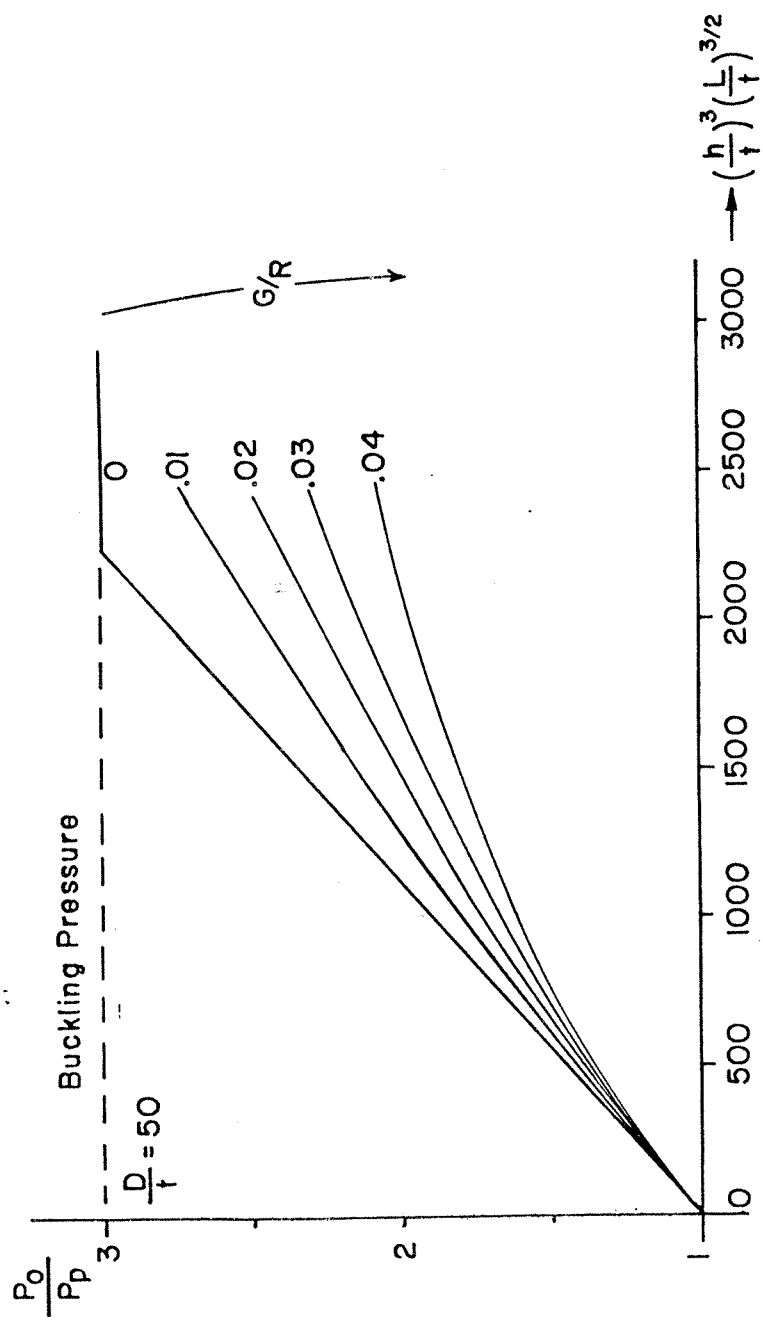

FIG. 5.17 CROSSOVER PRESSURE VS ARRESTOR GEOMETRIC PARAMETERS FOR DIFFERENT GAP SIZES

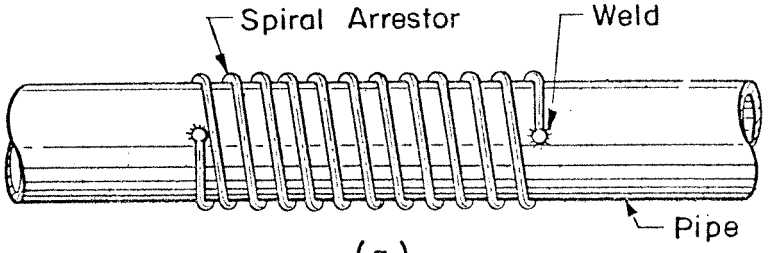

(a)

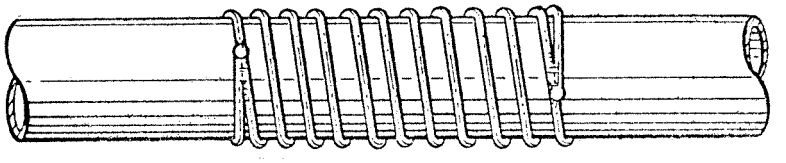

(b)

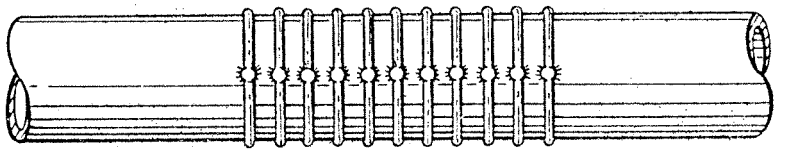

(c)

FIG.5.18 DIFFERENT SPIRAL ARRESTOR ARRANGEMENTS AND WELDING METHODS

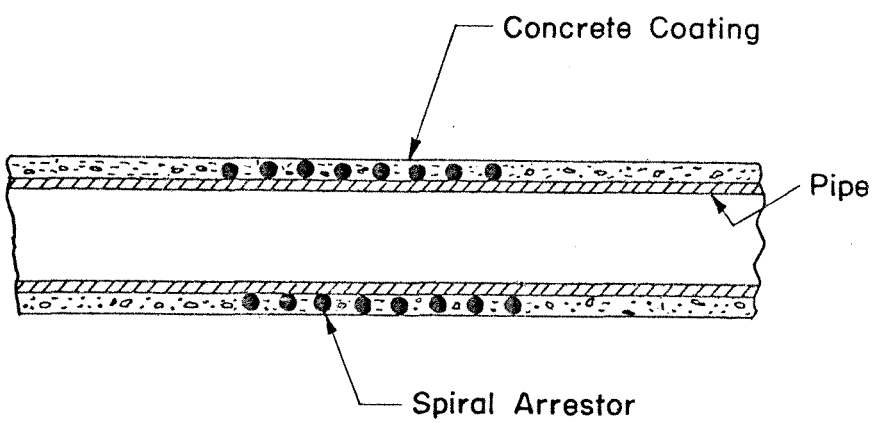

FIG.5.19 SPIRAL ARRESTOR USED UNDER CONCRETE COATING

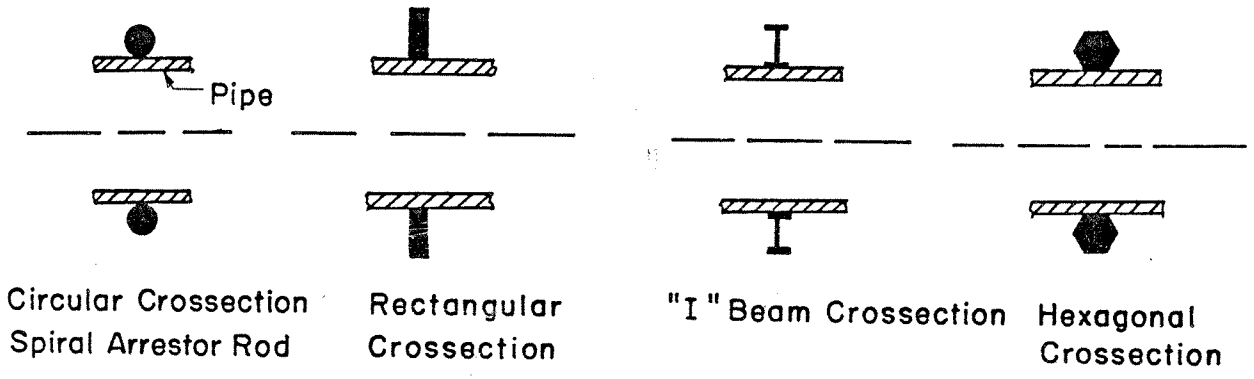

FIG.5.20 POSSIBLE CROSSECTIONS FOR SPIRAL ARRESTOR RODS

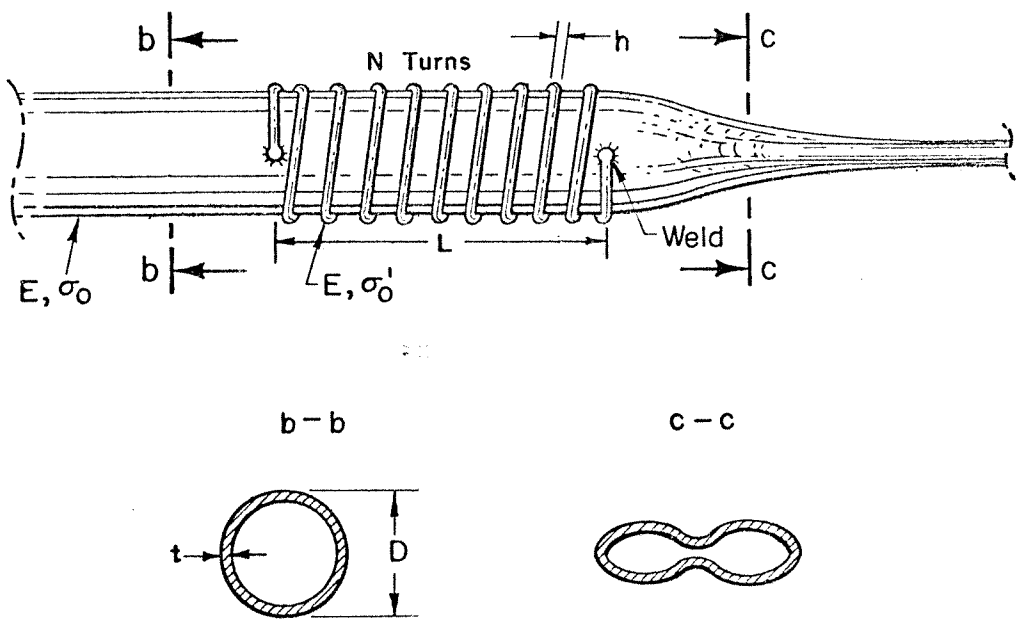

FIG.5.21 PARAMETERS OF THE ARREST PROBLEM

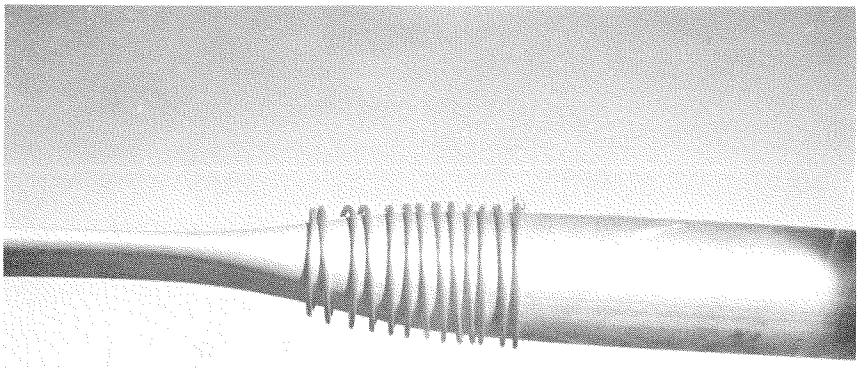

FIG. 5.22 SPIRAL ARRESTOR STOPPING A PROPAGATING BUCKLE

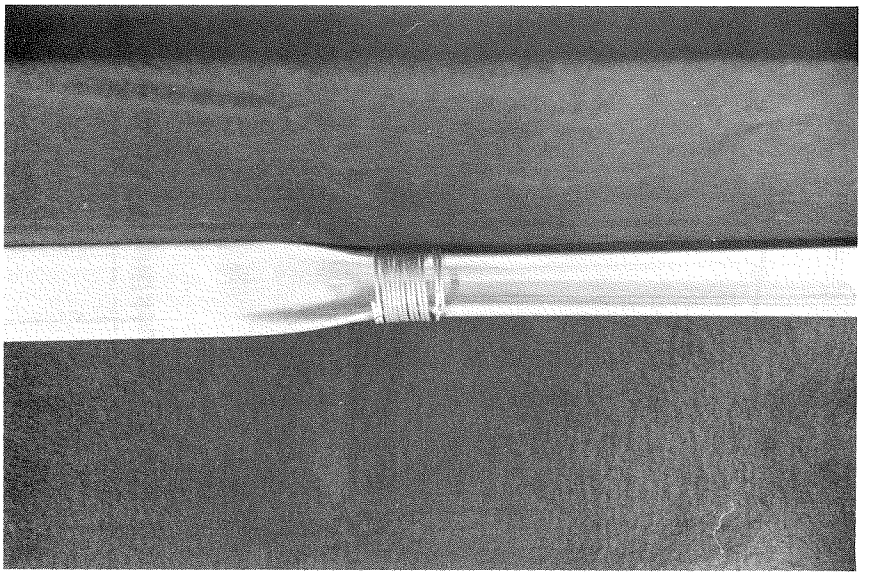

FIG. 5.23 BUCKLE PENETRATED ARRESTOR IN "U" MODE.

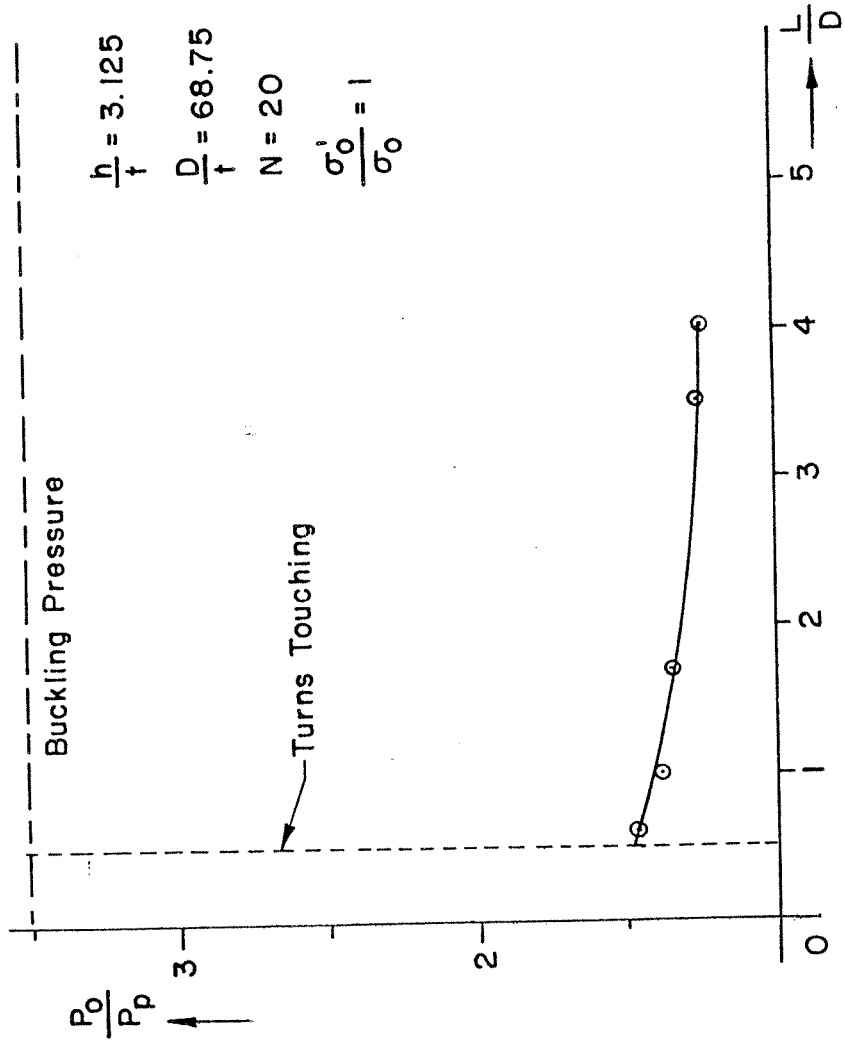

FIG. 5.24 VARIATION OF CROSSOVER PRESSURE WITH SPIRAL ARRESTOR PITCH

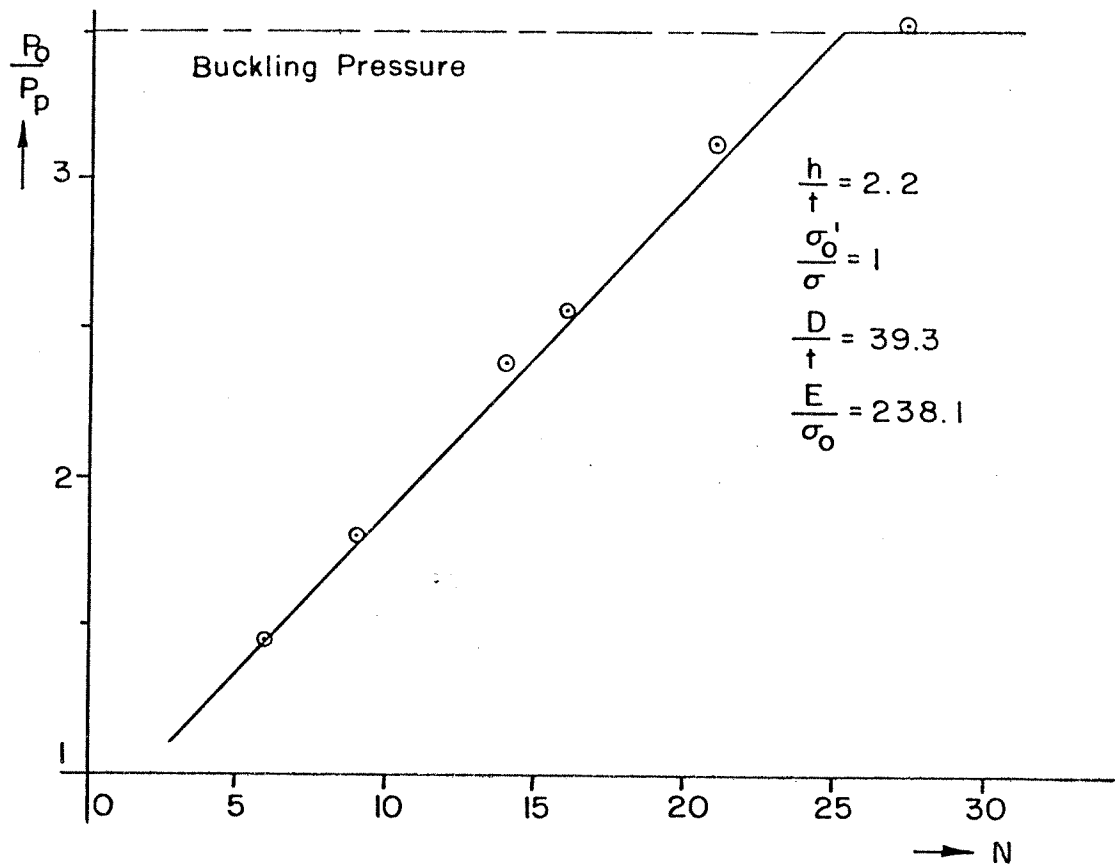

FIG.5.25 VARIATION OF CROSSOVER PRESSURE WITH NUMBER OF TURNS IN SPIRAL

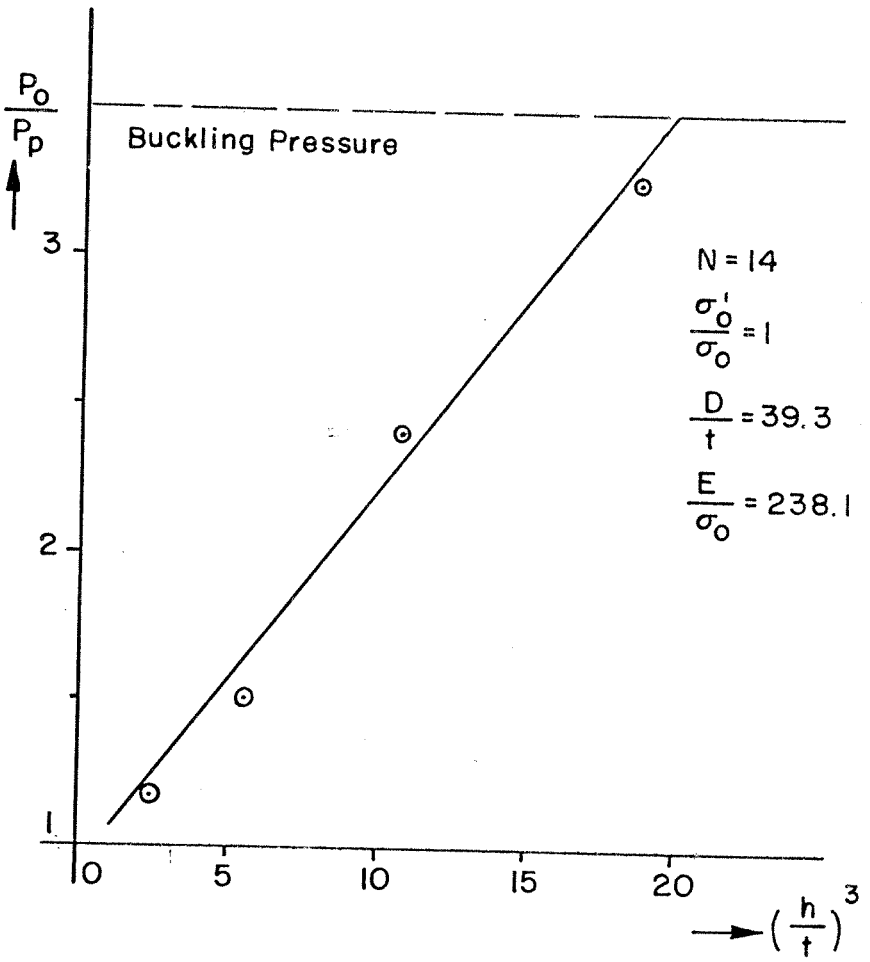

FIG.5.26 VARIATION OF CROSSOVER PRESSURE WITH SPIRAL ROD DIAMETER

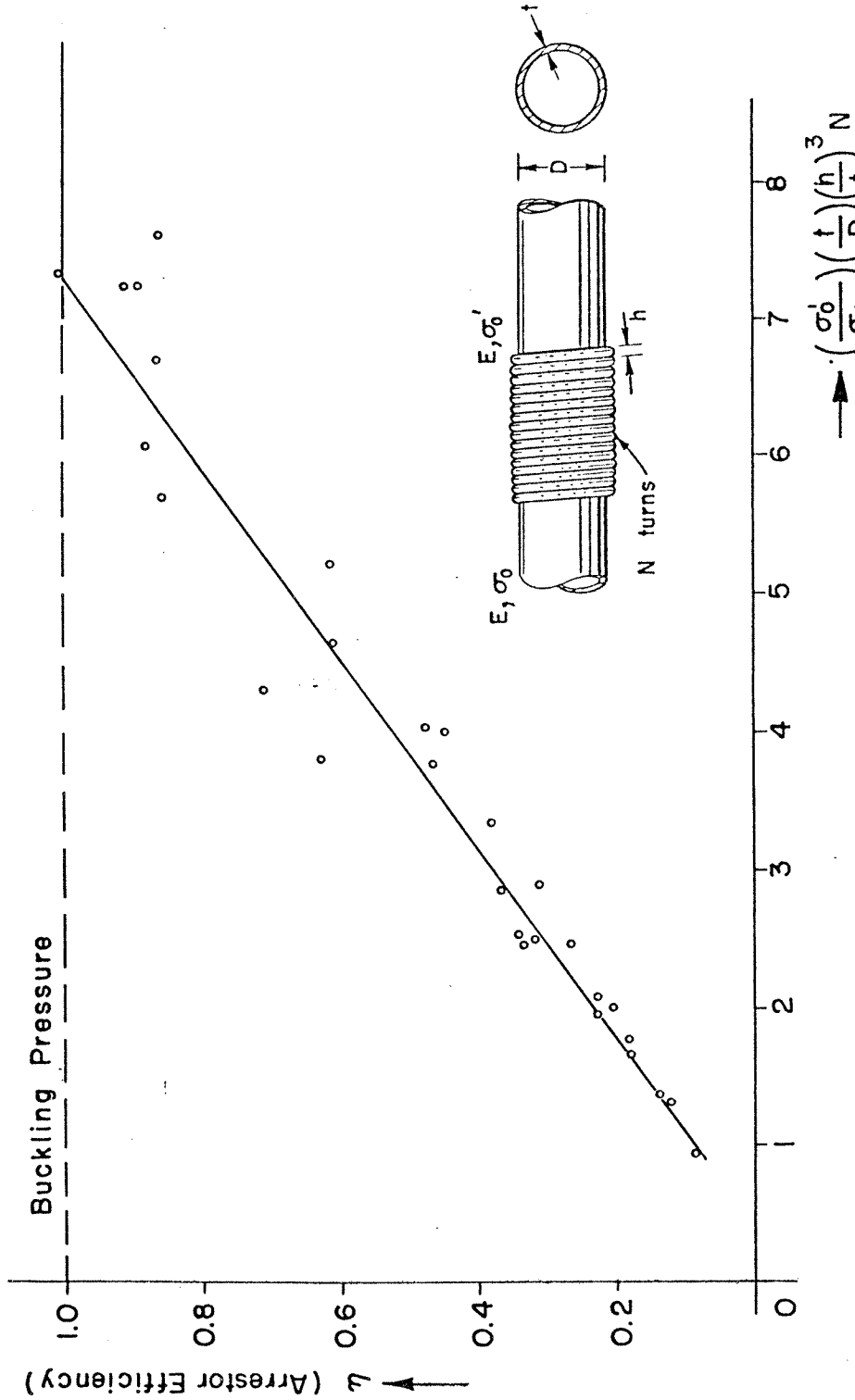

FIG. 5.27 EXPERIMENTAL RESULTS PLOTTED AGAINST THE EMPIRICAL EXPRESSION FOR THE ARRESTOR EFFICIENCY

Field	Brent. [5.1] (N. Sea)	Frigg [5.7] (N. Sea)	Loop [5.5] (G. Of Mexico)	Tunisia-Sicily Mediter. [5.6]	Forties [5.8] (N. Sea)
Pipeline Total Length Km (in.)	448 (278.5)	360 (225)	45 (28)	160 (100)	201 (125)
Average Depth m (ft.)	100 (328)	122 (400)	18+ (60+)	400+ (1310+)	122 (400)
Maximum Depth m (ft.)	165 (541)	158 (520)	46 (150)	500 (1970)	137 (450)
Pipe Diameter m (in.)	0.914 (36)	0.813 (32)	1.422 (56)	0.508 (20)	0.813 (32)
Pipe Thickness m (in.)	0.022 (0.867)	0.019 (0.75)	0.019 (0.75)	0.0206 (0.812)	0.019 (0.75)
Grade	5-LX-60	5-LX-65	5-LX-60	52X-X65	5-LX-65
Arrestor Type	Grouted	Grouted	Slip-On	Heavy Wall	Grouted
Arrestor Length m (in.)	1.143 (45)	1.830 (72)		3 (9.8)	
Arrestor Thick. m (in.)	0.032 (1.25)	0.025 (1.0)		0.030 (1.18)	
Gap Size	0.038 (1.5)	0.025 (1.0)			
Grout	Concrete	Concrete			
Arrestor Grade	5-LX-42	5-LX-65		52X-X65	
Pp. Bar (psi)	13.7 (199)	14.0 (203)	3.59 (52)		
Arrestor Space m (ft.)	150 (490)	500	152 (500)		

TABLE 5.1 EXAMPLES OF ARRESTORS USED IN FIELD SITUATIONS

	D mm(in)	t mm(in)	D/t	P_p bar(psi)	P_c bar(psi)
1	25.48 (1.003)	0.508 (0.020)	50.0	4.482 (65)	13.034 (189)
2	38.18 (1.503)	0.889 (0.035)	49.2	7.241 (105)	19.931 (289)
3	31.83 (1.253)	0.889 (0.035)	38.8	10.207 (148)	34.482 (500)
4	28.65 (1.128)	0.889 (0.035)	32.2	12.070 (175)	46.897 (680)
5	25.43 (1.001)	0.889 (0.035)	28.6	16.759 (243)	64.828 (940)
6	31.83 (1.252)	0.889 (0.035)	35.8	11.241 (163)	33.655 (488)
7	31.85 (1.254)	0.889 (0.013)	35.8	18.070 (262)	92.900 (1347)

TABLE 5.2 CHARACTERISTICS OF PIPES USED IN ARRESTOR EXPERIMENTS

PRE. MEDIUM	D/t	h/t	L/t	P_o/P_p	P_{oo}/P_p	U/U_o	$\eta_{St.}$	η_{Dy}	$\eta_{Dy}-\eta_{St.}/\eta_{St.}\%$
AIR	50	2.45	12.5	1.454	1.55	.60	.246	.275	11.8%
AIR	50	2.75	12.5	1.708	2.68	.91	.384	.912	137.5%
WATER	50	2.75	12.5	1.708	2.02	.30	.384	.528	37.5%
AIR	50	3.25	12.5	2.23	2.81	.95	.681	.937	37.6%
WATER	50	3.25	12.5	2.23	2.68	.36	.681	.916	34.5%
AIR	35.7	2.86	5.71	1.557	1.84	.85	.265	.397	49.8%
WATER	35.7	2.86	5.71	1.557	1.68	.36	.265	.322	21.5%
AIR	35.7	2.86	8.57	2.25	2.81	1.1	.588	.853	45.1%
WATER	35.7	2.86	8.57	2.25	2.59	.43	.588	.750	27.6%
AIR	35.7	2.86	11.43	2.55	3.12	★	.729	1.000	37.2%
WATER	35.7	2.86	11.43	2.55	2.91	★	.729	.912	25.1%

TABLE 5.3 COMPARISON OF DYNAMIC AND STATIC ARRESTOR EFFICIENCY

★ Flip-Flop Mode

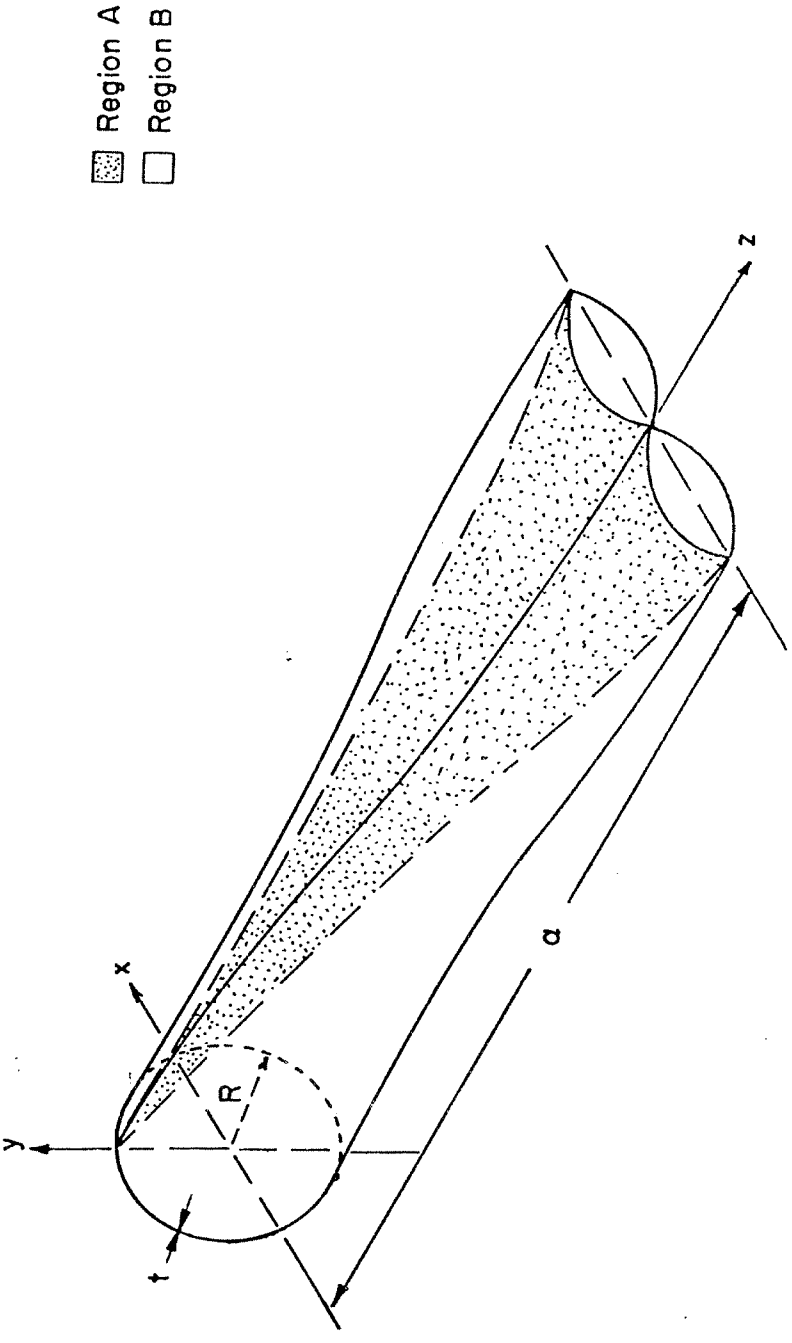

FIG. C.1 IDEALIZED GEOMETRY FOR BUCKLE FRONT